Department of Physics
UNIVERSITY OF COLORADO **BOULDER**

Ph.D. Thesis

On various aspects of ion collisions analyzed via a hydrodynamic hybrid approach

Mathis Habich

M.Sc., University of Colorado Boulder, USA

B.Sc., Goethe University Frankfurt, Germany

November 17, 2017

A thesis submitted to the Faculty of the Graduate School of the
University of Colorado Boulder in partial fulfillment of the requirements
for the degree of Doctor of Philosophy
Department of Physics

This Ph.D. thesis entitled

"On various aspects of ion collisions analyzed via a hydrodynamic hybrid approach"

written by Mathis Habich
has been approved by the Department of Physics, University of Colorado Boulder

_____ November 20, 2017

Prof. Paul Romatschke

_____ November 20, 2017

Prof. James L. Nagle

The final version of this very thesis has been examined by the signatories, and they find that both the content and the form meet acceptable presentation standards of scholarly work in the discipline of theoretical nuclear physics.

Mathis Habich (Ph.D., Department of Physics)

On various aspects of ion collisions analyzed via a hydrodynamic hybrid approach

Thesis directed by Prof. Dr. Paul Romatschke

Abstract

In this thesis, various theoretical results surrounding the quark–gluon plasma which is created in the ultrarelativistic collisions of ions are presented. The many-body, strong-coupling, and real-time characteristics of those collisions partially exclude first-principle quantum chromodynamics calculations, whereas the effective theory of hydrodynamics allows for a rather successful description of the quark–gluon plasma. A criterion of hydrodynamic stability is used to restrict the transport coefficient bulk viscosity. In addition, various collisional systems over a wide range of energy are successfully modeled for particle spectra, yields, flow coefficients, and HBT radii. Despite questions of hydrodynamic applicability to few-particle systems, there is reasonable agreement with experimental data for $p + p$ collisions in this framework. Notably, the strong dependence on the bulk viscosity of simulation results for $p + p$ collisions could help constrain this transport coefficient. All of those aspects solidify our quantitative understanding of the quark–gluon plasma produced in ion collisions.

Acknowledgments

During my work, I received a lot of support from many people. First, I would like to thank my advisor Prof. Paul Romatschke for all the years of working for him. His scientific guidance and knowledge were crucial to my success while he still allowed me to explore other aspects of academia during my graduate student career. My gratitude also is due to Javier Orjuela–Koop for being an amazing friend and wise academic colleague who assisted me in answering questions arising from the experimental side of heavy-ion collisions, as well as life decisions. Next, I would like to acknowledge Prof. Dennis Perepelitsa's help in connecting me with researchers and providing me with PHENIX data. Furthermore, I would like to thank Ryan Weller for clarifying conversations on a proton model.

Darüberhinaus gilt mein Dank meinem ältesten Freund Sebastian Köhlerschmidt, der mit Diskussionen, Humor und Unterhaltung in den anstrengenden Zeiten stets zur Hilfe war und ein verlässlicher, sowie weiser Ratgeber ist.
Schlussendlich möchte ich mich bei meiner Familie bedanken. Dies schließt meine Eltern Christine und Gernot, sowie meinen Bruder Johannes und seine Frau Dana ein. Es war die Erziehung meiner Eltern im kritischen Denken und der Wertschätzung von Wissen und die Vorbildfunktion meines Bruders und Danas durch ihre wissenschaftlichen Karrieren, welche mich stets inspirierten und motivierten weiterzumachen. Es sind diese positiv prägenden Einflüsse, welchen ich rückblickend am meisten zu verdanken habe.

Contents

Contents v

List of Figures vi

1. Introduction 1

2. Overview of heavy-ion collisions 3
2.1. Pre-equilibrium phase or initial conditions 5
2.2. Hydrodynamic phase 9
2.3. Hadronic phase, freeze-out, and free streaming 14

3. SONIC framework 18

4. Relevance of the bulk viscosity 21

5. Results for large collisional systems 27

6. Initial conditions for p+p 30

7. Conclusion 35

Bibliography 37

Appendix 47

A. Publications 48
A.1. Onset of cavitation in the quark–gluon plasma 48
A.2. Particle spectra and HBT radii for simulated central nuclear collisions of $C+C$, $Al+Al$, $Cu+Cu$, $Au+Au$, and $Pb+Pb$ from $\sqrt{s}$=62.4 – 2760 GeV 60
A.3. Testing hydrodynamic descriptions of p+p collisions at $\sqrt{s}$=7 TeV 67

List of Figures

2.1. Schematic Minkowski diagram of the four stages of heavy-ion collisions . . 3
2.2. Schematics of the initial geometry of large, colliding nuclei represented as idealized disks 5
2.3. Woods–Saxon profile 7
2.4. Glauber initial conditions for central $Au + Au$ in the transverse plane . . 9
2.5. Glauber initial conditions for non-central $Au + Au$ in the transverse plane 10
2.6. Sketch of the initial energy density distribution 11
2.7. Coordinate system for HBT radii 17

3.1. Execution steps of `SONIC` for event-by-event simulations 20

4.1. Sketch of cavitation and bubble formation inside the QGP 22
4.2. The upper bound of the bulk viscosity ζ/s for various flow profiles in $Au + Au$ collisions 23
4.3. Various parametrizations for the bulk viscosity over entropy density ratio 25

5.1. Pion spectrum for various large collisional systems all simulated via `SONIC` 28
5.2. Pion HBT radii for different collision systems 29

6.1. Initial conditions for the RND and FLC model for non-central $p + p$ collisions in the transverse plane 32
6.2. Elliptic flow coefficients for $p + p$ collisions 33
6.3. Charged hadron multiplicity for $p + p$ collisions 34

Prologue

This is a cumulative thesis comprising the peer-reviewed publications by the author of this very thesis:

- Mathis Habich and Paul Romatschke. "Onset of cavitation in the quark-gluon plasma". In: *JHEP* 12 (2014), p. 054. DOI: 10.1007/JHEP12(2014)054. arXiv: 1405.1978 [hep-ph]
- M. Habich, J.L. Nagle, and P. Romatschke. "Particle spectra and HBT radii for simulated central nuclear collisions of C + C, Al + Al, Cu + Cu, Au + Au, and Pb + Pb from $\sqrt{s} = 62.4$ - 2760 GeV". in: *Eur.Phys.J.* C75.1 (2015), p. 15. DOI: 10.1140/epjc/s10052-014-3206-7. arXiv: 1409.0040 [nucl-th]
- M. Habich, G. A. Miller, P. Romatschke, and W. Xiang. "Testing hydrodynamic descriptions of p+p collisions at $\sqrt{s} = 7$ TeV". in: *Eur. Phys. J.* C76.7 (2016), p. 408. DOI: 10.1140/epjc/s10052-016-4237-z. arXiv: 1512.05354 [nucl-th]

1. Introduction

The strong force is one of the four fundamental forces of nature, among the gravitational force, the electrodynamic force, and the weak force. Despite being so fundamental, the interactions of the strong force proved much more difficult to probe and explore than the other three remaining forces. From an experimental point of view, extreme temperatures must be reached in order to overcome the confinement of the strong force which creates all baryonic matter with which humans interact on an ordinary basis. These high-temperature requirements demand for vast machines, such as the Relativistic Heavy Ion Collider or the Large Hadron Collider that accelerate ions to ultrarelativistic velocities and overcome the strong coupling of the constituting nucleons by colliding two ions. The emerging matter with a yoctosecond lifetime is the so-called quark–gluon plasma (QGP). The word "plasma" in QGP is appropriate in so far as the quarks and gluons are no longer bound, akin to the state of an ordinary plasma where ions and electrons are no longer bound either. The nature of the strong force and its underlying theory quantum chromodynamics (QCD) render real-time calculations of the QGP very difficulty although QCD equations of state[1], describing the thermodynamics, have been calculated and are a quintessential ingredient in the theoretical description of heavy-ion collisions. In the absence of first-principle calculations for a real-time evolution, several effective theories have been proposed, including the currently most successful one: hydrodynamics.
Furthermore, the field of heavy-ion collisions has recently been extended to additionally include small systems, such as proton–proton ($p+p$) or proton–nucleus collisions which *might* also result in the formation of the QGP. This suggests that the name *ion collisions* should be used for the entire field. However, the existence of a hydrodynamic medium for such small systems is currently intensely debated in the community because mean-free-path length and system size are of the same order — a criterion which normally marks the break-down of hydrodynamics.
In this thesis, an overview of the phases of the collision is given, assuming the hydrodynamic paradigm. In Ch. 4, an upper threshold for the hydrodynamic transport coefficient bulk viscosity will be discussed and compared to commonly used values; the results in this chapter have been published in the peer-reviewed journal *Journal of High Energy Physics* (publication attached in App. A.1, Ref. [1]). In Ch. 5, the simulations for

[1] Note that those equations of state are solutions of QCD in equilibrium.

central collisions of systems, including bulk observables and Hanbury–Brown–Twiss radii for the QGP, are presented; the results in this chapter have been published in the peer-reviewed journal *The European Physical Journal C* (publication attached in App. A.2, Ref. [2]). In Ch. 6, initial condition models for protons are presented, simulated, and compared to data; the results in this chapter have been published in the peer-reviewed journal *The European Physical Journal C* (publication attached in App. A.3, Ref. [3]). Ch. 7 summarizes the findings and provides an outlook for future projects.

2. Overview of heavy-ion collisions

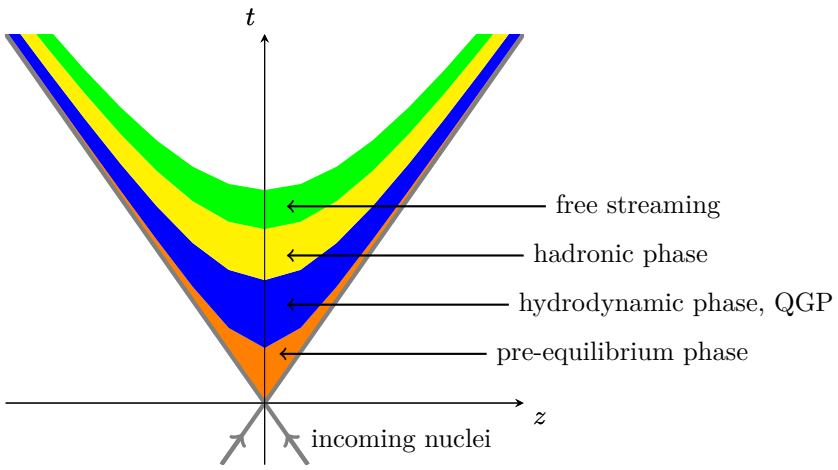

Figure 2.1.: Schematic Minkowski diagram of the four stages of heavy-ion collisions. The colliding nuclei are moving at ultrarelativistic speeds; therefore, their trajectories are very close to the light cones shown in gray. The lines of constant proper time $\tau = \sqrt{t^2 - z^2}$ correspond to hyperbolas in this sketch. As discussed in the text, the first phase is the pre-equilibrium phase directly after and during the longitudinally extended, incoming nuclei collide, followed by the hydrodynamic phase. The final state of the hydrodynamic phase yields an isothermal hypersurface which is in turn the initial state for seeding the hadronic phase. The hadronic phase includes the decay cascades of particles and the interactions among those particles which after some distance and time free-stream without interactions.

As mentioned in the introduction, the first-principle approach to describe heavy-ion collisions would be using QCD directly. However, the large strong-coupling constant α_S

adversely affects the reliability of standard tools, such as perturbative QCD calculations. Additionally, non-perturbative approaches, such as lattice QCD, are not applicable to heavy-ion collisions dynamics because of the infamous sign problem. To that end, a theoretical model is required, based on the underlying principles of QCD [4] that captures the relevant features — this is often called an effective theory.
Common models of heavy-ion collisions separate the evolution in at least four stages whose exact regimes and boundaries are still actively discussed [5], see Fig. 2.1. It is common convention to use coordinates where the actual collision begins at the proper time $\tau = \sqrt{t^2 - z^2} \approx 0$ fm/c. In terms of proper time, the four stages are defined as:

1. **Phase:** The pre-equilibrium phase happens directly after the collision of the ions, and it is dominated by very large gradients. The phase's duration is roughly $\tau \approx 0 - 1$ fm/c [6]. The end of the pre-equilibrium phase will serve as input (initial conditions) for the subsequent hydrodynamic phase.

2. **Phase:** The hydrodynamic phase begins at $\tau \approx 1$ fm/c, is marked by strong-coupling dynamics, and lasts roughly till 10 fm/c [6]. The end of the hydrodynamic phase will serve as input for the subsequent hadronic cascade phase.

3. **Phase:** The hot hadron gas phase takes place at the boundary of the hydrodynamic medium when the fluid's temperature drops below the decoupling temperature and the emerging particles still interact and decay. This happens at the surface of the fluid bubble both simultaneously with the hydrodynamic phase, as well as after the hydrodynamic phase has ended. Furthermore, this hot hadron gas continues to interact even after the hydrodynamic evolution has ceased for a given fluid cell.

4. **Phase:** The free-streaming phase consists of the generated particles that fly into the detectors without interacting with other particles.

Fig. 2.1 schematically shows those stages. N.b., based on particular theories of initial conditions affecting the pre-equilibrium phase, a finer distinction of stages can be made. Likewise, this holds true for the hydrodynamic stage (e.g., viscous hydrodynamics, ideal hydrodynamics) due to the hydrodynamic transport coefficients.
In order to properly combine those different stages that have different physical descriptions, certain assumptions need to be made for each stage. At the end of each stage, the results are the starting point for the next stage; thus, errors in one phase normally propagate forward — not necessarily in a linear fashion.
The second phase is described by relativistic hydrodynamics. The theoretical framework of the governing equations is well established[1]. In the following, we will use the gradient

[1] N.b., there are several different approaches who differ slightly, e.g.: Müller–Israel–Stewart [7], Denicol–Niemi–Molnár–Rischke [8], and gradient expansion [6].

expansion approach because of its relation to conformal theories. This will prove useful upon employing AdS/CFT for the pre-equilibrium phase. Furthermore, the transport coefficients inherent to hydrodynamics pose an uncertainty since they are experimentally hard to measure via direct means due to the extreme temperatures and short lifetimes. The next two phases are governed by hadron decays and interactions. Those decays and their associated probabilities have been analyzed in depth by other experiments, whereas the in-medium interaction between particles still carries sizable uncertainties. To recapitulate, the central paradigm of heavy-ion collisions today is the hydrodynamic evolution. This evolution strongly depends on the initial conditions, which are in turn determined by the pre-equilibrium phase and ultimately, by the geometry of the colliding ions. The interplay of geometry and evolution is by no means trivial due to the inherent non-linearity of hydrodynamics and the challenges accessing the pre-equilibrium phase with QCD from first-principles.

2.1. Pre-equilibrium phase or initial conditions

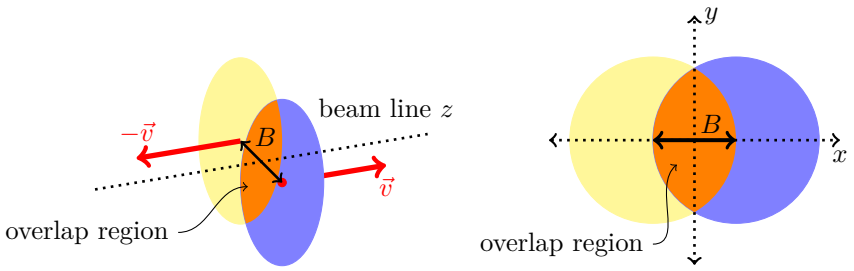

Figure 2.2.: Schematics of the initial geometry of large, colliding nuclei represented as idealized disks. The Lorentz contraction close to the speed of light renders the nuclei flat in the laboratory frame. Left: perspective view of the colliding nuclei with opposing velocities v. Right: Transversal view of the colliding nuclei with the impact parameter B.

The pre-equilibrium phase begins directly when the two nuclei come in "contact", as depicted in Fig. 2.2 and is the first phase of the evolution process. At the moment, the pre-equilibrium phase contributes probably the most to the overall uncertainty of ion collisions since the current techniques are not sufficient to directly solve QCD for this phase. Hence, one needs to resort to other approaches. The Anti-de Sitter space/conformal field theory (AdS/CFT) correspondence [9] is one of those approaches. This conjecture states

the duality between a strongly coupled quantum field theory ($\mathcal{N} = 4$) in four dimensions and a five-dimensional theory of classical gravity [10, 11, 12, 13]. In particular, supersymmetric $\mathcal{N} = 4$ Yang–Mills theory is believed to behave similarly when compared to QCD if:

- The non-conformal nature of QCD can be neglected, e.g., vanishing bulk viscosity;
- The strong-coupling constant α_S is assumed to be very large [11];
- The number of colors can be taken to be very large;
- The number and type of the degrees of freedom of QCD become unimportant.

To be specific, AdS/CFT might provide more insight about thermalization times which would constrain the initialization times of hydrodynamic models [14, 15, 16], as well as pre-equilibrium flow profiles[2] [18]. The successful numerical merger of black holes in AdS_5 [19] might advance the understanding of the pre-equilibrium phase by providing early-time dynamics, as well as initial energy density profiles which can subsequently be used to initialize hydrodynamic calculations.
While AdS/CFT aims to describe the actual dynamics of the pre-equilibrium phase, other model approaches have been proposed to generate initial conditions for the consecutive hydrodynamic phase. Particularly, those approaches focus on the final state of the pre-equilibrium phase and use this final state as input for the hydrodynamic phase. Normally, these inputs are the initial conditions in form of initial energy densities which are necessary for solving the hydrodynamic equations (akin to all partial differential equations that are initial-value problems), in addition to the initial flow profiles. Those approaches can per definition not describe the pre-equilibrium dynamics in contrast to the previously described AdS/CFT ansatz. One commonly used initial condition model is the optical Glauber model. The optical Glauber model is based on the Woods–Saxon distribution (shown in Fig. 2.3)

$$\varrho_A(r) \quad = \quad \frac{\varrho_0}{1 + \exp\frac{r-R_0}{a_0}}\,, \tag{2.1}$$

where R_0 and a_0 are the nuclear radius and skin thickness, respectively, while ϱ_0 is defined via $A = \int_V \mathrm{d}^3\vec{r}\,\varrho_A(r)$ with A being the total number of nucleons in the nucleus. By overlapping two Woods–Saxon distribution and shifting both density profiles by half an impact parameter $\vec{B}$, respectively, as shown in Fig. 2.2, one would generate smooth

[2] Historically, those initial flow profiles were not known; thus, it was customary to start hydrodynamic simulations with zero fluid flows — an assumption which is most likely incorrect [17].

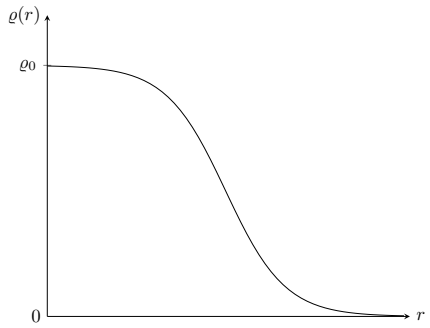

Figure 2.3.: Woods–Saxon profile from Eq. (2.1) for a nucleus of charge A. The larger a_0, the steeper the fall-off at $r \sim R_0$; the larger R_0, the wider the "plateau" of height ϱ_0 for small r. The area under the curve is the nucleon number A.

initial energy densities for the hydrodynamic phase via

$$\epsilon(\vec{x}_T) \quad \sim \quad T_A(\vec{x}_T + \vec{B}/2) T_A(\vec{x}_T - \vec{B}/2) \sigma_{\mathrm{AA}}^{\mathrm{inel}}(\sqrt{s}) \,, \tag{2.2}$$

where $\sigma_{\mathrm{AA}}^{\mathrm{inel}}$ is the inelastic nucleon–nucleon cross-section[3] with the *thickness function*

$$T_A(\vec{x}_T) \quad = \quad \int_{-\infty}^{+\infty} \mathrm{d}z \varrho_A(\vec{r}) \,, \tag{2.3}$$

stemming from the Lorentz contraction along the longitudinal direction and projecting the entire density into the transverse plane. The proportionality (2.3) is the so-called *binary collision scaling* and works reasonably well in phenomenology [20] by a simple scaling to experimental results. Furthermore, this model is based on the proportionality between charge and energy density.

The Glauber model — strictly speaking — determines the geometry of the colliding nuclei while the amount of deposited energy stems from the binary collision scaling in Eq. (2.2); thus, Glauber modeling can be used to describe the initial state of the pre-equilibrium phase. In contrast, AdS/CFT allows for a better understanding of the pre-equilibrium dynamics and deposited overall energy, but cannot describe the geometry of the nuclei. However, given a geometry, the energy densities can then be inferred from AdS/CFT; in fact, AdS/CFT predicts $\epsilon \sim \varrho^2$ in Ref. [18] which is basically Eq. (2.2) for vanishing $\vec{B}$.

[3] Cross-sections can be thought of as probabilities for a reaction to occur.

The original, optical Glauber model always creates smooth initial conditions with a mirror symmetry for non-vanishing impact parameter as can be seen in the left panels of Fig. 2.4 and Fig. 2.5, respectively. Since this model was not able to explain certain experimental observables, such as elliptic flow in central collisions, the Glauber model was refined to also include fluctuations via stochastic sampling. An overview of the Monte Carlo Glauber model is provided in Ref. [21] and the employed implementation is described in Ref. [22, 23]. In total, A nucleon positions are Monte Carlo sampled from the Woods-Saxon distribution (2.1) [22, 23]. Repeating these steps for two nuclei, a collision is said to occur if the distance between two sampled nucleon centers is less than $\sqrt{\sigma_{NN}^{\text{inel}}(\sqrt{s})/\pi}$ ($\sigma_{NN}^{\text{inel}}(200\,\text{GeV}) = 42.3$ mb). This motivates introducing two integers:

- Number of participants N_{part} is the number of nucleons with at least one collision.
- Number of collisions N_{coll} is the total number of binary collisions.

With the corresponding transverse densities , i.e., $\mathrm{d}N_i/\mathrm{d}\vec{x}_T$, one can relate these integers to the energy density of a collision via

$$\epsilon \sim \alpha \frac{\mathrm{d}N_{\text{coll}}}{\mathrm{d}\vec{x}_T} + (1-\alpha)\frac{\mathrm{d}N_{\text{part}}}{\mathrm{d}\vec{x}_T}\,, \tag{2.4}$$

where $\alpha \in [0,1]$ is a parameter expressing the relative strength of the contributions in this two-component model [21, 24]. For most simulations, α is a freely tunable parameter.

As shown in the right panels of Fig. 2.4 and Fig. 2.5, strong fluctuations are present for single events and decrease upon averaging numerous events as demonstrated by the central panels in the same figures. For hydrodynamic models, it is exactly these fluctuations that allow a better description of the experimental data; furthermore, these fluctuations seem more realistic as collisions basically take a snapshot of the current nucleonic (or even subnucleonic) configuration of the ions [25, 26].

Besides AdS/CFT and Glauber, other frameworks exist to explore the pre-equilibrium phase; e.g., the color-glass condensate (CGC) where a high, but saturated density of gluons is assumed. This weak coupling would allow for a classical-field descriptions at leading order [27, 28, 29]; the CGC/Glasma framework is described in more detail in Ref. [30].

The plethora of disparate approaches for the pre-equilibrium phase indicates the need for a better understanding of precisely this phase. To exacerbate the situation, many observables of this first phase are altered by the evolution in subsequent phases.

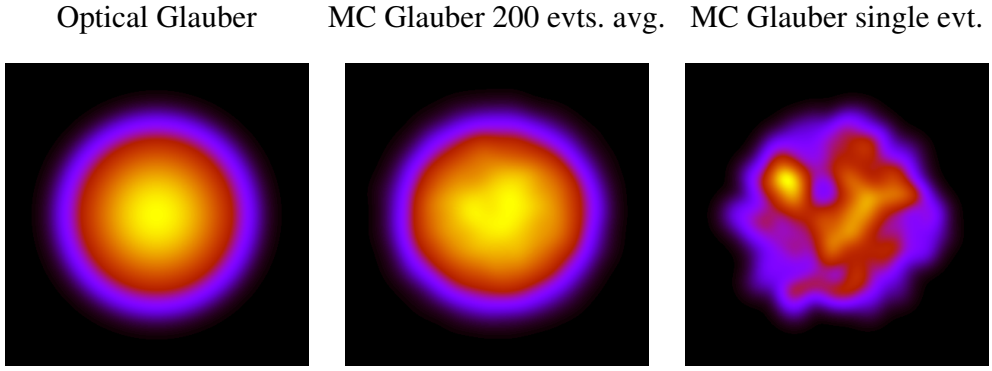

Figure 2.4.: Glauber initial conditions for central $Au+Au$ in the transverse plane, $B = 0$ fm. Left: Smooth Glauber initial conditions. Center: Averaged Monte Carlo Glauber over 200 events. Right: Single event Monte Carlo Glauber.

2.2. Hydrodynamic phase

As discussed in the previous section, the overlap region of two ions gives rise to a local deposition of energy density ϵ. This energy density is the starting point for a hydrodynamic treatment in which pressure gradients drive the fluid velocities; this is the fundamental concept of hydrodynamics. To very good accuracy, the medium surrounding the QGP is vacuum with zero pressure. Hydrodynamic evolution leads in the end to an expanding QGP that cools down while expanding because the pressure gradients are directed from the inside of the QGP to the outside vacuum. In Fig. 2.6, this situation is shown for an initial energy density that is elliptically shaped, e.g, the result of an off-center collision ($B \neq 0$). In this case, the pressure gradients are larger along the horizontal direction than along the vertical direction because the difference in pressure from the center to the outside is the same, yet the distance is shorter along the horizontal axis, leading to a larger horizontal pressure gradient; therefore, the fluid's momentum must be larger in this direction. This rather trivial concepts of fluid velocities following pressure gradients has profound consequences for heavy-ion collisions and is experimentally measured as collective flow in the QGP.

The theory of hydrodynamics is comparatively old, and despite its relevance in various

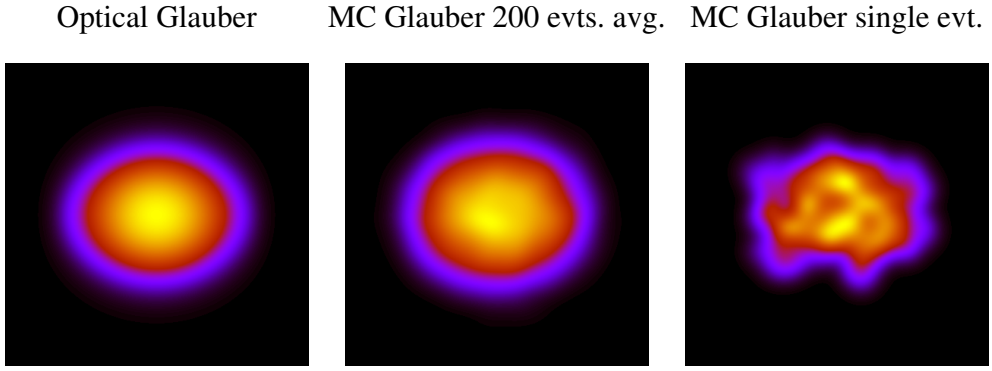

Figure 2.5.: Glauber initial conditions for non-central $Au + Au$ in the transverse plane, $B = 5$ fm along the x-axis. Left: Smooth Glauber initial conditions. Center: Averaged Monte Carlo Glauber over 200 events. Right: Single event Monte Carlo Glauber.

fields of physics[4], it has virtually disappeared from the physics curriculum. Therefore, a review of second-order hydrodynamics will be provided[5] to set the stage for the following chapters. Relativistic[6] hydrodynamics is simply the conservation of energy and momentum for a particular set of fields: namely the energy density ϵ, the fluid velocity u^μ, and the pressure p. Before constructing the energy–momentum tensor, the following definitions render the mathematical expressions shorter in a mostly minus metric

[4] For instance, hydrodynamics, also called fluid dynamics, has applications in condensed matter physics, cosmology, or biophysics.
[5] A complete derivation has been performed numerous times in the literature, for instance [6, 31, 32]
[6] Velocities near the speed of light make it necessary to use a relativistic formulation.

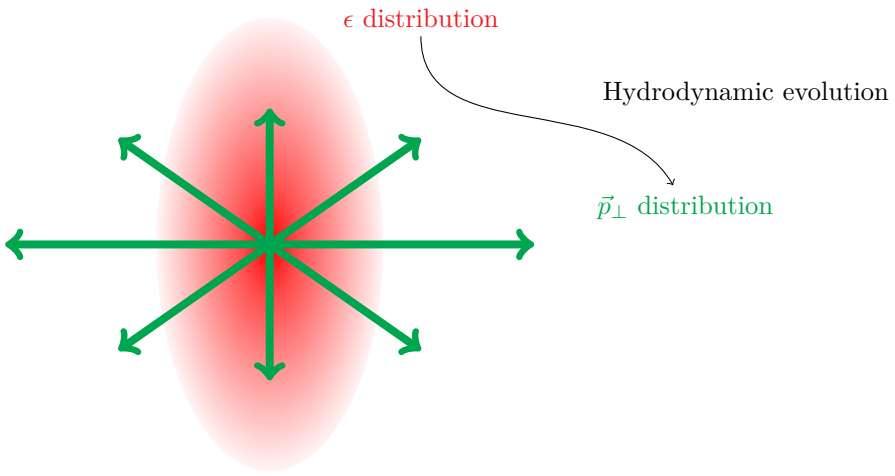

Figure 2.6.: Sketch of the initial energy density distribution. The initial energy density distribution (red) is translated via hydrodynamics into a transverse momentum ($p_\perp$) distribution of the fluid. The elliptical shape leads to an anisotropy in the momentum distribution.

$(\eta^{\mu\nu}) = \mathrm{diag}(+,-,-,-)$:

$$\Delta^{\mu\nu} \equiv \eta^{\mu\nu} - u^\mu u^\nu \,, \tag{2.5}$$

$$\nabla_\perp^\mu = \Delta^{\mu\nu}\nabla_\nu \,, \tag{2.6}$$

$$\nabla_\mu u^\mu = \partial_\mu u^\mu + \Gamma^\mu_{\mu\alpha} u^\alpha \,, \tag{2.7}$$

$$\mathrm{D} \equiv u^\mu \nabla_\mu \,, \tag{2.8}$$

$$A^{(\mu} B^{\nu)} \equiv \frac{1}{2}\left(A^\mu B^\nu + A^\nu B^\mu\right) \,, \tag{2.9}$$

$$A^{\langle\mu} B^{\nu\rangle} \equiv \frac{1}{2}\Delta^{\mu\xi}\Delta^{\nu\varrho}\left(A_\xi B_\varrho + A_\varrho B_\xi\right) - \frac{1}{3}\Delta^{\mu\nu}\Delta^{\xi\varrho}A_\xi B_\varrho \,, \tag{2.10}$$

$$\sigma^{\mu\nu} \equiv \nabla_\perp^\mu u^\nu + \nabla_\perp^\nu u^\mu - \frac{2}{3}\Delta^{\mu\nu}\Delta^{\xi\varrho}\nabla_\xi u_\varrho \tag{2.11}$$

$$= 2\nabla^{\langle\mu} u^{\nu\rangle} \,. \tag{2.12}$$

where $\Delta^{\mu\nu}$ in Eq. (2.5) is a projector along the transverse direction, and $A^{\langle\mu}B^{\nu\rangle}$ in Eq. (2.10) is a traceless product.

If gradients of the hydrodynamic fields are *not* allowed, symmetry dictates a unique form of the energy–momentum tensor for ideal hydrodynamics, i.e.,

$$T^{\mu\nu}_{\rm id} = \epsilon u^\mu u^\nu - p\Delta^{\mu\nu}. \tag{2.13}$$

By requiring the conservation of the energy–momentum tensor

$$\nabla_\mu T^{\mu\nu} = 0\,, \tag{2.14}$$

and projecting it along the longitudinal (u^μ) and transverse direction ($\Delta^{\mu\nu}$) of the fluid flow, one obtains the relevant equations for ideal hydrodynamics [6]

$$0 = D\epsilon + (\epsilon + p)\nabla_\mu u^\mu\,, \tag{2.15}$$
$$0 = (\epsilon + p)Du^\alpha - \nabla^\alpha_\perp\,. \tag{2.16}$$

The ideal equations are also referred to as Euler equations. However, those equations are only valid in the absence of friction or viscous effects. When including viscous effects by allowing gradient terms in $T^{\mu\nu}$, one arrives at the following equations [6]

$$T^{\mu\nu} = \epsilon u^\mu u^\nu - p\Delta^{\mu\nu} + \Pi^{\mu\nu}\,, \tag{2.17}$$
$$0 = D\epsilon + (\epsilon + p)\nabla_\xi u^\xi - \Pi^{\xi\varrho}\nabla_{(\xi}u_{\varrho)}\,, \tag{2.18}$$
$$0 = (\epsilon + p)Du^\mu - \nabla^\mu_\perp p + \Delta^\mu{}_\xi\nabla_\varrho\Pi^{\xi\varrho}\,, \tag{2.19}$$

where the tensor $\Pi^{\mu\nu}$ contains all the viscous contributions to hydrodynamics.
The tensor (2.17) is normally expanded up to second order in gradients of the fields[7] while an expansion up to first order would constitute the relativistic Navier–Stokes equations. For brevity, only the few, most relevant terms of the tensor $\Pi^{\mu\nu}$ will be listed[8] since these remain in the focus throughout this thesis[9]:

$$\Pi^{\mu\nu} = \eta\sigma^{\mu\nu} + \Delta^{\mu\nu}\zeta\nabla_\xi u^\xi \tag{2.20}$$
$$-\tau_\pi\eta\left[\mathrm{D}\sigma^{\mu\nu} + \frac{1}{3}\sigma^{\mu\nu}\nabla_\xi u^\xi\right] - \Delta^{\mu\nu}\zeta\tau_\Pi D\nabla_\xi u^\xi + \mathcal{O}(\partial^2 u)\,, \tag{2.21}$$

where $\sigma^{\mu\nu}$ is the gradient term (2.11).
If the order of expansion is fixed, i.e., higher-order terms will be dropped, one can split

[7] This is referred to as the *gradient approach*.
[8] Refs. [6, 33] list the complete set of terms.
[9] The other terms are still implemented and used in the calculations; see Refs. [6, 18, 33].

the viscous tensor into shear $\pi^{\mu\nu}$ and bulk contributions Π [34], that is,

$$\Pi^{\mu\nu} = \pi^{\mu\nu} + \Delta^{\mu\nu}\Pi\,, \tag{2.22}$$

$$\pi^{\mu\nu} = \eta\sigma^{\mu\nu} - \eta\tau_\pi\left[\mathrm{D}\sigma^{\mu\nu} + \frac{1}{3}\sigma^{\mu\nu}\nabla_\xi u^\xi\right] + \mathcal{O}(\partial^2 u)\,, \tag{2.23}$$

$$\Pi = \zeta\nabla_\xi u^\xi - \zeta\tau_\Pi \mathrm{D}\nabla_\xi u^\xi + \mathcal{O}(\partial^2 u)\,, \tag{2.24}$$

and write the equations of motion for the two viscous contributions as

$$\pi^{\mu\nu} = \eta\sigma^{\mu\nu} - \tau_\pi\left[\mathrm{D}\pi^{\mu\nu} + \frac{4}{3}\pi^{\mu\nu}\nabla_\xi u^\xi\right] + \mathcal{O}(\partial^2 u)\,, \tag{2.25}$$

$$\Pi = \zeta\nabla_\xi u^\xi - \tau_\Pi \mathrm{D}\Pi + \mathcal{O}(\partial^2 u)\,. \tag{2.26}$$

To recapitulate, the terms $\sigma^{\mu\nu} = \pi^{\mu\nu}/\eta - \mathcal{O}(\partial^2 u) = \sigma^{\langle\mu\nu\rangle}$ and $\nabla_\xi u^\xi = \Pi/\zeta - \mathcal{O}(\partial^2 u)$ were again plugged into Eqs. (2.23) and (2.24), the identity $\mathrm{D}\eta = -\eta\nabla_\xi u^\xi$ was used [33], and terms higher than second-order were dropped. The η-term is the shear viscosity contribution which is responsible for the internal friction of a fluid; the ζ-term is the bulk or volume viscosity contribution which is a measure for a fluid's resistance to changes in volume. Those first two terms stem from first-order gradients. While the shear viscosity is ubiquitous in viscous hydrodynamics, the bulk viscosity is not allowed in conformal fluids. It is intensely being debated how close the QGP is to a conformal system since underlying QCD is definitely not conformal. The last two terms in Eq. (2.21) are proportional to the respective relaxation times τ_π and τ_Π for the shear and bulk stresses; those second order transport coefficients preserve causality [6] if non-zero.
In order to close this system of equations, an equation of state (EoS), relating energy density and pressure, is required. The EoS must be derived from QCD. To summarize, a hydrodynamic calculation for the QGP needs the following ingredients:

- Fully specified transport coefficients entering the hydrodynamic equations (2.18) and (2.19). For the shear viscosity, AdS/CFT calculations suggest a value of $\eta/s = 1/(4\pi)$ [35] while weak-coupling pQCD suggests much larger values [36, 37].
  The bulk viscosity is assumed to be small for high-temperatures [38, 39]. For temperatures close to the cross-over temperature, the situation is less clear [40]; thus, other approaches have been developed to constrain the bulk viscosity [1, 39, 41, 42]. Nowadays, bulk viscosity is considered important in simulations, and temperature-dependent values range from $\zeta/s \approx 0.01$–0.5 (e.g., Ref. [2, 41]) .

- Complete set of initial conditions for hydrodynamic fields: scalar energy density field ϵ and a 4-vector fluid velocity field u^μ. Such initial energy densities are

described in Sec. 2.1 while AdS/CFT suggests at least a radial flow profile for central collisions in Eq. (5.1).

- An EoS to close the system of equations. This EoS stems from lattice QCD results [43, 44]. As discussed in Ch. 4, the choice of EoS can influence transport parameters extracted from experiment.

With this knowledge, one can now attempt solving Eq. (2.17), (2.18), and (2.19) for given initial conditions. The structure of those equations require a numerical approach for basically all physical systems. A few highly symmetric or simplified cases possess symmetric flow profiles which in turn can be solved analytically, e.g., the so-called Bjorken and Gubser flows [45, 46].
As hydrodynamics can be understood as a gradient expansion [6], the relevance of higher order gradients should be addressed. Naïvely, one would presume that higher-order gradients, i.e., beyond second order, would deliver more accurate results. Indeed, higher-order expansions can be performed up to arbitrary order with an abundance of terms. In order to warrant truncating the expansion at an order — for instance second order —, convergent behavior must be present for the series. In fact, the series does not converge rapidly; on the contrary, it is divergent [47, 48]. However, Ref. [48] showed that hydrodynamic gradient expansions converge to an attractor solution when Borel-resummed for Bjorken flow. Since attractors for partial differential equations are strongly dependent on the exact, mathematical structure of the equations and the initial conditions, this needs to be tested for systems in more general. In the cased tested in Ref. [48], Bjorken flow showed indeed the convergent behavior when the Borel resummation was performed.

2.3. Hadronic phase, freeze-out, and free streaming

The cross-over from QGP to confined hadrons can be characterized by a switching temperature T_{sw} when the hydrodynamic description changes to kinetic theory. This condition constitutes an isothermal hypersurface and the hydrodynamic energy–momentum tensor at the boundary of the QGP is converted into a particle energy–momentum tensor if that fluid cell fulfills the temperature condition

$$T < T_{\mathrm{sw}}\,. \tag{2.27}$$

The procedure of translating the hydrodynamic fields to particles is referred to as Cooper–Frye prescription [49]. At this point in time, the cooled-down region of QGP transforms into particles (e.g., π, p) that might subsequently interact and decay into other particles which ultimately free-stream into the detector. The point of last interaction is referred

to as *freeze-out*. Since the initial energy density profile and its potential anisotropies are translated via hydrodynamics and the hadronic cascades into the final-state particles, the distribution of detected particles should have information about the initial state's anisotropy. The total number of detected particles is called *multiplicity*. As discussed in Sec. 2.1, each event displays one configuration of the initial energy distribution. Therefore, the final states of several events are averaged over many events. It is the primary experimental observable for ion collisions. Therefore, every theoretical description of the QGP and the other phases must correctly predict the total number of produced particles. In addition to overall multiplicity, the particles can be resolved with respect to their angles and transverse momenta. While the overall multiplicity is primarily governed by the total amount of deposited energy in a collision, the momentum and angular spectra are much more sensitive to the geometry and the kinetics of the QGP; thus, those spectra provide a very good test of the employed models. For instance, the transverse and angular distribution of the particles strongly correlates with the geometrical set-up of the collision: smooth Glauber initial conditions have — from a theoretical perspective — a well defined impact parameter $\vec{B}$ and thus reaction plane[10], whereas the impact parameter in real collisions is experimentally inaccessible. Moreover, the definition of the reaction plane becomes even theoretically difficult when considering Monte Carlo Glauber initial conditions. Given the particle spectra, it is customary to Fourier-expand them in the azimuthal angle φ, i.e. for a particular event k with a multiplicity N_k, one has

$$\frac{\mathrm{d}N_k}{p_\perp \mathrm{d}p_\perp \mathrm{d}\varphi \mathrm{d}y} = \frac{1}{2\pi}\frac{\mathrm{d}N_k}{p_\perp \mathrm{d}p_\perp \mathrm{d}y}\left[1 + 2\sum_{n=1}^{\infty} v_n^{(k)}(p_\perp, y)\cos\left[n\left(\varphi - \Psi_n^{(k)}(p_\perp, y)\right)\right]\right], \tag{2.28}$$

where y is the rapidity[11], and the Fourier coefficients v_n are called *flow coefficients*; furthermore, $\Psi_n^{(k)}$ are the flow angles. Hence, the average flow coefficients v_n can be calculated via [50]

$$v_n(p_\perp, y) = \frac{1}{N_{\mathrm{evts}}}\sum_{k=1}^{N_{\mathrm{evts}}}\left|v_n^{(k)}(p_\perp, y)\right| \tag{2.29}$$

$$= \frac{1}{N_{\mathrm{evts}}}\sum_{k=1}^{N_{\mathrm{evts}}}\left|\frac{1}{N_{\mathrm{k}}}\sum_{j=1}^{N_k}\exp\left[in\varphi_j^{(k)}(p_\perp, y)\right]\frac{\mathrm{d}N_k}{p_\perp \mathrm{d}p_\perp \mathrm{d}\varphi \mathrm{d}y}\right|, \tag{2.30}$$

[10] The impact parameter $\vec{B}$ and the beam line z span the reaction plane.
[11] Mid-rapidity is tantamount to $y \approx 0$.

where the term $|\ldots|$ denotes the absolute value of the average of a single event k with N_k particles produced while the out-most sum denotes the average over all events N_{evts} belonging to a particular centrality class, particle species, and momentum bin. Evidently, Eq. (2.30) is independent of the flow angles $\Psi_n^{(k)}$ [50].
The directed flow v_1 is mostly caused by the spectator nucleons, i.e., not part of the overlap region[12]. The elliptic flow coefficient v_2 is an important measure for the ellipticity of the system (e.g., the initial energy distribution in Fig. 2.6 would lead to a measurable v_2), and it is often considered an indicator for a hydrodynamic origin[13].

Besides the flow coefficients, other correlations can be calculated as well. For instance, Hanbury–Brown–Twiss (HBT) radii are another set of interesting observables because those radii might provide some insight about the spatial and temporal structure of the QGP [52] in contrast to the bulk observable multiplicity. Due to the fact, that "the QGP may feature inhomogenous temperature profiles and strong collective dynamics" [52], the radii measure just "space–time regions of homogeneity" [53, 54] with small variations of the momentum distributions to allow for those quantum correlations to occur [52]. HBT radii are defined via the two-particle correlation function

$$C(\vec{p}_1, \vec{p}_2) \equiv \frac{\langle N \rangle^2}{\langle N(N-1) \rangle} \frac{P_2(\vec{p}_1, \vec{p}_2)}{P_1(\vec{p}_1) P_1(\vec{p}_2)}\,, \tag{2.31}$$

where P_i are i-particle spectra and $\langle \ldots \rangle$ are normalizations by the average number of particles $\langle N \rangle$ and particle pairs $\langle N(N-1) \rangle$. For a Gaussian emission source and under the assumptions outlined in Ref. [55], this expression can be approximated as [52, 56, 57, 58, 59, 60]

$$C(\vec{K}, \vec{q}) = 1 + \exp\left(- \sum_{i,j=s,o,l} R_{ij}^2(\vec{K}) q_i q_j \right)\,, \tag{2.32}$$

where the momenta were re-expressed via

$$\vec{K} \equiv \frac{\vec{p}_1 + \vec{p}_2}{2}\,, \tag{2.33}$$

$$\vec{q} \equiv \vec{p}_1 - \vec{p}_2\,. \tag{2.34}$$

In the form (2.32), the diagonal tensor components R_{ii} are the so-called HBT radii with

[12] In granular models, this overlap region is no longer sharply defined by the geometry and event-by-event simulations are required to realize various nucleon distributions.
[13] However, it is indeed possible to have flow-like results by other means as well [51].

the geometry shown in Fig. 2.7, following the Bertsch–Pratt coordinate system [61]

- $R_{\mathrm{o(utward)}}$: extension parallel to the averaged transverse momenta of the particle pair;
- $R_{\mathrm{s(ideward)}}$: extension orthogonal to the *outward* and the *longitudinal* direction;
- $R_{\mathrm{l(ongitudinal)}}$: extension in the reaction plane[14].

Furthermore, the orientation of this coordinate system might not coincide with the principal axes of the emission source in the case of off-central collisions, as the region of homogeneity might be tilted with respect to the beam line [55]. Given this definition of the longitudinal direction within the reaction plane, the second-order event plane would seem a reasonable choice to compare to experimental data.

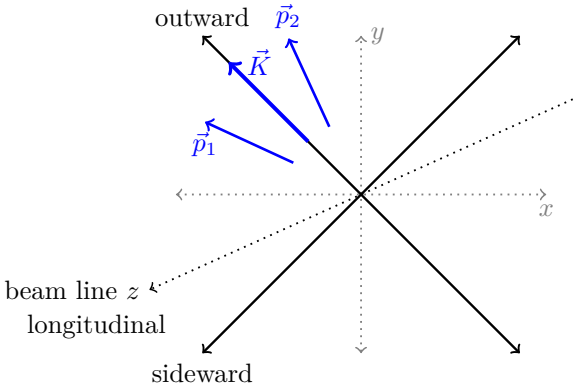

Figure 2.7.: Coordinate system for HBT radii. The *outward* and *sideward* directions are in the transverse plane. This "HBT" coordinate system can be thought of as a boost along the beamline and a rotation about the beam axis for the geometry with impact parameter along the x-axis in central, mid-rapidity collisions, as shown in Fig. 2.2.

[14] In central, mid-rapidity collisions, R_{l} is along the beam line [55].

3. SONIC framework

After establishing the concepts of heavy-ion collisions and the underlying ideas in the previous chapter, the main focus of this chapter will be the description of the used software for the individual stages. In this work, the pre-equilibrium phase is not fully dynamic, but its final state will be used to initialize the hydrodynamic phase. The software package SONIC consists, therefore, of two parts:

- UVH2+1: 2+1-dimensional, hydrodynamic partial-differential-equation solver for relativistic fluids including Glauber initial condition generator. Note that the three-dimensional system is reduced to a two-dimensional system using boost-invariance. The details of UVH2+1 are stated in Ref. [62];
- B3D: Monte Carlo event generator for the scattering dynamics including routines for correlations of emerging particles, notably the flow coefficients v_n, as well as the multiplicities. The exact details are stated in Ref. [63]

SONIC implements the following steps which are based on the hydrodynamic model of heavy-ion collision. First, initial energy density profiles are generated[1] via the Glauber model. Initial fluid velocities, including results from AdS/CFT black hole collisions are implemented as optional pre-equilibrium evolution. Each initial condition undergoes the hydrodynamic evolution via UVH2+1 till every fluid cell of the QGP drops below the switching temperature T_{sw}. Afterwards, the isothermal hypersurface defined via T_{sw} is passed to B3D which then generates multiple events per hypersurface, i.e., oversampling. Each event results in an ensemble of particles based on the energies and momenta of the fluid cells and particle production statistics. Those particles subsequently interact and decay. After all interactions have ceased, particle information is recorded and also analyzed, as well as averaged over the B3D events. The outputs from B3D can be compared to experimental data. The entire procedure is schematically shown in Fig. 3.1 with the multiple parallel branches indicating mathematically identical calculations of different initial seeds, so-called *events*.
For the papers leading to this thesis, the following new routines have been implemented into, or used in conjunction, with SONIC:

[1] N.b., one can use other initial conditions as well, but they are at the moment not part of SONIC.

- Calculation of the critical bulk viscosity for a fluid during runtime;
- Monte Carlo initial condition generator for two different proton models [64, 65];
- Thermal photon rates;
- Thermal lepton rates [66];
- Deployment routines for easier access to SONIC;
- Multi-event processing scripts to create sufficient statistics (rewritten and scripts added).

The entire SONIC package is publicly available under [67] and runs parallelized on modern machines or high-performance clusters.
Besides the presented SONIC package, other commonly used hydrodynamic simulations are VISHNU and MUSIC. VISHNU is akin to SONIC in that it also is a 2+1D simulation suite with integrated event-by-event initial condition generator and is publicly available under Ref. [68]. The hydrodynamic solver employs a regularization of the viscous stress tensor to "suppress numerical instabilities caused by large spatial gradients" [69]. After the hydrodynamic evolution ceases, the hadronic cascade is performed via the well known UrQMD package [70, 71]. The entire event-by-event version of VISHNU is described in Ref. [69].
MUSIC is a three-dimensional hydrodynamic code using the Kurganov–Tadmor method for solving the hydrodynamic equations; a numerical viscosity is artificially introduced to stabilize the system [72, 73, 74, 75]. The hadronic cascade is also performed via UrQMD in the newer versions [70, 71, 74, 76]. Mechanisms to stabilize hydrodynamic equations are standard practice in the field of fluid dynamics, and the terms must be sufficiently small to keep the discretized system similar to the physical one.
All three suites, that is, SONIC, MUSIC and VISHNU, enhance stability by introducing an artificial dampening. The hadronic cascades for MUSIC and VISHNU use UrQMD while SONIC uses B3D [63]. However, MUSIC stands out as the only three-dimensional code among those. The 3D description is more realistic as the real collision also occurs in three spatial dimensions. With those advantages, new physics can be explored, notably forward/backward-rapidity physics, i.e., $|\eta| > 0$, whereas VISHNU and SONIC are — strictly speaking —restricted to mid-rapidity descriptions of the system. However, for the mid-rapidity region in $A + A$ collisions, the differences between 2+1D and 3+1D are minute [17]

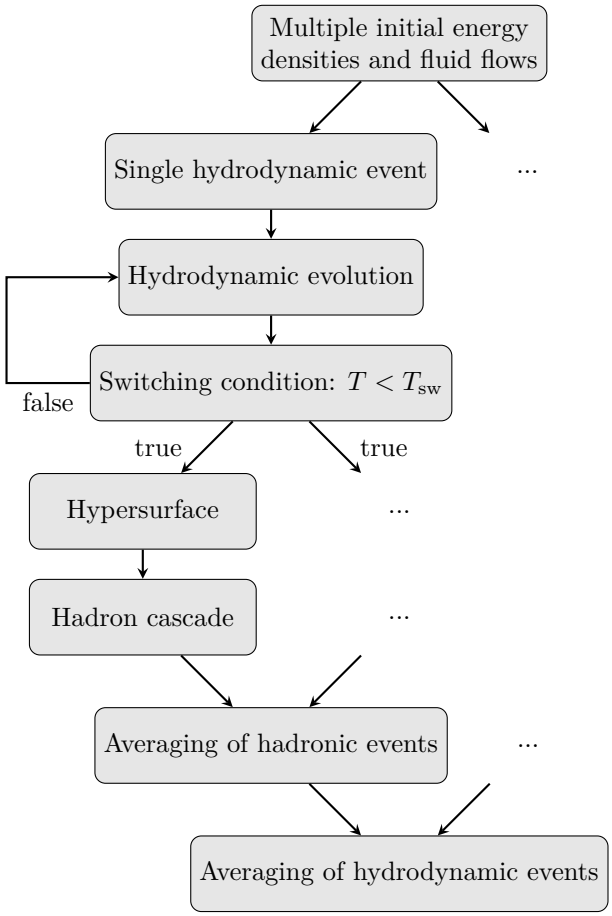

Figure 3.1.: Execution steps of SONIC event-by-event simulations. The dots symbolize parallel, execution steps which have different initial conditions. The details depend on the simulated collisional system. Note that the step *switching condition* means that the entire hypersurface is recorded and then single decay event are seeded in the next step for a given hypersurface, i.e., the physical description switches from hydrodynamics to kinetic theory.

4. Relevance of the bulk viscosity

Having provided the conceptional, mathematical, and computational framework in the previous chapters, it is now possible to focus on the physical aspects of heavy-ion collisions. Despite of possessing a solid mathematical framework for hydrodynamics, the values of transport coefficients are still actively discussed. In case of the shear viscosity, AdS/CFT duality provided a value of $\eta/s = 1/(4\pi)$ [35]. Much less is known about the bulk viscosity coefficient ζ/s. Prior to discussing specific values for ζ/s, the following question is worth considering: what values of the bulk viscosity are considered large?
The latter question inspired imposing an upper bound on ζ/s via the following prescription [1]: high fluid velocities reduce the pressure of a medium and can induce phase transitions [77]; requiring the fluid's pressure to remain above the vapour pressure p_v allows for calculating an upper bound on the bulk viscosity. The results on the upper limit of the bulk viscosity were published in the peer-reviewed journal *Journal of High Energy Physics*; the corresponding publication can be found in App. A.1, Ref. [1]. The effective pressure is defined from the energy–momentum tensor in Eq. (2.17) via the projection

$$p_\mathrm{eff} \equiv -\frac{1}{3}\Delta_{\mu\nu}T^{\mu\nu} = p - \Pi \approx p - \zeta\nabla_\mu u^\mu \,, \tag{4.1}$$

where the first-order constitutive relation $\Pi = \zeta\nabla_\mu u^\mu$ (cf. Sec. 2.2, especially Eqs. (2.24) and (2.26)) was used to expand the bulk viscous tensor Π. When, for a given flow profile u^μ and value of ζ/s, the effective pressure is reduced to the vapour pressure $p_\mathrm{eff}\,(\zeta/s) = p_\mathrm{v}$, the fluid has reached the maximum critical value for the bulk viscosity, thus becoming mechanically unstable [1]. Solving Eq. (4.1) for the bulk viscosity leads to

$$\left.\frac{\zeta}{s}\right|_\mathrm{crit} \equiv \frac{(p_\mathrm{v} - p)\,T}{(\epsilon + p)}\left(\nabla_\mu u^\mu\right)^{-1} \,, \tag{4.2}$$

where, again, the gradients enter only up to first order originating from Eq. (2.24).
Based on this method, there are two distinguishable cases:

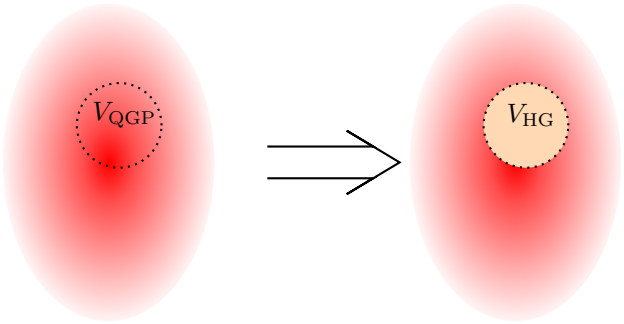

Figure 4.1.: Sketch of cavitation and bubble formation inside the QGP. A region of QGP with V_{QGP} undergoes a phase transition to a hadron gas occupying the volume V_{HG}.

- Stable region:

$$\frac{\zeta}{s} < \left.\frac{\zeta}{s}\right|_{\mathrm{crit}} \quad \Rightarrow \quad p > p_{\mathrm{v}} \tag{4.3}$$

  The fluid remains in its fluid phase and is safe from bubble formation.

- Unstable region:

$$\frac{\zeta}{s} \geqq \left.\frac{\zeta}{s}\right|_{\mathrm{crit}} \quad \Rightarrow \quad p \leqq p_{\mathrm{v}} \tag{4.4}$$

  The approximation (4.2) indicates a mechanical instability, i.e., *cavitation* which would lead to the formation of a hadron gas bubble. If this happens inside the QGP at high temperatures $T \gg T_{\mathrm{sw}}$, one would require a two-component description with interaction terms between the two phases which is currently not available. In Fig. 4.1, the hypothetical scenario is depicted where a region of QGP undergoes a phase transition to a hadron gas. In the absence of a full two-component description, cavitation would affect observables if hadronization occurs at $T \gg T_{\mathrm{sw}}$. Furthermore, statistical model fits of experimental data do not indicate that hadronization occurs at $T \gg T_{\mathrm{sw}}$; thus, it is unlikely that cavitation takes place either. Therefore, this entire argument establishes an upper bound on $\zeta/s < \zeta/s|_{\mathrm{crit}}$.

The results of this calculation on the upper bound of the bulk viscosity ζ/s are shown in Fig. 4.2 for $Au + Au$ collisions for various flow profiles. For convenience, the values

of the critical bulk viscosity are also tabulated in Tab. 4.1. The critical bulk viscosity, i.e., smallest value, is normally acquired at very early times because the medium has the largest gradients at this point in time. The early-time dominance becomes evident from the structure of eq. (4.2) with the gradients being in the denominator.

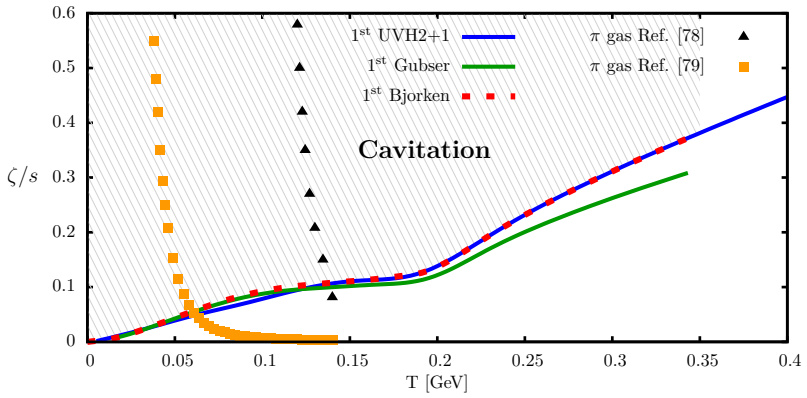

Figure 4.2.: The upper bound of the bulk viscosity ζ/s for various flow profiles in $Au+Au$ collisions shown alongside pion hadron gases for comparison. The values for `SONIC` are shown in Tab. 4.1. Figure from Ref. [1].

In Fig. 4.3, various parametrizations of ζ/s are shown, stemming from perturbative QCD [38, 80] and strong-coupling calculations for gauge theory plasmas [81, 82], respectively, i.e.,

$$\frac{\zeta}{s}(T) = \frac{15}{4\pi}\left(\frac{1}{3} - c_s^2(T)\right)^2 \quad \text{(pQCD)}\,, \tag{4.5}$$

$$\frac{\zeta}{s}(T) = \frac{1}{2\pi}\left(\frac{1}{3} - c_s^2(T)\right) \quad \text{(Buchel)}\,. \tag{4.6}$$

as well as a matching procedure from Ref. [83] for ζ/s (Denicol et al.) combining lQCD ($T > T_{\rm sw}$) [39] and hadron resonance gas calculations ($T < T_{\rm sw}$) [84]. For evaluating c_s^2 in Eqs. (4.5) and (4.6), the EoS[1] from Ref. [43] has been used[2].
Considerations on upper limits for ζ/s are important for heavy-ion collision phenomenology because inter alia flow coefficients or total multiplicity are influenced by the bulk viscosity [83]. The effect of the bulk viscosity becomes quite important in $p+p$ collisions due to the small size of the system and the associated large velocity gradients (see Ch. 6).

[1] Ref. [82] uses the EoS S95n-v1 [44] and for a form of ζ/s similar to Eq. (4.6), the EoS S95n-v1 results are fairly similar [44] to Ref. [43].
[2] N.b., for all parametrizations in Eqs. (4.5), (4.6), an ideal EoS would yield $\zeta/s = 0$ because $c_s^2 = 1/3$.

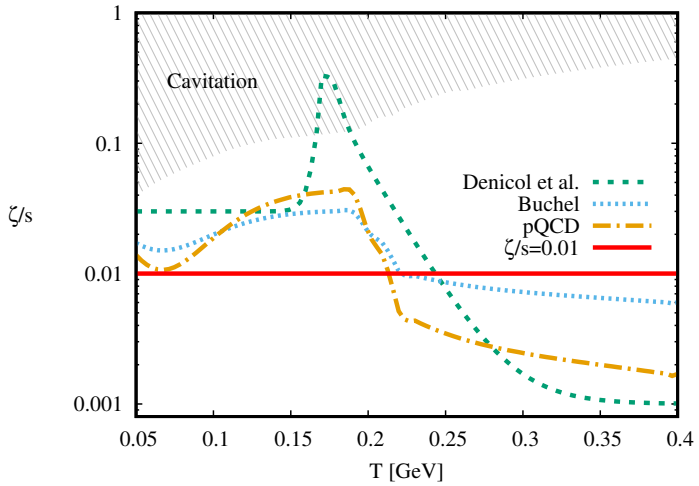

Figure 4.3.: Various parametrizations of the bulk viscosity over entropy density ratios. The shown bulk viscosities stem from *pQCD*, (cf. Eq. (4.5), Ref. [38, 80]), *Buchel* (cf. Eq. (4.6), Ref. [81]), as well as *Denicol et al.* (see text, cf. Ref. [39, 83, 84]), as well as $\zeta/s = 0.01$ (`SONIC`, cf. [2, 3, 85]). For comparison, the critical bulk viscosity over entropy density $\zeta/s|_{\text{crit}}$ is plotted as the shaded region, marking cavitation. For $\zeta/s < \zeta/s|_{\text{crit}}$, the fluid should not show signs of an instability.

T [GeV] $< T_{\mathrm{sw}}$	$\left.\frac{\zeta}{s}\right\|_{\mathrm{crit}}$
0.00469642	0.00169694
0.013057	0.00497383
0.022206	0.0125483
0.0296516	0.021164
0.0379349	0.02849
0.0462618	0.0359127
0.0545628	0.043125
0.0629548	0.0499432
0.0712237	0.0561936
0.079572	0.0625752
0.0878945	0.0693277
0.0962501	0.075808
0.10453	0.0837463
0.112806	0.0907254
0.121131	0.0965039
0.129377	0.101845
0.139845	0.107867
0.146004	0.10947
0.158309	0.112649
0.164542	0.114632

T [GeV] $> T_{\mathrm{sw}}$	$\left.\frac{\zeta}{s}\right\|_{\mathrm{crit}}$
0.176971	0.119278
0.183064	0.121507
0.189231	0.124561
0.195933	0.131252
0.212277	0.160206
0.212771	0.159683
0.221	0.179543
0.229499	0.197662
0.237644	0.216092
0.245966	0.233866
0.254476	0.251218
0.262512	0.252912
0.271587	0.267672
0.280239	0.281296
0.288455	0.293878
0.296251	0.305592
0.31051	0.326412
0.31701	0.335655
0.323119	0.344239
0.328859	0.352221
0.33932	0.366585
0.348569	0.379116
0.356772	0.390116
0.364074	0.399832
0.370601	0.40846
0.379159	0.419708
0.388683	0.432149
0.396475	0.442282
0.404248	0.452333
0.412173	0.462567

Table 4.1.: Approximate values of the critical bulk viscosity $\zeta/s|_{\mathrm{crit}}$ for central $Au + Au$ collision, obtained from hydrodynamic calculations with first-order gradients. The left table shows values of ζ/s below T_{sw}, whereas the right table shows values above T_{sw}.

5. Results for large collisional systems

Having set up the stage for large and small collisional systems, one can now use SONIC to simulate these systems. The results on these collision systems were published in the peer-reviewed journal *The European Physical Journal C*; the corresponding publication can be found in App. A.2, Ref. [2]. In the case of large collisional systems where the initial conditions can be simulated via Monte Carlo Glauber generators[1], the agreement between theoretical simulations and experimental data is striking. As can be seen in Fig. 5.1 for the multiplicities and mean pion transverse momenta, the majority of results lies within 5% of the experimental result and on average within 7% for Tab. II in Ref. [2]. All of the SONIC simulations, shown in Fig. 5.1, were initialized with the same transport coefficients $\eta/s = 0.08$ and $\zeta/s = 0.01$ (cf. Fig. 4.3), switching temperature $T_{\mathrm{sw}} = 170$ MeV from hydrodynamic to cascade description, same EoS, as well as an initial radial pre-equilibrium flow profile

$$v^r(\tau, r) = -\frac{\tau}{3.0}\partial_r \ln T_A^2(r)\,, \tag{5.1}$$

calculated in Ref. [18] with T_A from Eq. (2.3). The successful description of experimental data over a wide range of collision systems increases the confidence that the hydrodynamic paradigm does indeed capture the important physics of these collisions. Besides those benchmark observables, HBT radii can also be used as a more refined observable to establish confidence in a model (cf. Sec. 2.3). HBT radii are an interferometry technique from astronomy to classify star sizes that behave akin to a Gaussian emission source [52, 55, 56, 60, 86, 87]. In the past, the discrepancy between experimentally measured HBT data and ideal hydrodynamic simulations was named "the HBT puzzle". Specifically, it was possible to tune simulation parameters to match some observables, such as particle spectra, but not particle spectra, collective flows, and HBT radii simultaneously [55]. The geometry of HBT radii is explained in Sec. 2.3 and in Fig. 2.7. Over the years, there have been advances in hydrodynamic simulations by including pre-equilbrium flow, viscosity, and hadron cascade [86], all of which are part of modern simulation suites such as SONIC. By using the built-in routines of SONIC, simulations now agree with experimental data for those radii fairly well as shown in Fig. 5.2. However, when turning the

[1] The implementation employed can be found in Ref. [23].

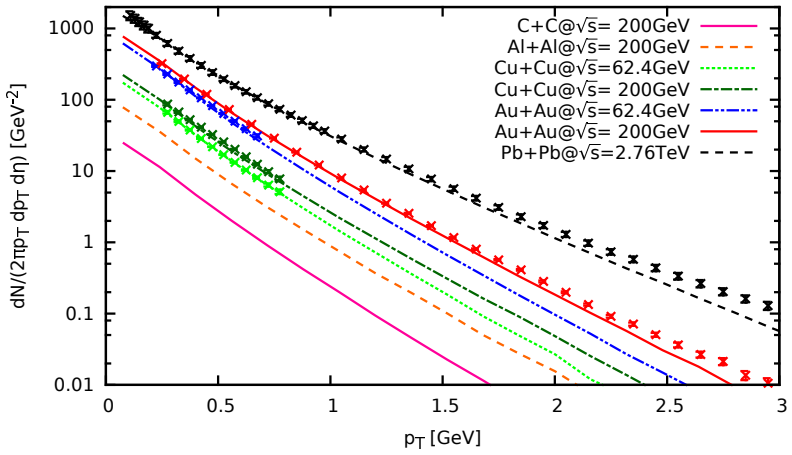

Figure 5.1.: Pion spectrum for various collisional systems all simulated via SONIC. Figure from Ref. [2].

attention to $p + p$, numerical problems emerged [2]. Since other initial conditions have become available for $p + p$ systems (see Ch. 6), future work might be able to accurately describe those.

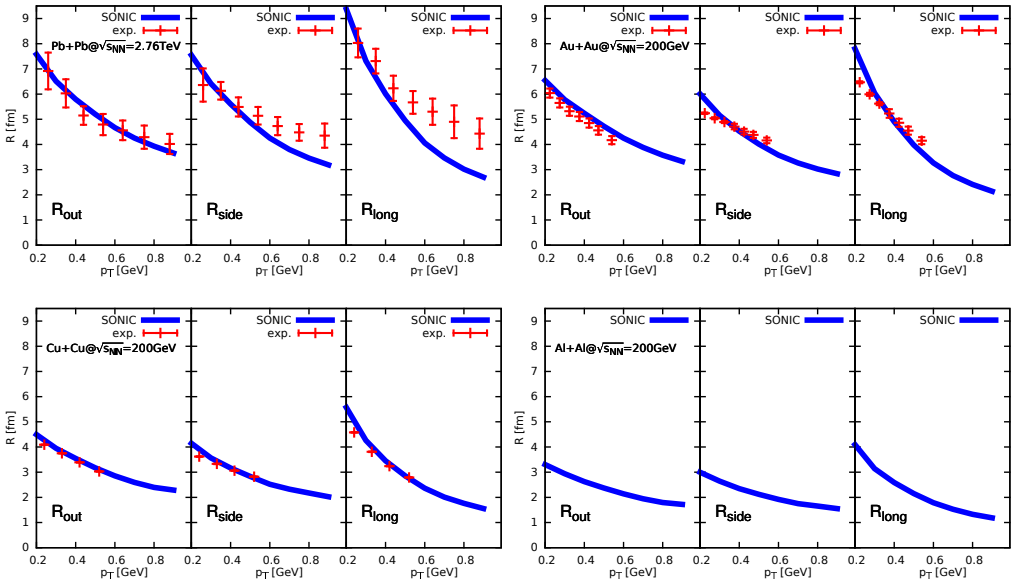

Figure 5.2.: Pion HBT radii for the different collision systems compared to experimental data from Ref. [88, 89, 90, 91]. The simulated data agrees well with experimental data where available. Figure from Ref. [2].

6. Initial conditions for p+p

Having established the methodology of comparing simulation to experiment, it is worth considering $p + p$ systems. The results on $p + p$ collisions were published in the peer-reviewed journal *The European Physical Journal C*; the corresponding publication can be found in App. A.3, Ref. [3]. By abstaining from the a priori discussion whether these systems lead to the formation of the QGP in the first place, one can still check whether hydrodynamic simulations would lead to sensible results[1]. Indeed, experimental data from ALICE, ATLAS, or CMS show that there is a measurable elliptic flow present in $p + p$ collisions [92, 93, 94]; thus, it is interesting to test hydrodynamic models against these experimental data. In order to test models against data, one requires proper initial conditions. Motivated by the fact that the Glauber model has the nucleon size as a scale for their granularity in heavy-ion collisions, the following proton model, presented in Ref. [95], was tested. Its transverse energy density is

$$T_{\mathrm{RND}}(\vec{x}_\perp) \quad = \quad \int \frac{\mathrm{d}^2 q}{(2\pi)^2} e^{-i\vec{q}\,\vec{x}_\perp} F_1(Q^2 = \vec{q}^{\,2}) = \int \frac{\mathrm{d}Q\, Q}{2\pi} J_0(Q x_\perp) F_1(Q^2)\,, \quad (6.1)$$

where F_1 is the Dirac from factor, and Q^2 is the squared transverse momentum transfer. This model assumes a direct proportionality between the charge and energy density. It will be labeled RND (from *RouND*) since it exclusively produces round protons. The difference in initial- and final-state wave functions of scattered protons during experiments motivates the infinite-momentum frame, effectively making the proton two-dimensional. In this frame, the momentum transfer via scattering occurs only in the transverse plane (with the infinite momentum being along the longitudinal direction), effectively projecting the proton's three-dimensional density onto the two-dimensional, transverse plane after Fourier-transforming in two dimensions [95, 96]. Combining those ideas yields Eq. (6.1) where the form factor F_1 is parametrized akin to Ref. [95].
Besides proton model (6.1), experimental results on the ratio of the electric and magnetic form factors $G_{\mathrm{E}}/G_{\mathrm{M}}$ show a fall-off for large Q^2 [97, 98]; this is tantamount to a constant Pauli to Dirac form factor ratio QF_2/F_1 [99, 100]. The constancy of the ratio QF_2/F_1

[1] Even if hydrodynamic models agree well with experimental data, it would not be a strict proof for the existence of the QGP in such small system; rather, it increases confidence in the entire hydrodynamic heavy-ion collision framework for a wide range of systems.

contradicts pQCD calculations which stipulate instead $Q^2F_2/F_1 = const.$ [99, 100, 101, 102, 103]. To resolve this conundrum, a relativistic constituent-quark model was proposed [104] which allows for a helicity flip[2] of a quark during scattering [105, 106]. All of these observations indicate an interplay of the constituents' angular momenta and spins with non-vanishing orbital angular momentum of the quarks [107]; in particular, this relativistic constituent-quark model is able to explain the constancy of QF_2/F_1 [100, 108] by allowing spins to contribute to the proton's shape. These facts lead to another proton model, calculated in Ref. [100], labeled "FLC" (from *FLuCtuating*). The FLC model shares some similarities with the Monte Carlo Glauber because it also generates fluctuating initial conditions; furthermore, the FLC model seems more realistic than the Glauber-like RND model which basically collides two "disks" (cf. Fig. 2.2. According to this model, a single proton has the transverse energy density

$$T_{\mathrm{FLC}}(\vec{x}_\perp) \quad = \quad \int_{-\infty}^{\infty} \mathrm{d}z \left[\frac{\varrho_U(r)\,(1+\hat{n}\cdot\hat{s})}{2N} + \frac{\varrho_L(r)\,[1+2\,(\hat{r}\cdot\hat{s})\,(\hat{r}\cdot\hat{n})-\hat{n}\cdot\hat{s})}{2N} \right] , \tag{6.2}$$

where $\vec{x}_\perp = (x, y)$ is the position vector in the transverse direction, that is after integrating out z, while $\hat{s}$ is the proton's spin, $\hat{n}$ is the direction of the quark's spin, and $\hat{r}$ is the vector from the proton's center of mass to the quark; the functions $\varrho_{L/U}$ are proton form factors which exist in tabulated form. This model conceptually depicts the proton as a two-body system in terms of its spins, stemming from a three-quark wave function [99, 100, 108, 109]. Given the model's success in explaining the constancy of the form factor ratios, testing it in relativistic ion collisions seems appropriate. When Monte Carlo sampling the vectors $\hat{n}$, $\hat{s}$, and $\hat{r}$ in Eq. (6.2), the majority of generated protons resemble spheres; however, in some cases, non-spherical shapes emerge that resemble tori or peanuts, with the latter having two distinct concentrations of energy.

The initial condition generators are publicly available from Ref. [64, 65]. Equipped with the energy densities of single protons, namely RND (6.1) and FLC (6.2), one can now generate initial conditions by Monte Carlo sampling the impact parameter and then obtain the deposited energy from

$$\epsilon(\vec{x}_T, \tau_0) = \kappa(\tau_0) T_1\left(x + \frac{b}{2}, y\right) T_2\left(x - \frac{b}{2}, y\right) , \tag{6.3}$$

where κ is an overall normalization constant determined by the experimentally measured multiplicity of the collision (cf. Eq. (2.2)). Both models (6.1) and (6.2) have been simulated using the previously described `SONIC` suite; see Fig. 6.1 and Ref. [3].

[2] Helicity is defined as the projection of spin onto the unit momentum vector.

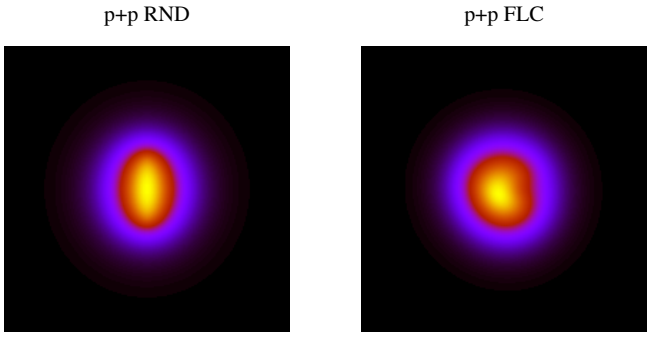

Figure 6.1.: Initial conditions for the RND and FLC model for non-central $p+p$ collisions in the transverse plane. The FLC model clearly exhibits fluctuating spin couplings from Eq. (6.2), whereas the RND model overlaps spherical shapes yielding a clearly elliptical shape. N.b., for the FLC model, non-spherical shapes are fairly rare.

The results are shown in Figs. 6.2 and 6.3. For $p + p$ collisions, the integrated elliptic flow was experimentally measured to be approximately flat[3] [111, 112] as a function of multiplicity while the simulation shows a clear multiplicity dependence in Fig. 6.2. A possible interpretation of those results is that the RND and FLC models possess insufficient fluctuations, particularly for describing central $p + p$ collisions.
In Ref. [85], a phenomenological, three-quark model (OSU model) for the proton was presented, i.e., there are three positions where energy is deposited controlled. When Monte Carlo sampled, this model is able to explain the second-, third-, and fourth-order flow coefficients, and can be tweaked to match the integrated elliptic flow for high- and medium-multiplicity events.

[3]Note that the published results are for $\sqrt{s} = 5.02\,, 13$ TeV; results for $\sqrt{s} = 7$ TeV are expected to lie somewhere in between.

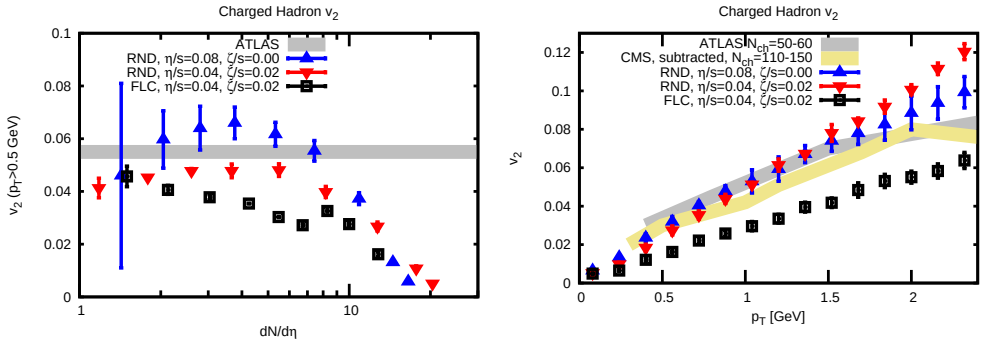

Figure 6.2.: Elliptic flow coefficients for $p + p$ collisions. Left: Integrated elliptic flow as a function of centrality. The high- and low-multiplicity data cannot be described well [92] by `SONIC` when initialized with the RND (6.1) and FLC model (6.2). Right: Non-integrated elliptic flow spectrum for 40–50% centrality class. The simulation can be tuned to agree with the experimental data [92, 110]. Figures from Ref. [3].

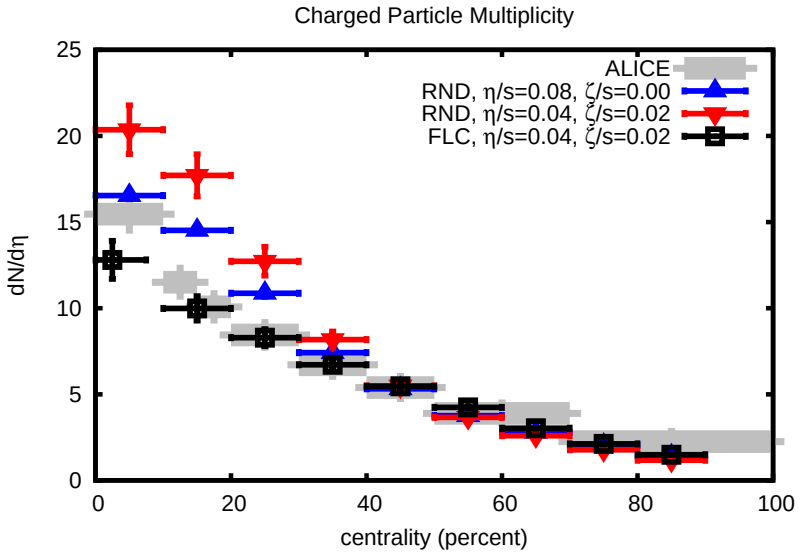

Figure 6.3.: Charged hadron multiplicity for $p+p$ collisions. The 40–50% centrality class was used as input to calibrate the simulation. While the high-multiplicity events are accurately modeled via both models, the peripheral collisions are better described by the FLC model. Figure from Ref. [2].

7. Conclusion

The field of heavy-ion collisions has now been extended to also include light ions, as seen in $p + p$ collisions. The hydrodynamic paradigm describes many of the QGP's aspects very well as shown in Ch. 5 where a wide range of collisional systems can be described by the same physical model without tweaking transport coefficients. Confirming the benchmark observations of particle spectra and collective flow (cf. with Fig. 5.1), the same approach is quite successful in describing formerly elusive Hanburry–Brown–Twiss radii as shown in Fig. 5.2, implying an increased understanding of those large systems. In contrast to those systems, the collision of $p + p$ requires indeed new techniques, i.e., a better understanding of the initial conditions, most likely including a quark substructure, whereas large systems are accurately described within the Glauber nucleon approach. With respect to small systems, the overall bulk quantities, such as multiplicity, are modeled well in Fig. 6.3. However, when using the RND (6.1) and FLC (6.2) model, the integrated elliptic flow coefficient v_2 compares poorly to experimental data for $p + p$ (see Fig. 6.2). An additional complication arises from the fact that flow coefficients are no longer unambiguously defined. Using different procedure, ATLAS measured a multiplicity-independent integrated elliptic flow coefficient [92], whereas CMS found an increasing elliptic flow coefficient for these events [93].
Proton models, including the substructure *OSU* model (cf. Ref. [85]), describe the CMS data, but disagree with the "flat" ATLAS data [113, 114] at low multiplicity. Since the fluctuating models with proton substructure exhibit the most promising results, changing the sampling procedure to generate less round protons could be an interesting alley to pursue for the FLC model (6.2).
Sensitivity of model results to the bulk and shear viscosity (shown in Fig. 6.2) suggest the possibility of constraining bulk viscosity and eventually also shear viscosity values. The upper limit of the bulk viscosity based on the cavitation criterion in Ch. 4 can be considered an estimate. Recent hydrodynamic approaches to constrain transport coefficients include massively parallel computations of the parameter space. Those results can then give best-fit approaches of parameter combinations to existing data (e.g., see Ref. [115, 116]).

Giving an outlook, extensions to measure forward physics [117] will require full 3+1D simulations on the theoretical side (e.g., MUSIC from Ref. [72, 73], publicly available

since summer 2017). Access to such 3+1D frameworks would facilitate the implementation of new observables for which theoretical three-dimensional calculations exist.
In this author's opinion, the theoretical side arguably lacks simulation capabilities despite the available computational power with respect to modular codes that allow for easy modification and implementation of new routines, as well as dissemination.
To conclude, the field of ion collisions has seen an increase in scope with the inclusion of $p + p$ or other small-size systems while the physical understanding of large-size systems has become more precise. The initial conditions for hydrodynamic simulations pose one of the primary challenges, for which the answer need to come from outside the hydrodynamic framework. Lastly, going to higher energies (e.g., the Future Circular Collider [118]) or smaller systems (e.g., $e^+ + e^-$) will show how well current theories can make predictions for these new regimes which either confirm or shatter our current understanding.

Bibliography

[1] Mathis Habich and Paul Romatschke. "Onset of cavitation in the quark-gluon plasma". In: *JHEP* 12 (2014), p. 054. DOI: 10.1007/JHEP12(2014)054. arXiv: 1405.1978 [hep-ph].

[2] M. Habich, J.L. Nagle, and P. Romatschke. "Particle spectra and HBT radii for simulated central nuclear collisions of C + C, Al + Al, Cu + Cu, Au + Au, and Pb + Pb from $\sqrt{s} = 62.4$ - 2760 GeV". In: *Eur.Phys.J.* C75.1 (2015), p. 15. DOI: 10.1140/epjc/s10052-014-3206-7. arXiv: 1409.0040 [nucl-th].

[3] M. Habich et al. "Testing hydrodynamic descriptions of p+p collisions at $\sqrt{s} = 7$ TeV". In: *Eur. Phys. J.* C76.7 (2016), p. 408. DOI: 10.1140/epjc/s10052-016-4237-z. arXiv: 1512.05354 [nucl-th].

[4] Edmond Iancu. "QCD in heavy ion collisions". In: *Proceedings, 2011 European School of High-Energy Physics (ESHEP 2011): Cheile Gradistei, Romania, September 7-20, 2011*. 2014, pp. 197–266. DOI: 10.5170/CERN-2014-003.197. arXiv: 1205.0579 [hep-ph]. URL: https://inspirehep.net/record/1113441/files/arXiv:1205.0579.pdf.

[5] Paul Romatschke. "Do nuclear collisions create a locally equilibrated quark–gluon plasma?" In: *Eur. Phys. J.* C77.1 (2017), p. 21. DOI: 10.1140/epjc/s10052-016-4567-x. arXiv: 1609.02820 [nucl-th].

[6] Paul Romatschke. "New Developments in Relativistic Viscous Hydrodynamics". In: *Int. J. Mod. Phys.* E19 (2010), pp. 1–53. DOI: 10.1142/S0218301310014613. arXiv: 0902.3663 [hep-ph].

[7] Azwinndini Muronga. "Causal theories of dissipative relativistic fluid dynamics for nuclear collisions". In: *Phys. Rev.* C69 (2004), p. 034903. DOI: 10.1103/PhysRevC.69.034903. arXiv: nucl-th/0309055 [nucl-th].

[8] G. S. Denicol et al. "Derivation of transient relativistic fluid dynamics from the Boltzmann equation". In: *Phys. Rev.* D85 (2012), p. 114047. DOI: 10.1103/PhysRevD.85.114047, 10.1103/PhysRevD.91.039902. arXiv: 1202.4551 [nucl-th].

[9] Juan Martin Maldacena. "The Large N limit of superconformal field theories and supergravity". In: *Int. J. Theor. Phys.* 38 (1999), pp. 1113–1133. DOI: 10.1023/A:1026654312961. arXiv: hep-th/9711200 [hep-th].

[10] Paul M. Chesler and Wilke van der Schee. "Early thermalization, hydrodynamics and energy loss in AdS/CFT". In: *Int. J. Mod. Phys.* E24.10 (2015), p. 1530011. DOI: 10.1142/S0218301315300118. arXiv: 1501.04952 [nucl-th].

[11] Romuald A. Janik. "AdS/CFT for the early stages of heavy ion collisions". In: *Nucl. Phys.* A931 (2014), pp. 176–184. DOI: 10.1016/j.nuclphysa.2014.09.098. arXiv: 1409.7571 [hep-ph].

[12] Wilke van der Schee, Paul Romatschke, and Scott Pratt. "Fully Dynamical Simulation of Central Nuclear Collisions". In: *Phys.Rev.Lett.* 111.22 (2013), p. 222302. DOI: 10.1103/PhysRevLett.111.222302. arXiv: 1307.2539.

[13] Wilke van der Schee. "Gravitational collisions and the quark-gluon plasma". PhD thesis. Utrecht U., 2014. arXiv: 1407.1849 [hep-th]. URL: http://inspirehep.net/record/1305268/files/arXiv:1407.1849.pdf.

[14] Paul M. Chesler and Laurence G. Yaffe. "Holography and colliding gravitational shock waves in asymptotically AdS_5 spacetime". In: *Phys. Rev. Lett.* 106 (2011), p. 021601. DOI: 10.1103/PhysRevLett.106.021601. arXiv: 1011.3562 [hep-th].

[15] Paul M. Chesler and Laurence G. Yaffe. "Horizon formation and far-from- equilibrium isotropization in supersymmetric Yang-Mills plasma". In: *Phys. Rev. Lett.* 102 (2009), p. 211601. DOI: 10.1103/PhysRevLett.102.211601. arXiv: 0812.2053 [hep-th].

[16] Michal P. Heller, Romuald A. Janik, and Przemyslaw Witaszczyk. "The characteristics of thermalization of boost-invariant plasma from holography". In: *Phys. Rev. Lett.* 108 (2012), p. 201602. DOI: 10.1103/PhysRevLett.108.201602. arXiv: 1103.3452 [hep-th].

[17] Joshua Vredevoogd and Scott Pratt. "Viscous Hydrodynamics and Relativistic Heavy Ion Collisions". In: *Phys. Rev.* C85 (2012), p. 044908. DOI: 10.1103/PhysRevC.85.044908. arXiv: 1202.1509 [nucl-th].

[18] Paul Romatschke and J. Drew Hogg. "Pre-Equilibrium Radial Flow from Central Shock-Wave Collisions in AdS5". In: *JHEP* 04 (2013), p. 048. DOI: 10.1007/JHEP04(2013)048. arXiv: 1301.2635 [hep-th].

[19] Hans Bantilan and Paul Romatschke. "Simulation of Black Hole Collisions in Asymptotically Anti-de Sitter Spacetimes". In: *Phys. Rev. Lett.* 114.8 (2015), p. 081601. DOI: 10.1103/PhysRevLett.114.081601. arXiv: 1410.4799 [hep-th].

[20] P. F. Kolb et al. "Centrality dependence of multiplicity, transverse energy, and elliptic flow from hydrodynamics". In: *Nucl. Phys.* A696 (2001), pp. 197–215. DOI: 10.1016/S0375-9474(01)01114-9. arXiv: hep-ph/0103234 [hep-ph].

[21] Michael L. Miller et al. "Glauber modeling in high energy nuclear collisions". In: *Ann. Rev. Nucl. Part. Sci.* 57 (2007), pp. 205–243. DOI: 10.1146/annurev.nucl.57.090506.123020. arXiv: nucl-ex/0701025 [nucl-ex].

[22] B. Alver et al. "The PHOBOS Glauber Monte Carlo". In: (2008). arXiv: 0805.4411 [nucl-ex].

[23] Alver Burak et al. https://tglaubermc.hepforge.org.

[24] Dmitri Kharzeev and Marzia Nardi. "Hadron production in nuclear collisions at RHIC and high density QCD". In: *Phys. Lett.* B507 (2001), pp. 121–128. DOI: 10.1016/S0370-2693(01)00457-9. arXiv: nucl-th/0012025 [nucl-th].

[25] Mike Miller and Raimond Snellings. "Eccentricity fluctuations and its possible effect on elliptic flow measurements". In: (2003). arXiv: nucl-ex/0312008 [nucl-ex].

[26] Paul Sorensen. "Implications of space-momentum correlations and geometric fluctuations in heavy-ion collisions". In: *J. Phys.* G37 (2010), p. 094011. DOI: 10.1088/0954-3899/37/9/094011. arXiv: 1002.4878 [nucl-ex].

[27] R. Venugopalan. "The color glass condensate: A classical effective theory of high energy QCD". In: *J. Phys. Conf. Ser.* 50 (2006), pp. 70–78. DOI: 10.1088/1742-6596/50/1/008.

[28] Larry McLerran. "Quark gluon plasma, color glass condensate and glasma: 3 lectures at Lake Baikal". In: *Phys. Part. Nucl. Lett.* 8 (2011), pp. 673–682. DOI: 10.1134/S1547477111070132.

[29] Francois Gelis et al. "The Color Glass Condensate". In: *Ann. Rev. Nucl. Part. Sci.* 60 (2010), pp. 463–489. DOI: 10.1146/annurev.nucl.010909.083629. arXiv: 1002.0333 [hep-ph].

[30] F. Gelis. "Color Glass Condensate and Glasma". In: *Int. J. Mod. Phys.* A28 (2013), p. 1330001. DOI: 10.1142/S0217751X13300019. arXiv: 1211.3327 [hep-ph].

[31] Dirk H. Rischke. "Fluid dynamics for relativistic nuclear collisions". In: (1998). [Lect. Notes Phys.516,21(1999)]. DOI: 10.1007/BFb0107310. arXiv: nucl-th/9809044 [nucl-th].

[32] Rudolf Baier, Paul Romatschke, and Urs Achim Wiedemann. "Dissipative hydrodynamics and heavy ion collisions". In: *Phys. Rev.* C73 (2006), p. 064903. DOI: 10.1103/PhysRevC.73.064903. arXiv: hep-ph/0602249 [hep-ph].

[33] Rudolf Baier et al. "Relativistic viscous hydrodynamics, conformal invariance, and holography". In: *JHEP* 04 (2008), p. 100. DOI: 10.1088/1126-6708/2008/04/100. arXiv: 0712.2451 [hep-th].

[34] Paul Romatschke. "Relativistic Viscous Fluid Dynamics and Non-Equilibrium Entropy". In: *Class. Quant. Grav.* 27 (2010), p. 025006. DOI: 10.1088/0264-9381/27/2/025006. arXiv: 0906.4787 [hep-th].

[35] P. Kovtun, Dan T. Son, and Andrei O. Starinets. "Viscosity in strongly interacting quantum field theories from black hole physics". In: *Phys. Rev. Lett.* 94 (2005), p. 111601. DOI: 10.1103/PhysRevLett.94.111601. arXiv: hep-th/0405231 [hep-th].

[36] Simon C. Huot, Sangyong Jeon, and Guy D. Moore. "Shear viscosity in weakly coupled N = 4 super Yang-Mills theory compared to QCD". In: *Phys. Rev. Lett.* 98 (2007), p. 172303. DOI: 10.1103/PhysRevLett.98.172303. arXiv: hep-ph/0608062 [hep-ph].

[37] Markus H. Thoma. "Viscosity coefficient of the quark - gluon plasma in the weak coupling limit". In: *Phys. Lett.* B269 (1991), pp. 144–148. DOI: 10.1016/0370-2693(91)91466-9.

[38] Peter Brockway Arnold, Caglar Dogan, and Guy D. Moore. "The Bulk Viscosity of High-Temperature QCD". In: *Phys. Rev.* D74 (2006), p. 085021. DOI: 10.1103/PhysRevD.74.085021. arXiv: hep-ph/0608012 [hep-ph].

[39] Frithjof Karsch, Dmitri Kharzeev, and Kirill Tuchin. "Universal properties of bulk viscosity near the QCD phase transition". In: *Phys. Lett.* B663 (2008), pp. 217–221. DOI: 10.1016/j.physletb.2008.01.080. arXiv: 0711.0914 [hep-ph].

[40] Guy D. Moore and Omid Saremi. "Bulk viscosity and spectral functions in QCD". In: *JHEP* 09 (2008), p. 015. DOI: 10.1088/1126-6708/2008/09/015. arXiv: 0805.4201 [hep-ph].

[41] S. Ryu et al. "Importance of the Bulk Viscosity of QCD in Ultrarelativistic Heavy-Ion Collisions". In: *Phys. Rev. Lett.* 115.13 (2015), p. 132301. DOI: 10.1103/PhysRevLett.115.132301. arXiv: 1502.01675 [nucl-th].

[42] G. S. Denicol, S. Jeon, and C. Gale. "Transport Coefficients of Bulk Viscous Pressure in the 14-moment approximation". In: *Phys. Rev.* C90.2 (2014), p. 024912. DOI: 10.1103/PhysRevC.90.024912. arXiv: 1403.0962 [nucl-th].

[43] Mikko Laine and York Schröder. "Quark mass thresholds in QCD thermodynamics". In: *Phys. Rev.* D73 (2006), p. 085009. DOI: 10.1103/PhysRevD.73.085009. arXiv: hep-ph/0603048 [hep-ph].

[44] Pasi Huovinen and Pter Petreczky. "QCD Equation of State and Hadron Resonance Gas". In: *Nucl. Phys.* A837 (2010), pp. 26–53. DOI: 10.1016/j.nuclphysa.2010.02.015. arXiv: 0912.2541 [hep-ph].

[45] J. D. Bjorken. "Highly Relativistic Nucleus-Nucleus Collisions: The Central Rapidity Region". In: *Phys. Rev.* D27 (1983), pp. 140–151. DOI: 10.1103/PhysRevD.27.140.

[46] Steven S. Gubser. "Symmetry constraints on generalizations of Bjorken flow". In: *Phys. Rev.* D82 (2010), p. 085027. DOI: 10.1103/PhysRevD.82.085027. arXiv: 1006.0006 [hep-th].

[47] Paul Romatschke. "Far From Equilibrium Fluid Dynamics". In: (2017). arXiv: 1704.08699 [hep-th].

[48] Michal P. Heller and Michal Spalinski. "Hydrodynamics Beyond the Gradient Expansion: Resurgence and Resummation". In: *Phys. Rev. Lett.* 115.7 (2015), p. 072501. DOI: 10.1103/PhysRevLett.115.072501. arXiv: 1503.07514 [hep-th].

[49] Fred Cooper and Graham Frye. "Comment on the Single Particle Distribution in the Hydrodynamic and Statistical Thermodynamic Models of Multiparticle Production". In: *Phys. Rev.* D10 (1974), p. 186. DOI: 10.1103/PhysRevD.10.186.

[50] Ulrich Heinz, Zhi Qiu, and Chun Shen. "Fluctuating flow angles and anisotropic flow measurements". In: *Phys. Rev.* C87.3 (2013), p. 034913. DOI: 10.1103/PhysRevC.87.034913. arXiv: 1302.3535 [nucl-th].

[51] Paul Romatschke. "Collective flow without hydrodynamics: simulation results for relativistic ion collisions". In: *Eur. Phys. J.* C75.9 (2015), p. 429. DOI: 10.1140/epjc/s10052-015-3646-8. arXiv: 1504.02529 [nucl-th].

[52] Ulrich W. Heinz. "How to extract physics from HBT radius parameters". In: *Nucl. Phys.* A610 (1996), pp. 264C–277C. DOI: 10.1016/S0375-9474(96)00361-2. arXiv: nucl-th/9608002 [nucl-th].

[53] S. V. Akkelin and Yu. M. Sinyukov. "The HBT interferometry of expanding sources". In: *Phys. Lett.* B356 (1995), pp. 525–530. DOI: 10.1016/0370-2693(95)00765-D.

[54] A. N. Makhlin and Yu. M. Sinyukov. "Hydrodynamics of Hadron Matter Under Pion Interferometric Microscope". In: *Z. Phys.* C39 (1988), p. 69. DOI: 10.1007/BF01560393.

[55] Michael Annan Lisa et al. "Femtoscopy in relativistic heavy ion collisions". In: *Ann. Rev. Nucl. Part. Sci.* 55 (2005), pp. 357–402. DOI: 10.1146/annurev.nucl.55.090704.151533. arXiv: nucl-ex/0505014 [nucl-ex].

[56] S. Pratt. "Pion Interferometry for Exploding Sources". In: *Phys. Rev. Lett.* 53 (1984), pp. 1219–1221. DOI: 10.1103/PhysRevLett.53.1219.

[57] Edward V. Shuryak. "The Correlation of identical pions in multibody production". In: *Phys. Lett.* 44B (1973), pp. 387–389. DOI: 10.1016/0370-2693(73)90414-0.

[58] M. Gyulassy, S. K. Kauffmann, and L. W. Wilson. "Pion Interferometry of Nuclear Collisions. 1. Theory". In: *Phys. Rev.* C20 (1979), pp. 2267–2292. DOI: 10.1103/PhysRevC.20.2267.

[59] Scott Chapman and Ulrich W. Heinz. "HBT correlators: Current formalism versus Wigner function formulation". In: *Phys. Lett.* B340 (1994), pp. 250–253. DOI: 10.1016/0370-2693(94)01277-6. arXiv: hep-ph/9407405 [hep-ph].

[60] Scott Pratt. "Resolving the HBT Puzzle in Relativistic Heavy Ion Collision". In: *Phys. Rev. Lett.* 102 (2009), p. 232301. DOI: 10.1103/PhysRevLett.102.232301. arXiv: 0811.3363 [nucl-th].

[61] G. F. Bertsch. "Pion Interferometry as a Probe of the Plasma". In: *Nucl. Phys.* A498 (1989), pp. 173C–180C. DOI: 10.1016/0375-9474(89)90597-6.

[62] Matthew Luzum and Paul Romatschke. "Conformal Relativistic Viscous Hydrodynamics: Applications to RHIC results at s(NN)**(1/2) = 200-GeV". In: *Phys. Rev.* C78 (2008). [Erratum: Phys. Rev.C79,039903(2009)], p. 034915. DOI: 10.1103/PhysRevC.78.034915,10.1103/PhysRevC.79.039903. arXiv: 0804.4015 [nucl-th].

[63] John Novak et al. "Determining Fundamental Properties of Matter Created in Ultrarelativistic Heavy-Ion Collisions". In: *Phys. Rev.* C89.3 (2014), p. 034917. DOI: 10.1103/PhysRevC.89.034917. arXiv: 1303.5769 [nucl-th].

[64] Mathis Habich. https://bitbucket.org/mhabich/pp-ic-fluc.

[65] Mathis Habich. https://bitbucket.org/mhabich/pp-ic-rnd.

[66] Yannis Burnier and Chiara Gastaldi. "Contribution of next-to-leading order and Landau-Pomeranchuk-Migdal corrections to thermal dilepton emission in heavy-ion collisions". In: *Phys. Rev.* C93.4 (2016), p. 044902. DOI: 10.1103/PhysRevC.93.044902. arXiv: 1508.06978 [nucl-th].

[67] Mathis Habich et al. https://bitbucket.org/mhabich/sonic.

[68] Chun Shen et al. https://u.osu.edu/vishnu.

[69] Chun Shen et al. "The iEBE-VISHNU code package for relativistic heavy-ion collisions". In: *Comput. Phys. Commun.* 199 (2016), pp. 61–85. DOI: 10.1016/j.cpc.2015.08.039. arXiv: 1409.8164 [nucl-th].

[70] M. Bleicher et al. "Relativistic hadron hadron collisions in the ultrarelativistic quantum molecular dynamics model". In: *J. Phys.* G25 (1999), pp. 1859–1896. DOI: 10.1088/0954-3899/25/9/308. arXiv: hep-ph/9909407 [hep-ph].

[71] S. A. Bass et al. "Microscopic models for ultrarelativistic heavy ion collisions". In: *Prog. Part. Nucl. Phys.* 41 (1998). [Prog. Part. Nucl. Phys.41,225(1998)], pp. 255–369. DOI: 10.1016/S0146-6410(98)00058-1. arXiv: nucl-th/9803035 [nucl-th].

[72] Bjoern Schenke, Sangyong Jeon, and Charles Gale. http://www.physics.mcgill.ca/music/.

[73] Bjoern Schenke, Sangyong Jeon, and Charles Gale. "(3+1)D hydrodynamic simulation of relativistic heavy-ion collisions". In: *Phys. Rev.* C82 (2010), p. 014903. DOI: 10.1103/PhysRevC.82.014903. arXiv: 1004.1408 [hep-ph].

[74] Jean-François Paquet et al. "Production of photons in relativistic heavy-ion collisions". In: *Phys. Rev.* C93.4 (2016), p. 044906. DOI: 10.1103/PhysRevC.93.044906. arXiv: 1509.06738 [hep-ph].

[75] Bjorn Schenke, Sangyong Jeon, and Charles Gale. "Elliptic and triangular flow in event-by-event (3+1)D viscous hydrodynamics". In: *Phys. Rev. Lett.* 106 (2011), p. 042301. DOI: 10.1103/PhysRevLett.106.042301. arXiv: 1009.3244 [hep-ph].

[76] Chun Shen et al. "Collectivity and electromagnetic radiation in small systems". In: *Phys. Rev.* C95.1 (2017), p. 014906. DOI: 10.1103/PhysRevC.95.014906. arXiv: 1609.02590 [nucl-th].

[77] Krishna Rajagopal and Nilesh Tripuraneni. "Bulk Viscosity and Cavitation in Boost-Invariant Hydrodynamic Expansion". In: *JHEP* 03 (2010), p. 018. DOI: 10.1007/JHEP03(2010)018. arXiv: 0908.1785 [hep-ph].

[78] Egang Lu and Guy D. Moore. "The Bulk Viscosity of a Pion Gas". In: *Phys. Rev. C* 83 (2011), p. 044901. DOI: 10.1103/PhysRevC.83.044901. arXiv: 1102.0017 [hep-ph].

[79] Antonio Dobado, Felipe J. Llanes-Estrada, and Juan M. Torres-Rincon. "Bulk viscosity of low-temperature strongly interacting matter". In: *Phys.Lett.* B702 (2011), pp. 43–48. DOI: 10.1016/j.physletb.2011.06.059. arXiv: 1103.0735 [hep-ph].

[80] Roger Horsley and Wim Schoenmaker. "Quantum Field Theories Out of Thermal Equilibrium. 1. General Considerations". In: *Nucl. Phys.* B280 (1987), pp. 716–734. DOI: 10.1016/0550-3213(87)90170-2.

[81] Alex Buchel. "Bulk viscosity of gauge theory plasma at strong coupling". In: *Phys. Lett.* B663 (2008), pp. 286–289. DOI: 10.1016/j.physletb.2008.03.069. arXiv: 0708.3459 [hep-th].

[82] Jacquelyn Noronha-Hostler et al. "Bulk Viscosity Effects in Event-by-Event Relativistic Hydrodynamics". In: *Phys. Rev.* C88.4 (2013), p. 044916. DOI: 10.1103/PhysRevC.88.044916. arXiv: 1305.1981 [nucl-th].

[83] G. S. Denicol et al. "Effect of bulk viscosity on Elliptic Flow near QCD phase transition". In: *Phys. Rev.* C80 (2009), p. 064901. DOI: 10.1103/PhysRevC.80.064901. arXiv: 0903.3595 [hep-ph].

[84] Jacquelyn Noronha-Hostler, Jorge Noronha, and Carsten Greiner. "Transport Coefficients of Hadronic Matter near T(c)". In: *Phys. Rev. Lett.* 103 (2009), p. 172302. DOI: 10.1103/PhysRevLett.103.172302. arXiv: 0811.1571 [nucl-th].

[85] Ryan D. Weller and Paul Romatschke. "One fluid to rule them all: viscous hydrodynamic description of event-by-event central p+p, p+Pb and Pb+Pb collisions at $\sqrt{s} = 5.02$ TeV". In: (2017). arXiv: 1701.07145 [nucl-th].

[86] Scott Pratt. "Femtoscopy overview and the HBT puzzle". In: *Acta Phys. Polon. Supp.* 1 (2008), pp. 489–492.

[87] Scott Pratt. "The Long Slow Death of the HBT Puzzle". In: *Nucl. Phys.* A830 (2009), pp. 51C–57C. DOI: 10.1016/j.nuclphysa.2009.10.010. arXiv: 0907.1094 [nucl-th].

[88] K. Aamodt et al. "Two-pion Bose-Einstein correlations in central Pb-Pb collisions at $\sqrt{s_{NN}} = 2.76$ TeV". In: *Phys. Lett.* B696 (2011), pp. 328–337. DOI: 10.1016/j.physletb.2010.12.053. arXiv: 1012.4035 [nucl-ex].

[89] J. Adams et al. "Pion interferometry in Au+Au collisions at S(NN)**(1/2) = 200-GeV". In: *Phys. Rev.* C71 (2005), p. 044906. DOI: 10.1103/PhysRevC.71.044906. arXiv: nucl-ex/0411036 [nucl-ex].

[90] B. I. Abelev et al. "Pion Interferometry in Au+Au and Cu+Cu Collisions at RHIC". In: *Phys. Rev.* C80 (2009), p. 024905. DOI: 10.1103/PhysRevC.80.024905. arXiv: 0903.1296 [nucl-ex].

[91] K. Aamodt et al. "Femtoscopy of *pp* collisions at $\sqrt{s} = 0.9$ and 7 TeV at the LHC with two-pion Bose-Einstein correlations". In: *Phys. Rev.* D84 (2011), p. 112004. DOI: 10.1103/PhysRevD.84.112004. arXiv: 1101.3665 [hep-ex].

[92] Georges Aad et al. "Observation of Long-Range Elliptic Azimuthal Anisotropies in $\sqrt{s}$ =13 and 2.76 TeV *pp* Collisions with the ATLAS Detector". In: *Phys. Rev. Lett.* 116.17 (2016), p. 172301. DOI: 10.1103/PhysRevLett.116.172301. arXiv: 1509.04776 [hep-ex].

[93] Vardan Khachatryan et al. "Evidence for collectivity in pp collisions at the LHC". In: *Phys. Lett.* B765 (2017), pp. 193–220. DOI: 10.1016/j.physletb.2016.12.009. arXiv: 1606.06198 [nucl-ex].

[94] Jaroslav Adam et al. "Insight into particle production mechanisms via angular correlations of identified particles in pp collisions at $\sqrt{s} = 7$ TeV". In: *Eur. Phys. J.* C77.8 (2017), p. 569. DOI: 10.1140/epjc/s10052-017-5129-6. arXiv: 1612.08975 [nucl-ex].

[95] Siddharth Venkat et al. "Realistic Transverse Images of the Proton Charge and Magnetic Densities". In: *Phys. Rev.* C83 (2011), p. 015203. DOI: 10.1103/PhysRevC.83.015203. arXiv: 1010.3629 [nucl-th].

[96] Steven Weinberg. "Dynamics at infinite momentum". In: *Phys. Rev.* 150 (1966), pp. 1313–1318. DOI: 10.1103/PhysRev.150.1313.

[97] M. K. Jones et al. "G(E(p)) / G(M(p)) ratio by polarization transfer in polarized $\vec{e}p \to e\vec{p}$". In: *Phys. Rev. Lett.* 84 (2000), pp. 1398–1402. DOI: 10.1103/PhysRevLett.84.1398. arXiv: nucl-ex/9910005 [nucl-ex].

[98] O. Gayou et al. "Measurement of G(Ep) / G(Mp) in $\vec{e}p \to e\vec{p}$ to Q**2 = 5.6-GeV**2". In: *Phys. Rev. Lett.* 88 (2002), p. 092301. DOI: 10.1103/PhysRevLett.88.092301. arXiv: nucl-ex/0111010 [nucl-ex].

[99] Gerald A. Miller and Michael R. Frank. "Q**2 independence of QF(2) / F(1), Poincare invariance and the nonconservation of helicity". In: *Phys. Rev.* C65 (2002), p. 065205. DOI: 10.1103/PhysRevC.65.065205. arXiv: nucl-th/0201021 [nucl-th].

[100] Gerald A. Miller. "Shapes of the proton". In: *Phys. Rev.* C68 (2003), p. 022201. DOI: 10.1103/PhysRevC.68.022201. arXiv: nucl-th/0304076 [nucl-th].

[101] G. Peter Lepage and Stanley J. Brodsky. "Exclusive Processes in Perturbative Quantum Chromodynamics". In: *Phys. Rev.* D22 (1980), p. 2157. DOI: 10.1103/PhysRevD.22.2157.

[102] Stanley J. Brodsky and G. Peter Lepage. "Helicity Selection Rules and Tests of Gluon Spin in Exclusive QCD Processes". In: *Phys. Rev.* D24 (1981), p. 2848. DOI: 10.1103/PhysRevD.24.2848.

[103] Gerald A. Miller. "Non-Spherical Shapes of the Proton: Existence, Measurement and Computation". In: *Nucl. Phys. News* 18 (2008), pp. 12–16. DOI: 10.1080/10506890802123721. arXiv: 0802.3731 [nucl-th].

[104] Felix Schlumpf. "Relativistic constituent quark model for baryons". PhD thesis. Zurich U., 1992. arXiv: hep-ph/9211255 [hep-ph].

[105] Thierry Gousset, Bernard Pire, and John P. Ralston. "Hadron helicity violation in exclusive processes: Quantitative calculations in leading order QCD". In: *Phys. Rev.* D53 (1996), pp. 1202–1215. DOI: 10.1103/PhysRevD.53.1202. arXiv: hep-ph/9504281 [hep-ph].

[106] Vladimir M. Braun et al. "Light cone sum rules for the nucleon form-factors". In: *Phys. Rev.* D65 (2002), p. 074011. DOI: 10.1103/PhysRevD.65.074011. arXiv: hep-ph/0112085 [hep-ph].

[107] Alexander Kvinikhidze and Gerald A. Miller. "Shapes of the nucleon". In: *Phys. Rev.* C73 (2006), p. 065203. DOI: 10.1103/PhysRevC.73.065203. arXiv: nucl-th/0603035 [nucl-th].

[108] M. R. Frank, B. K. Jennings, and G. A. Miller. "The Role of color neutrality in nuclear physics: Modifications of nucleonic wave functions". In: *Phys. Rev.* C54 (1996), pp. 920–935. DOI: 10.1103/PhysRevC.54.920. arXiv: nucl-th/9509030 [nucl-th].

[109] Gerald A. Miller. "Light front cloudy bag model: Nucleon electromagnetic form-factors". In: *Phys. Rev.* C66 (2002), p. 032201. DOI: 10.1103/PhysRevC.66.032201. arXiv: nucl-th/0207007 [nucl-th].

[110] CMS Collaboration. "Azimuthal anisotropy harmonics from long-range correlations in high multiplicity pp collisions at sqrts = 7 TeV". In: (2015).

[111] Morad Aaboud et al. "Measurement of multi-particle azimuthal correlations with the subevent cumulant method in *pp* and *p*+Pb collisions with the ATLAS detector at the LHC". In: (2017). arXiv: 1708.03559 [hep-ex].

[112] Mingliang Zhou. "Observation of long-range elliptic anisotropies in $\sqrt{s}$=13 and 2.76 TeV pp collisions with the ATLAS detector". In: *Nucl. Phys.* A956 (2016), pp. 769–772. DOI: 10.1016/j.nuclphysa.2016.04.005.

[113] Ryan Weller. Personal communication. Mar. 2017.

[114] Ryan Weller. Personal communication. Oct. 2017.

[115] H. Niemi et al. "Fluid dynamical response to initial state fluctuations". In: *Nucl. Phys.* A926 (2014), pp. 109–114. DOI: 10.1016/j.nuclphysa.2014.03.014.

[116] Jussi Auvinen, Jonah E. Bernhard, and Steffen A. Bass. "Systematic Extraction of QGP Properties". In: 2016. arXiv: 1610.00590 [nucl-th]. URL: http://inspirehep.net/record/1489219/files/arXiv:1610.00590.pdf.

[117] Klaus Dehmelt. "The path through sPHENIX and fsPHENIX toward an EIC detector at eRHIC". In: *PoS* DIS2016 (2016), p. 255.

[118] CERN. https://fcc.web.cern.ch/.

Appendix

A. Publications

This chapter includes all the publications mentioned in the Prologue. Since the following papers are verbatim includes, the styling of those pages deviates from the rest of this thesis.

A.1. Onset of cavitation in the quark–gluon plasma

Published for SISSA by Springer

Received: *July 11, 2014*
Revised: *October 21, 2014*
Accepted: *November 20, 2014*
Published: *December 5, 2014*

JHEP12(2014)054

Onset of cavitation in the quark-gluon plasma

Mathis Habich and Paul Romatschke

Department of Physics, 390 UCB, University of Colorado, Boulder, CO 80309-0390, U.S.A.

E-mail: mathis.habich@colorado.edu, paul.romatschke@colorado.edu

Abstract: We study the onset of bubble formation (cavitation) in the quark-gluon plasma as a result of the reduction of the effective pressure from bulk-viscous corrections. By calculating velocity gradients in typical models for quark-gluon plasma evolution in heavy-ion collisions, we obtain results for the critical bulk viscosity above which cavitation occurs. Since present experimental data for heavy-ion collision seems inconsistent with the presence of bubbles above the phase transition temperature of QCD, our results may be interpreted as an upper limit of the bulk viscosity in nature. Our results indicate that bubble formation is consistent with the expectation of hadronisation in low-temperature QCD.

Keywords: QCD Phenomenology, Heavy Ion Phenomenology

ArXiv ePrint: 1405.1978

doi:10.1007/JHEP12(2014)054

Contents

1 Introduction 1

2 Bulk-viscous bubble formation in relativistic hydrodynamics 2
- 2.1 Thermodynamics of cavitation in QCD 3
- 2.2 Critical bulk viscosity in first and second order hydrodynamics 3

3 Cavitation in heavy-ion collisions 5
- 3.1 Bjorken flow 5
- 3.2 Gubser flow 5
- 3.3 Numerical results 6
- 3.4 QCD equation of state 7

4 Conclusion 7

JHEP12(2014)054

1 Introduction

The experimental heavy-ion collisions programme conducted at the Relativistic Heavy Ion Collider and the Large Hadron Collider strongly suggests that the quark-gluon plasma (QGP) formed in these collisions behaves like an almost ideal fluid [1–4]. This fluid is very well-described by relativistic hydrodynamics [5]. For an ordinary fluid such as water, the effective pressure can be different than the equilibrium pressure and, in particular, in some situations it can drop below the vapour pressure. In this case, the thermodynamically preferred phase becomes the gas phase, and a vapour bubble forms inside the fluid, a phenomenon known as 'cavitation'.[1] Mainly, high fluid velocities trigger cavitation in liquids. In the case of relativistic fluids such as the QGP studied in heavy-ion collisions, cavitation would imply a phase transition from a deconfined plasma phase of quarks and gluons to a confined hadron-gas phase. The resulting medium would be highly inhomogeneous with (possibly short-lived) hadron gas bubbles expanding and collapsing in an otherwise laminar fluid. Maybe more importantly, hadron gas dynamics would take over at temperatures above the QCD phase transition, which would have immediate consequences on the measured particle spectra. The apparent success of describing experimental data by relatively simple, laminar fluid flows and subsequent freeze-out at the QCD phase transition temperature seems inconsistent with the presence of hadron gas bubbles, or even the onset of fluid instabilities in the high-temperature QGP. In the present work, we will thus make the assumption that cavitation does *not* occur in the experimentally observed QGP. We

[1] We note that if the bubble is unstable, then it quickly collapses. Nevertheless, the onset of cavitation signals an instability in the fluid evolution.

will study cavitation in relativistic fluids with a given bulk viscosity coefficient and then proceed to rule out bulk viscosity values under the above assumption.

In this article, the effective pressure is defined as one third of the trace of the pressure tensor [6]. For this definition, the shear viscous contribution to the pressure cancels, whereas the bulk-viscous contribution remains present. This differs from other approaches taken in the literature, which focused on single components of the pressure tensor [7–11] where the shear viscous contribution is present and important. Because shear-viscous effects will add on to the effects considered in this work, cavitation could occur in regions which — in our analysis — are found to be stable, but not the other way around. One caveat of our approach is that in the calculations that follow, the bulk-viscous contributions to the fluid flow profiles themselves have been neglected for simplicity. In principle, these contributions should be taken into account, but in practice, one expects the corrections to be small as long as the bulk viscosity coefficient itself is small [12]. Thus, our approach essentially amounts to a linear-response treatment of bulk-viscous effects in fully non-linear, shear-viscous fluid dynamics.

This work is organised as follows: in section 2, cavitation for relativistic hydrodynamics is defined. In section 2.2, the main idea of constraining bulk viscosity is elucidated for 1st and 2nd order hydrodynamics. Section 3 applies this framework to heavy-ion collisions, i.e., the critical bulk viscosity for cavitation is calculated for analytical and numerical flow profiles, as well as different equations of state. We present our conclusions and an upper limit for the QCD bulk viscosity in section 4.

2 Bulk-viscous bubble formation in relativistic hydrodynamics

Cavitation can be defined as the drop of pressure below the saturated vapour pressure of the particular liquid (see p. 6 in ref. [13]). This definition needs to be revisited for relativistic fluids which can have a pressure tensor that differs strongly from equilibrium. Formally, starting from a standard decomposition of the energy-momentum tensor

$$T^{\mu\nu} = \epsilon u^\mu u^\nu + (p - \Pi)\,\Delta^{\mu\nu} + \pi^{\mu\nu}\,, \tag{2.1}$$

with ϵ, p, u^μ the energy density, pressure and fluid four velocity, and the projector $\Delta^{\mu\nu} = g^{\mu\nu} - u^\mu u^\nu$ with a mostly minus signature metric tensor $g^{\mu\nu}$, we identify $\Pi, \pi^{\mu\nu}$ as the bulk- and shear-viscous stress tensor components. In this work, we concentrate on the effective, local pressure defined in three dimensions as

$$p_{\text{eff}} \equiv -\frac{1}{3}\Delta_{\mu\nu}T^{\mu\nu} = p - \Pi\,. \tag{2.2}$$

This preserves the normal, intuitive definition of pressure in the rest frame and, being a scalar, is easy to interpret in non-equilibrium situation.

Akin to ref. [13], the *occurrence of cavitation* can be mathematically defined as

$$p_{\text{eff}} < p_{\text{v}}\,, \tag{2.3}$$

with p_{v} the 'vapour' pressure of a different thermodynamic phase having the same temperature. In words, this means that if the effective pressure p_{eff} of a QGP falls below p_{v}, then

JHEP12(2014)054

the liquid will undergo a phase transition to the hadron-gas phase (often referred to as 'freeze-out' in the language of heavy-ion collisions) and a (small) gas bubble will form. The definition (2.3) is intuitively much easier to interpret than the case considered by most other authors [7–11], where a single component of the pressure tensor drops below the vapour pressure, whereas other component(s) will generally be larger than the vapour pressure.

2.1 Thermodynamics of cavitation in QCD

In ordinary fluids such as water, the transition from vapour to liquid is first order, and cavitation leads to the formation of vapour bubbles having the same temperature but different density than the surrounding liquid. The confinement-deconfinement transition in QCD at vanishing baryon density has been calculated to be an analytic crossover from hadron gas to QGP using lattice gauge theory [14]. As a consequence, one may worry if cavitation in QCD may occur at all, given that the thermodynamic properties such as energy density are continuous accross the phase boundary.

In the following, we will assume that cavitation in QCD is possible in principle in the sense of forming hadron gas domains ('cavities') inside the QGP liquid. Our assumption is based on two arguments: first, note that while the confinement-deconfinement transition in QCD is an analytic crossover in equilibrium situations at vanishing baryon density, our present work focusses on *non-equilibrium transitions*[2] induced by strong fluid flow gradients. In particular, these strong fluid gradients may lead to confinement-deconfinement transitions induced at temperatures well above the critical temperature of equilibrium QCD T_c. The nature of the non-equilibrium confinement-deconfinement transition induced at $T > T_c$ is not known, but it is possible to be a true phase transition, given that one may expect the energy density between QGP and hadron gas phase to be discontinuous at constant temperatures $T > T_c$.

Second, if the non-equilibrium confinement-deconfinement transition at $T > T_c$ *continued to be* an analytic crossover, one would still expect the drop in effective liquid pressure to be associated with phase-separated domains, possibly with extended domain walls (thick-walled bubbles), or more in line with elements found in spinodal decomposition if there is no energy barrier separating the two phases. This would be in-line with the expectation for $Z(3)$ domains studied in [15].

Once created, we expect the inhomogeneous liquid-gas domains to evolve in a non-trivial fashion; we reserve a study of this fascinating subject for future work.

2.2 Critical bulk viscosity in first and second order hydrodynamics

After establishing a criterion for cavitation, the critical bulk viscosity for the onset of cavitation can be calculated by assuming the validity of hydrodynamics.

For 1st order hydrodynamics. The effective pressure (2.2) up to 1st order gradients [16] for a non-conformal fluid is

$$p_{\text{eff}} = p - \Pi \approx p - \zeta \nabla_\mu u^\mu \,. \tag{2.4}$$

[2]Note that by *non-equilibrium*, we mean slightly off equilibrium for which hydrodynamics is still valid, in contrast to far-from-equilibrium transitions.

JHEP12(2014)054

The critical bulk viscosity is defined as the maximum value of ζ for which the fluid flow is still *non-cavitating*. Assuming the sign of the gradient $\nabla_\mu u^\mu$ to be positive (this is the case for all the scenarios we consider below), one finds

$$\left.\frac{\zeta}{s}\right|_{\rm crit} \equiv \frac{(p-p_{\rm v})\,T}{(\epsilon+p)\,\nabla_\mu u^\mu}\,, \tag{2.5}$$

where the bulk viscosity was divided by the entropy density $s = (\epsilon + p)/T$, yielding a dimensionless ratio.

For 2nd order hydrodynamics. In order to assess the accuracy of 1st order calculation, one can consider the effect of 2nd order gradients. Expanding the viscosity scalar Π of eq. (2.2) up to 2nd order in gradients yields for a flat space-time [16]

$$p_{\rm eff} = p - \zeta\nabla_\mu u^\mu + \zeta\tau_\Pi {\rm D}\left(\nabla_\mu u^\mu\right) + \xi_1\sigma^{\mu\nu}\sigma_{\mu\nu} + \xi_2\left(\nabla_\mu u^\mu\right)^2\,. \tag{2.6}$$

Most of the 2nd order transport coefficients τ_Π, ξ_1, ξ_2 are poorly known for most quantum field theories. However, in a particular strong coupling[3] (see ref. [17]), these have been calculated [16]:

$$\eta = \frac{3\zeta}{2(1-3c_{\rm s}^2)}\,, \tag{2.7}$$

$$\zeta\tau_\Pi = \zeta\tau_\pi = \frac{\zeta}{\epsilon+p}\eta(4-\ln 4)\,, \tag{2.8}$$

$$\xi_1 = \frac{\lambda_1}{3}\left(1-3c_{\rm s}^2\right) = \frac{2\eta^2}{3(\epsilon+p)}\left(1-3c_{\rm s}^2\right) = \frac{\zeta}{\epsilon+p}\eta\,, \tag{2.9}$$

$$\xi_2 = \frac{2\eta\tau_\Pi c_{\rm s}^2}{3}\left(1-3c_{\rm s}^2\right) = \frac{\zeta\tau_\Pi c_{\rm s}^2}{1-3c_{\rm s}^2} = \frac{\zeta}{\epsilon+p}\eta c_{\rm s}^2(4-\ln 4)\,. \tag{2.10}$$

By expressing these transport coefficients in terms of the speed of sound squared $c_{\rm s}^2$, ζ, and shear viscosity η, one finds the critical bulk viscosity in 2nd order hydrodynamics:

$$\left.\frac{\zeta}{s}\right|_{\rm crit} \equiv \frac{(p_{\rm v}-p)\,T}{(\epsilon+p)}\left[\nabla_\mu u^\mu - \frac{\eta}{s}\frac{(4-\ln 4)\big({\rm D}\nabla_\mu u^\mu + c_s^2\left(\nabla_\mu u^\mu\right)^2\big) + \sigma^{\mu\nu}\sigma_{\mu\nu}}{T}\right]^{-1}\,. \tag{2.11}$$

Note that in the 2nd order result, there is a pole in the critical bulk viscosity once the 2nd order gradient terms become as large as the 1st order terms. We find that for QCD this typically happens at very low temperatures (far below T_c), where one does not expect a hydrodynamic description to be applicable in the first place. In weak coupling, the transport coefficients typically lead to a quadratic dependence of ζ/s [18, 19] which is beyond the scope of our linear-response treatment.

To recapitulate, this method assumes a conformal, hydrodynamic description and uses the resulting flow profile to constrain the maximum value of ζ/s by requiring that the *effective pressure does not drop below zero.*

[3] Note that by construction, this particular theory only includes terms of linear order in bulk viscosity, e.g., terms of the form ζ^2 are absent in the transport coefficients.

JHEP12(2014)054

3 Cavitation in heavy-ion collisions

In this section, the critical bulk viscosity coefficient for the onset of cavitation is calculated for specific flow profiles used in the modelling of heavy-ion collisions. Specifically, the flow gradients are calculated for Bjorken flow [20]; Gubser flow [21, 22]; and a numerical solver for relativistic, viscous hydrodynamics in 2+1 dimensions [23, 24]. All these flow profiles are for *conformal fluids*, e.g., they ignore effects of bulk viscosity in the flow itself (see the discussion in section 1). In this entire section, the vapour pressure $p_{\rm v}$ is chosen to be zero:

$$p_{\rm v} \equiv 0\,, \tag{3.1}$$

which will result in the most conservative estimates of cavitation since higher values of $p_{\rm v}$ would decrease $\zeta/s|_{\rm crit}$ (e.g., see eq. (2.5)).

3.1 Bjorken flow

The set-up that was suggested by Bjorken [20] in 1982 can be utilised to extract a benchmark value on the bulk viscosity. It is particularly simple to use Milne coordinates $x^\mu = (\tau, x, y, \eta)$ because the fluid velocity becomes $u^\mu = (1, 0, 0, 0)^T$, i.e., the fluid is locally at rest. The velocity gradient simply depends on the Christoffel symbols for Milne coordinates

$$\nabla_\mu u^\mu = \frac{1}{\tau}\,, \tag{3.2}$$

whereas the temperature evolution is governed by

$$T = T_0\,(\tau/\tau_0)^{-c_{\rm s}^2}\,. \tag{3.3}$$

This framework is comparatively simple because it entirely neglects transverse, spatial dynamics of the QGP. For an ideal equation of state the dynamics is completely governed by the gradients: evidently, the gradient is always positive for $\tau > 0$ for 1st order hydrodynamics; however, for 2nd order gradients, the gradients become negative after diverging for early times and/or low temperatures ($\tau T \ll 1$).

The critical bulk viscosity for Bjorken flow is monotonously increasing with temperature. By taking 2nd order gradients into account, only small changes are present, as can be seen in figure 1. The effect of these higher-order terms is small due to the small numerical values of the 2nd order transport coefficients.

3.2 Gubser flow

By expressing the flow profile that was proposed by Gubser [21] in Milne coordinates, one finds a fluid flow profile

$$u^\mu = \left(\frac{1 + q^2 r^2 + q^2 \tau^2}{2q\tau\sqrt{1+g^2}},\, \frac{qr}{\sqrt{1+g^2}},\, 0,\, 0\right)^{\rm T} \tag{3.4}$$

JHEP12(2014)054

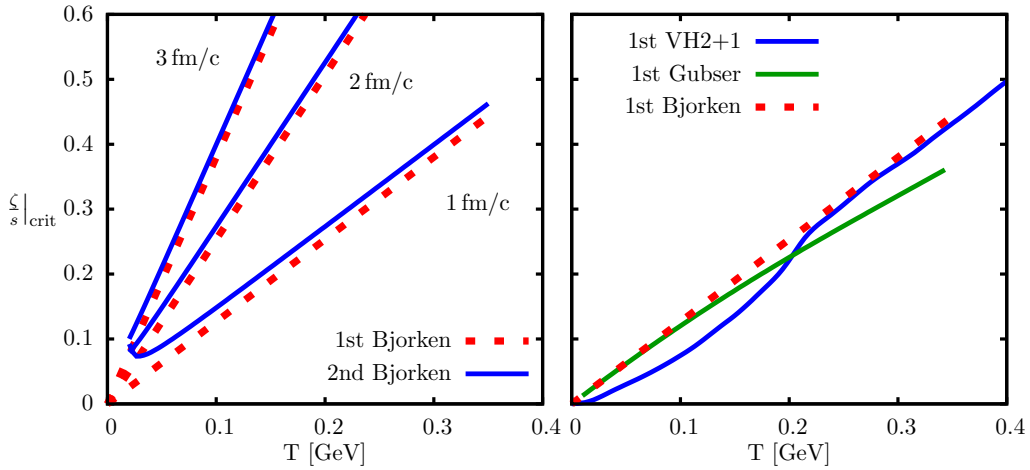

Figure 1. Critical bulk viscosity as a function of temperature for ideal equation of state. Areas above respective lines of $\zeta/s|_{\rm crit}$ are regions where cavitation occurs. Left: comparison of 1st and 2nd order results for Bjorken flow. Right: comparison between Bjorken flow, Gubser flow, and numerical computations.

and a temperature profile

$$T = \frac{1}{\tau f_*^{1/4}} \left\{ \frac{\hat{T}_0}{(1+g^2)^{1/3}} + \frac{H_0}{\sqrt{1+g^2}} \left[1 - (1+g^2)^{1/6} \, {}_2F_1\left(\frac{1}{2}, \frac{1}{6}, \frac{3}{2}, -g^2 \right) \right] \right\}, \quad (3.5)$$

where

$$g = \frac{1 + q^2 r^2 - q^2 \tau^2}{2q\tau}, \quad f_*^{1/4}, \quad \hat{T} = 5.55\,, \quad H_0 = 0.33\,, \quad 1/q = 4.3\text{fm}\,.$$

The variables τ and r denote the proper time and radial distance, respectively. The specific form of fluid velocity and temperature arises from symmetry considerations [21, 22]. In comparison to Bjorken flow, this flow profile is more realistic because radial velocities are non-vanishing; hence, the transverse dynamics is not neglected but fixed to have a unique, analytical form. By comparing the different orders of Gubser flow, one sees a similar behaviour to Bjorken flow, i.e., higher-order gradients decrease the denominator; thus, 2nd order terms increase the value of $\zeta/s|_{\rm crit}$ (see figure 1).

3.3 Numerical results

The last flow profile stems from a numerical simulation that fully includes transverse dynamics ("VH2+1", see refs. [23, 24] for details) for an initial condition of a central $Au+Au$ collision at $\sqrt{s} = 200\,\text{GeV}$ per nucleon pair. It was initialised with vanishing flow at early times, such that the high-temperature $\zeta/s|_{\rm crit}$ behaviour matches the Bjorken flow result, as it should. For late times, the significant fluid velocity gradients differ from both the Bjorken and Gubser flow results, resulting in a different $\zeta/s|_{\rm crit}$ behaviour at low temperatures (see figure 1).

JHEP12(2014)054

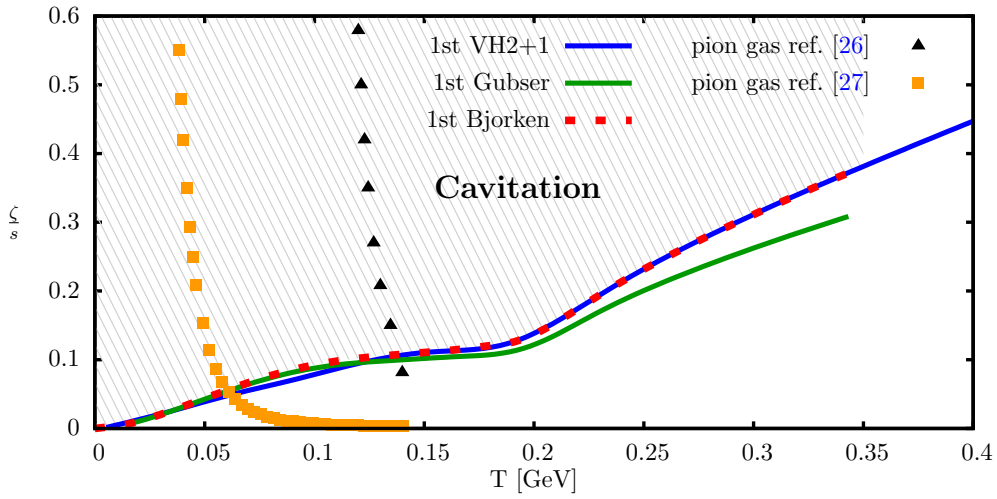

Figure 2. Bulk viscosity over entropy density ratio as a function of temperature. Shown are results for the lowest critical bulk viscosity coefficient $\zeta/s|_{\text{crit}}$ using different flow profiles and a QCD equation of state. For higher viscosity values, we predict bubbles to form in the liquid ('cavitation'). For comparison we also show the result of a calculation of ζ/s for two pion gases from refs. [26, 27]. The pion gas is calculated up to $T = 140\,\text{MeV}$.

3.4 QCD equation of state

For a realistic model of the QGP, we have repeated the above calculations for $\zeta/s|_{\text{crit}}$ with a QCD equation of state (see ref. [25]). In figure 2, the *lowest* value of $\zeta/s|_{\text{crit}}$ for Bjorken, Gubser and numerical flow profiles, respectively, is shown. For comparison, we also show the result of calculations of ζ/s for a pion gas from refs. [26, 27]. The former is performed at chemical equilibrium; whereas, the latter being an out-of-chemical equilibrium calculation for which elastic scattering is the dominant process [27, 28]. In dynamical heavy-ion collisions ζ/s is most likely to lie between these curves. At very high temperature, one could also compare to perturbative QCD calculations from ref. [29] where $\zeta/s \sim 0.01\alpha_s^2$, which tends to fall as a function of temperature, whereas $\zeta/s|_{\text{crit}}$ rises with temperature. Thus, we presume that cavitation is a phenomenon of low temperatures — not of high temperatures.

4 Conclusion

In this work, we have studied the onset of bubble formation (cavitation) in the QGP resulting from the presence of bulk-viscous terms in relativistic hydrodynamics. We found that at temperatures $T < 140\,\text{MeV}$, a bulk viscosity coefficient smaller than that expected from a pion gas leads to the formation of hadron gas bubbles in the QGP liquid (see also refs. [6–10, 26, 27, 30, 31]). This may be interpreted as the known freeze-out phenomenon in heavy-ion collisions where the plasma undergoes a phase transition to a hadron gas. At around the QCD phase transition temperature, we predict that for values of $\zeta/s \gtrapprox 0.1$, cavitation in the QGP will occur. Under the assumption that experimental data on the

JHEP12(2014)054

QGP from heavy-ion collisions is inconsistent with the presence of hadron gas bubbles, our results for $\zeta/s|_{\text{crit}}$ may be interpreted as an upper bound on the bulk viscosity in high-temperature QCD. At very high temperatures, this interpretation seems consistent with known perturbative values of ζ/s. Several aspects of our work can and should be improved in subsequent studies: first, it is possible to implement the corrections from bulk viscosity in the flow profiles used in the calculations of $\zeta/s|_{\text{crit}}$, eliminating the approximation we have used in this work. Second, one can repeat our study with more realistic approximations for the hadron gas pressure than our choice: $p_{\text{v}} \equiv 0$. Ultimately, and maybe most importantly, it would be interesting to calculate the particle spectra from a numerical simulation including the presence of hadron gas bubbles. This could potentially be done using state-of-the-art numerical hydrodynamical solvers [5, 32, 33] and could verify the assumption that cavitating fluids are inconsistent with experimental data on heavy-ion collisions.

Acknowledgments

This work was supported by the *Sloan Foundation*, Award No. BR2012-038 and the *Deutsche Forschungsgemeinschaft* (DFG), Grant No. RO 4513/1-1.

References

[1] P. Romatschke, *New developments in relativistic viscous hydrodynamics*, *Int. J. Mod. Phys.* **E 19** (2010) 1 [arXiv:0902.3663] [INSPIRE].

[2] U. Heinz and R. Snellings, *Collective flow and viscosity in relativistic heavy-ion collisions*, *Ann. Rev. Nucl. Part. Sci.* **63** (2013) 123 [arXiv:1301.2826] [INSPIRE].

[3] B. Müller, J. Schukraft and B. Wyslouch, *First results from Pb+Pb collisions at the LHC*, *Ann. Rev. Nucl. Part. Sci.* **62** (2012) 361 [arXiv:1202.3233] [INSPIRE].

[4] T. Schäfer and D. Teaney, *Nearly perfect fluidity: from cold atomic gases to hot quark gluon plasmas*, *Rept. Prog. Phys.* **72** (2009) 126001 [arXiv:0904.3107] [INSPIRE].

[5] C. Gale, S. Jeon, B. Schenke, P. Tribedy and R. Venugopalan, *Event-by-event anisotropic flow in heavy-ion collisions from combined Yang-Mills and viscous fluid dynamics*, *Phys. Rev. Lett.* **110** (2013) 012302 [arXiv:1209.6330] [INSPIRE].

[6] A. Buchel, X.O. Camanho and J.D. Edelstein, *Cavitation effects on the confinement/deconfinement transition*, *Phys. Lett.* **B 734** (2014) 131 [arXiv:1303.6300] [INSPIRE].

[7] K. Rajagopal and N. Tripuraneni, *Bulk viscosity and cavitation in boost-invariant hydrodynamic expansion*, *JHEP* **03** (2010) 018 [arXiv:0908.1785] [INSPIRE].

[8] A. Klimek, L. Leblond and A. Sinha, *Cavitation in holographic sQGP*, *Phys. Lett.* **B 701** (2011) 144 [arXiv:1103.3987] [INSPIRE].

[9] J.R. Bhatt, H. Mishra and V. Sreekanth, *Cavitation and thermal photon production in relativistic heavy ion collisions*, arXiv:1005.2756 [INSPIRE].

JHEP12(2014)054

[10] J.R. Bhatt, H. Mishra and V. Sreekanth, *Shear viscosity, cavitation and hydrodynamics at LHC*, *Phys. Lett.* **B 704** (2011) 486 [arXiv:1103.4333] [INSPIRE].

[11] J.R. Bhatt, H. Mishra and V. Sreekanth, *Thermal photons in QGP and non-ideal effects*, *JHEP* **11** (2010) 106 [arXiv:1011.1969] [INSPIRE].

[12] H. Song and U.W. Heinz, *Interplay of shear and bulk viscosity in generating flow in heavy-ion collisions*, *Phys. Rev.* **C 81** (2010) 024905 [arXiv:0909.1549] [INSPIRE].

[13] C. Brennen, *Cavitation and bubble dynamics*, Oxford engineering science series, Oxford University Press, Oxford U.K. (1995).

[14] Y. Aoki, G. Endrodi, Z. Fodor, S.D. Katz and K.K. Szabo, *The order of the quantum chromodynamics transition predicted by the standard model of particle physics*, *Nature* **443** (2006) 675 [hep-lat/0611014] [INSPIRE].

[15] U.S. Gupta, R.K. Mohapatra, A.M. Srivastava and V.K. Tiwari, *Simulation of $Z(3)$ walls and string production via bubble nucleation in a quark-hadron transition*, *Phys. Rev.* **D 82** (2010) 074020 [arXiv:1007.5001] [INSPIRE].

[16] P. Romatschke, *Relativistic viscous fluid dynamics and non-equilibrium entropy*, *Class. Quant. Grav.* **27** (2010) 025006 [arXiv:0906.4787] [INSPIRE].

[17] I. Kanitscheider and K. Skenderis, *Universal hydrodynamics of non-conformal branes*, *JHEP* **04** (2009) 062 [arXiv:0901.1487] [INSPIRE].

[18] R.S. Bhalerao, A. Jaiswal, S. Pal and V. Sreekanth, *Particle production in relativistic heavy-ion collisions: A consistent hydrodynamic approach*, *Phys. Rev.* **C 88** (2013) 044911 [arXiv:1305.4146] [INSPIRE].

[19] A. Jaiswal, R.S. Bhalerao and S. Pal, *Complete relativistic second-order dissipative hydrodynamics from the entropy principle*, *Phys. Rev.* **C 87** (2013) 021901 [arXiv:1302.0666] [INSPIRE].

[20] J.D. Bjorken, *Highly relativistic nucleus-nucleus collisions: the central rapidity region*, *Phys. Rev.* **D 27** (1983) 140 [INSPIRE].

[21] S.S. Gubser, *Symmetry constraints on generalizations of Bjorken flow*, *Phys. Rev.* **D 82** (2010) 085027 [arXiv:1006.0006] [INSPIRE].

[22] S.S. Gubser and A. Yarom, *Conformal hydrodynamics in Minkowski and de Sitter spacetimes*, *Nucl. Phys.* **B 846** (2011) 469 [arXiv:1012.1314] [INSPIRE].

[23] P. Romatschke and U. Romatschke, *Viscosity information from relativistic nuclear collisions: how perfect is the fluid observed at RHIC?*, *Phys. Rev. Lett.* **99** (2007) 172301 [arXiv:0706.1522] [INSPIRE].

[24] R. Baier and P. Romatschke, *Causal viscous hydrodynamics for central heavy-ion collisions*, *Eur. Phys. J.* **C 51** (2007) 677 [nucl-th/0610108] [INSPIRE].

[25] M. Laine and Y. Schröder, *Quark mass thresholds in QCD thermodynamics*, *Phys. Rev.* **D 73** (2006) 085009 [hep-ph/0603048] [INSPIRE].

[26] E. Lu and G.D. Moore, *The bulk viscosity of a pion gas*, *Phys. Rev.* **C 83** (2011) 044901 [arXiv:1102.0017] [INSPIRE].

[27] A. Dobado, F.J. Llanes-Estrada and J.M. Torres-Rincon, *Bulk viscosity of low-temperature strongly interacting matter*, *Phys. Lett.* **B 702** (2011) 43 [arXiv:1103.0735] [INSPIRE].

[28] J.M. Torres-Rincon, personal communication, (2014).

JHEP12(2014)054

[29] P.B. Arnold, C. Dogan and G.D. Moore, *The bulk viscosity of high-temperature QCD*, *Phys. Rev.* **D 74** (2006) 085021 [hep-ph/0608012] [INSPIRE].

[30] G. Torrieri, B. Tomasik and I. Mishustin, *Bulk viscosity driven clusterization of quark-gluon plasma and early freeze-out in relativistic heavy-ion collisions*, *Phys. Rev.* **C 77** (2008) 034903 [arXiv:0707.4405] [INSPIRE].

[31] G. Torrieri and I. Mishustin, *Instability of boost-invariant hydrodynamics with a QCD inspired bulk viscosity*, *Phys. Rev.* **C 78** (2008) 021901 [arXiv:0805.0442] [INSPIRE].

[32] P. Romatschke, M. Mendoza and S. Succi, *A fully relativistic lattice Boltzmann algorithm*, *Phys. Rev.* **C 84** (2011) 034903 [arXiv:1106.1093] [INSPIRE].

[33] G.S. Denicol, S. Jeon and C. Gale, *Transport coefficients of bulk viscous pressure in the* 14*-moment approximation*, arXiv:1403.0962 [INSPIRE].

JHEP12(2014)054

A.2. Particle spectra and HBT radii for simulated central nuclear collisions of $C + C$, $Al + Al$, $Cu + Cu$, $Au + Au$, and $Pb + Pb$ from $\sqrt{s}$=62.4 – 2760 GeV

Eur. Phys. J. C (2015) 75:15
DOI 10.1140/epjc/s10052-014-3206-7

THE EUROPEAN PHYSICAL JOURNAL C

Regular Article - Theoretical Physics

Particle spectra and HBT radii for simulated central nuclear collisions of C + C, Al + Al, Cu + Cu, Au + Au, and Pb + Pb from $\sqrt{s} = 62.4$–2760 GeV

M. Habich, J. L. Nagle, P. Romatschke[a]
University of Colorado Boulder, Boulder, USA

Received: 11 September 2014 / Accepted: 27 November 2014 / Published online: 14 January 2015

Abstract We study the temperature profile, pion spectra, and HBT radii in central, symmetric, and boost-invariant nuclear collisions, using a super hybrid model for heavy-ion collisions (SONIC), combining pre-equilibrium flow with viscous hydrodynamics and late-stage hadronic rescatterings. In particular, we simulate Pb + Pb collisions at $\sqrt{s} = 2.76$ TeV, Au + Au, Cu + Cu, Al + Al, and C + C collisions at $\sqrt{s} = 200$ GeV, and Au + Au and Cu + Cu collisions at $\sqrt{s} = 62.4$ GeV. We find that SONIC provides a good match to the pion spectra and HBT radii for all collision systems and energies, confirming earlier work that a combination of pre-equilibrium flow, viscosity, and QCD equation of state can resolve the so-called HBT puzzle. For reference, we also show p + p collisions at $\sqrt{s} = 7$ TeV. We make tabulated data for the 2 + 1 dimensional temperature evolution of all systems publicly available for the use in future jet energy loss or similar studies.

1 Introduction

With the advent of gauge/gravity duality, it has become possible to effectively simulate far-from-equilibrium thermalization in central (and smooth) nuclear collisions [1]. Combining this pre-equilibrium dynamics with hydrodynamics [2] and a late-stage hadronic cascade [3], one obtains a 'Super hybrid mOdel simulatioN for relativistic heavy-Ion Collisions' (SONIC for short) that effectively has only a limited number of parameters, namely those specifying the properties of the incoming nuclei, the speed of sound, and shear and bulk viscosities in the quark–gluon plasma. In this work, we use this model to study symmetric nuclear collisions of different nuclei (Pb, Au, Cu, Al, C) at collision energies ranging from $\sqrt{s} = 62.4$ GeV to $\sqrt{s} = 2.76$ TeV. We study the temperature evolution, pion spectra, and HBT radii for these different collision systems with the aim of both testing the model against experimental data where available and providing model predictions for the design of future experimental studies. In addition, we also show results for SONIC for central p + p collisions at $\sqrt{s} = 7$ TeV energy, even though evidence for forming an equilibrated quark–gluon plasma in these systems is currently lacking.

A fundamental question regarding the quark–gluon plasma is at what temperature and what scale a strong coupling description is most appropriate versus weak coupling. Near-inviscid hydrodynamic modeling indicates strong coupling, though the exact sensitivity of final state hadrons to the temperature dependence of η/s is currently under investigation. There are experimental observables when compared to model calculations that are potential indicators of stronger coupling at temperatures near the transition point. Inclusion of this strongest coupling near the transition is proposed to help reconcile the full suite of jet quenching observables including the anisotropy in mid-central collisions [4,5], the larger than expected v_2 and v_3 of direct photons [6] and heavy quark observables [7]. An important motivation for the sPHENIX upgrade [8] is to answer the question regarding the underlying nature of the quark–gluon plasma near the point of strongest coupling. A key question is whether high statistics data sets in Au + Au collisions at $\sqrt{s} = 200$ GeV at RHIC and Pb + Pb collisions at $\sqrt{s} = 2.76$ TeV at the LHC are substantially augmented by hard process observables at lower RHIC energies and with different nuclear geometries for emphasizing emission and parton quenching interactions closer or further away from this transition temperature. In this work, we explore the temperature evolution of different systems and provide access to the space-time snapshots for utilization in jet quenching, photon emission, and heavy quark diffusion calculations.

[a] e-mail: paul.romatschke@colorado.edu

2 Methodology

We model heavy-ion collisions by using a super hybrid model which we call SONIC which combines pre-equilibrium flow with hydrodynamics and a late-stage hadronic afterburner. Introducing the radius $r = \sqrt{x^2 + y^2}$, the different nuclei are modeled by employing an overlap function

$$T_A(r) = \epsilon_0 \int_{-\infty}^{\infty} \mathrm{d}z \left[1 + \mathrm{e}^{-(r^2+z^2-R)/a}\right] \tag{1}$$

with R, a the charge radius and skin depth parameters listed in Table 1. ϵ_0 is an overall normalization constant that controls the total final multiplicity. The pre-equilibrium flow has been calculated numerically assuming an infinite number of colors and infinite coupling for central (and smooth) Pb–Pb collisions at $\sqrt{s} = 2.76$ TeV in Ref. [1]. We re-analyzed the results from Ref. [1], finding that after the system has thermalized, the velocity is consistent with the early-time analytic result derived in Ref. [9] up to an overall factor of two (see Fig. 1). Therefore, in the following we will employ the pre-equilibrium radial flow velocity

$$v^r(\tau, r) = -\frac{\tau}{3}\partial_r \ln T_A^2(r), \tag{2}$$

where $\tau = \sqrt{t^2 - z^2}$; see Fig. 1. Using Eq. (2) and an initial energy density profile given by (cf. Ref. [9])

$$\epsilon(\tau, r) = T_A^2(r)\,, \tag{3}$$

we start the hydrodynamic evolution at a time τ_{sw}. Note that we have chosen the energy density to scale as the overlap function squared because this scaling is well known to give a simple description of the centrality dependence of multiplicity, cf. [10]. Following the observations in Refs. [1,11], τ_{sw} has to be large enough such that a local rest-frame can be defined as ($\tau_{\mathrm{sw}} \gtrsim 0.35$ fm/c) and before non-linear effects prohibit the use of Eq. (2) ($\tau_{\mathrm{sw}} \lesssim 0.6$ fm/c).

Table 1 Model parameters for different collision systems [12,13]. For all systems we use $T_S = 170$ MeV, $\eta/s = 0.08$, $\zeta/s = 0.01$, and QCD equation of state at zero baryon density [14]. The parameters R and a correspond to Eq. (1) except for p-1 where a denotes the width of a Gaussian, i.e., $T_A(r) = \epsilon_0 \int \mathrm{d}z \mathrm{e}^{-r^2/2/a^2}$

Isotope	$\sqrt{s}$ (GeV)	R (fm)	a (fm)	T_0 ($\tau = 0.5$ fm) (MeV)
p-1	7000	–	0.4	390
C-12	200	2.355	0.522	238
Al-27	200	3.061	0.519	287
Cu-63	62.4	4.163	0.606	300
Cu-63	200	4.163	0.606	327
Au-197	62.4	6.380	0.535	340
Au-197	200	6.380	0.535	370
Pb-208	2760	6.624	0.549	470

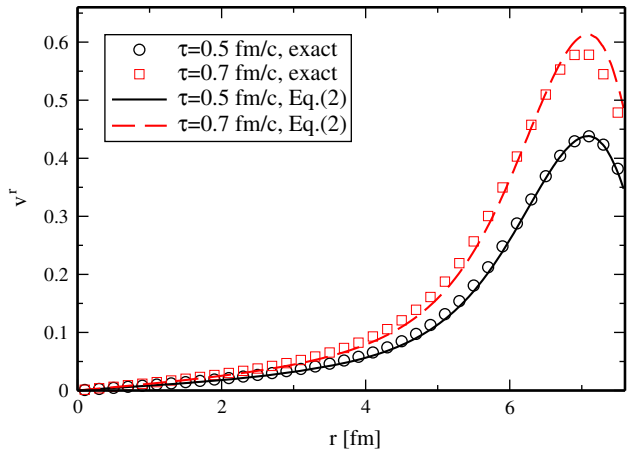

Fig. 1 Comparison between the pre-equilibrium radial flow velocity obtained for Pb + Pb collisions at $\sqrt{s} = 2.76$ TeV using a full numerical relativity simulation [1] ("exact") and the model equation (2)

Using the energy density from Eq. (3), the flow profile from Eq. (2), and setting the initial shear and bulk stresses to zero, we can solve the subsequent system evolution using the relativistic viscous hydrodynamics solver VH2 + 1 [2,15], version 1.7. The fluid shear viscosity over entropy ratio is set to $\eta/s = 0.08$ and the bulk viscosity over entropy ratio is set to $\zeta/s = 0.01$. The equation of state used is that from Ref. [14] which is consistent with lattice QCD data [16,17] at vanishing baryon density and matches a hadron resonance gas at low temperatures. We monitor the isothermal hypersurface defined by $T_S = 170$ MeV throughout the system evolution until the last fluid cell has cooled below T_S.

From the information about fluid temperature, velocity, and dissipative stress components we generate hadrons with masses up to 2.2 GeV and follow their rescattering dynamics using the hadron cascade code B3D [3]. Details for the freeze-out procedure can be found in the original reference [3], but for completeness we mention that the particle spectra take into account deformations from shear and bulk stresses independent of particle type as outlined in [18] such that the full energy-momentum tensor is continuous across the freeze-out hypersurface. We then generate 5000 B3D events for each hydro event. Once the particles have stopped interacting we collect information about the particle spectra and report the total charged multiplicity $\frac{\mathrm{d}N_{\mathrm{ch}}}{\mathrm{d}y}$, the mean pion transverse momentum $\langle p_T \rangle$ and the pion HBT radii R_{out}, R_{side}, and R_{long}.

With the pre-equilibrium flow given by Eq. (2), and adjusting ϵ_0 so that total multiplicity is constant, we find that the final particle $\langle p_T \rangle$ and the extracted HBT radii are insensitive to the choice of τ_{sw}, just as in the full gauge/gravity+hydro+cascade calculation (cf. Ref. [1]). Thus, τ_{sw} is not a relevant parameter of SONIC. This leaves a total of six relevant parameters for the system evolution: three numbers (R, a, T_S) and three functions (the temperature

Table 2 Details for collision systems compared to experimental data. $\langle p_T \rangle$ is for pion transverse momentum except for p + p collisions where report $\langle p_T \rangle$ for π, K, p. We use $\frac{dN_{ch}}{dy} = 1.1\frac{dN_{ch}}{d\eta}$ to convert model multiplicity to pseudorapidity distribution

Isotope	$\sqrt{s_{NN}}$ (GeV)	N_{part}	N_{coll}	$dN_{ch}/d\eta$	$\langle p_T \rangle$ (MeV)	Comments
p-1	7000	–	–	7	599	for $p_T > 0.15$ GeV
p-1 (exp.)	7000	–	–	6	622±21	[19,23], min.-bias
C-12	200	17	19	21	396	
Al-27	200	45	70	68	415	
Cu-63 (th.)	62.4	111	227	144	403	
Cu-63 (exp.)	62.4	106 ± 3	162 ± 13	138±10	379±20	[20,24,25], 0–10 % most central
Cu-63 (th.)	200	113	227	193	421	
Cu-63 (exp.)	200	108 ± 4	189 ± 14	198±15	420±20	[20,24,25], 0–10 % most central
Au-197 (th.)	62.4	375	1173	508	402	
Au-197 (exp.)	62.4	356 ± 11	–	472 ±41	405±11.0	[20,26], 0–5 % most central
Au-197 (th.)	200	378	1173	677	424	
Au-197 (exp.)	200	361 ± 11	1065 ± 105	691±52	453±33	[20,27], 0–5 % most central
Pb-208 (th.)	2760	399	1217	1635	503	
Pb-208 (exp.)	2760	382 ± 27	–	1584 ±80	517±19	[21,28], 0–5 % most central

dependent ratios η/s, ζ/s, and the equation of state). Note that ϵ_0 is fixed by requiring the final charged multiplicity to match the experimental data, wherever it is available [19–21], cf. Table 2. For C + C and Al + Al collisions at $\sqrt{s} = 200$ GeV, we employ the formula

$$\frac{dN_{ch}}{dy} = \left[\alpha(\sqrt{s})N_{coll} + \frac{1-\alpha(\sqrt{s})}{2}N_{part}\right]\frac{dN_{pp}}{dy}, \qquad (4)$$

where $\frac{dN_{pp}}{dy}$ is the charged multiplicity for nucleon-nucleon collisions at a given collision energy $\sqrt{s}$, and $\alpha(\sqrt{s} = 200\ \text{GeV}) = 0.13$ (cf. Ref. [22]).

We note that a full 2 + 1 dimensional simulation of a single symmetric nuclear collision can be executed on a modern desktop in approximately one hour, which makes SONIC a viable tool to investigate collisions having granular initial conditions on an event-by-event basis in the future.

3 Results

Our results for the multiplicity and mean pion transverse momentum in the different systems are reported in Table 2 alongside with experimental results where available. Since the experimental multiplicity is used to fix one of the model parameters (ϵ_0), only the pion $\langle p_T \rangle$ is a non-trivial model output. Comparing experimental measurements of $\langle p_T \rangle$ with model output from SONIC, we find that with model-parameter choices $\eta/s = 0.08$, $\zeta/s = 0.01$, $T_S = 170$ MeV, and a QCD equation of state, there is good agreement with experimental data for all collision systems at all collision energies.

For reference, we also show SONIC runs for p + p collisions at $\sqrt{s} = 7$ TeV collision energy, even though this system may not form an equilibrated state of matter (and thus SONIC would not be applicable in this case). Note that, nevertheless, the $\langle p_T \rangle$ value for p + p collisions is not too far from the experimental value, which may just be a reflection of the fact that transverse flow is not an indicator of system equilibration (cf. [1]).

It should be noted that our current implementation of SONIC does not properly reproduce the experimentally measured proton spectra because the number of protons and antiprotons is too high. The reason for this has been identified to be the missing implementation of baryon–antibaryon annihilation [29,30]. For this reason, we currently are unable to report physically viable results for baryons.

The time evolution for the temperature in the center of the fireball ($r = 0$ fm) is reported in Fig. 2, where we distinguish between the evolution spent in the hydrodynamic phase ($T > T_S$) and the hadron gas phase at low temperature. Shown in Fig. 3 is the radial velocity profile for the different collision systems at $\tau = 2$ fm/c inside the hydrodynamic phase. Not surprisingly, larger systems tend to build up smaller radial flow and tend to live longer than smaller systems. However, possibly interesting features for temperature evolution between different systems may also be identified in Fig. 2. For instance, note that Fig. 2 implies that the central temperature evolution in Au + Au collisions at $\sqrt{s} = 62.4$ GeV starts out close to the Cu + Cu $\sqrt{s} = 200$ GeV results, but then eventually approaches the Au + Au $\sqrt{s} = 200$ GeV curve. We are making the full two-dimensional space-time evolution profiles available for

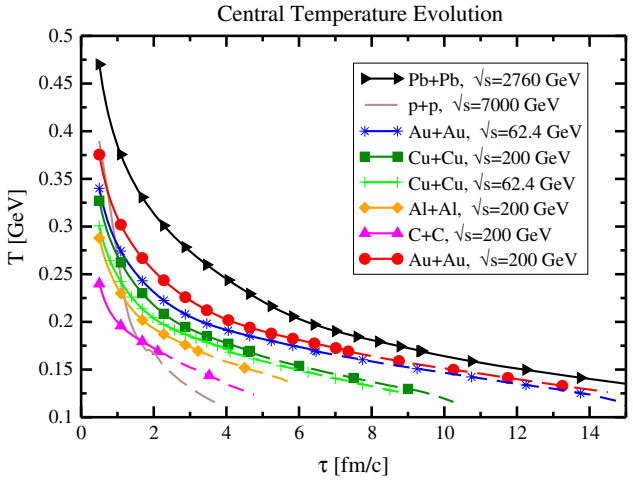

Fig. 2 Temperature evolution as a function of proper time at the center of the fireball ($r = 0$) for different collision systems and different collision energies. *Full lines* denote evolution within hydrodynamics ($T > T_S$), *dashed lines* denote hadron gas regime ($T < T_S$). For reference, also $p + p$ collisions at $\sqrt{s} = 7$ TeV are shown, even though this system may not equilibrate at all. The "kink" at 2 fm/c in the temperature evolution in the $p + p$ system around $T = T_S$ is due to the center $r = 0$ being cooler than the surrounding matter

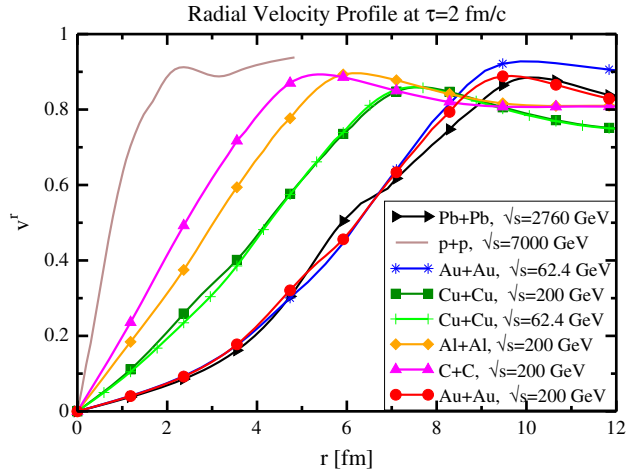

Fig. 3 Velocity profile at $\tau = 2$ fm/c for the different collision systems ($\tau = 1.9$ fm/c for p + p). The velocity profiles for the Pb + Pb and Au + Au systems are similar because the systems have similar geometry and the final-observed larger radial flow at higher $\sqrt{s}$ is simply due to the longer lifetime of the Pb + Pb system

potential use in studies of jet energy loss, direct photon emission and heavy quark diffusion [31].

Our results for pion HBT radii are calculated as described in [3] and the results are shown in Fig. 4 for the different collision systems. Despite some remaining discrepancies between our model results and experimental data, the overall agreement between SONIC and experiment for different collision energies and systems is striking, given that the inability of standard hydrodynamics to describe the data has been labeled the 'HBT puzzle' in the literature. As noted in Ref. [32], it is possible to resolve this 'puzzle' by a combination of different ingredients, notably pre-equilibrium flow, viscosity, and a QCD-like equation of state. Since all of these ingredients are naturally incorporated in SONIC, it is gratifying to observe that the HBT puzzle is no longer a puzzle but rather a (small) discrepancy in some of the data–model comparison.

In Fig. 5, we show the pion transverse momentum spectra for the different collision systems. As remarked above, we do find that with constant values of $\eta/s = 0.08$, $\zeta/s = 0.01$, and a QCD equation of state, SONIC provides a good overall description of the available experimental data. Note that the discrepancy in the pion spectra for Pb + Pb collisions at $p_T > 1.5$ GeV was not observed in Ref. [1]. The reason is that in Ref. [1], the actual calculation erroneously used a model parameter value of $R = 6.48$ fm instead of $R = 6.62$ fm (cf. Table 1) for Pb. Once correcting for this error, we do find slightly less transverse flow in Pb + Pb collsions, leading to the discrepancy observed in Fig. 5. However, it is expected that implementing more realistic granular initial conditions will lead to higher transverse flow velocities. This could help to improve the description of experimental data at $p_T > 1.5$ GeV in SONIC in the future.

4 Conclusions

We have presented SONIC, a new super hybrid model for heavy-ion collisions that combines pre-equilibrium flow, viscous hydrodynamics, and hadronic cascade dynamics into one package. SONIC was used to simulate boost-invariant, central, symmetric collisions of smooth nuclei (Pb, Au, Cu, Al, C) at energies ranging from $\sqrt{s} = 62.4$ GeV to $\sqrt{s} = 2.76$ TeV. We found that for a QCD equation of state and a choice of QCD viscosity over entropy ratios of $\eta/s = 0.08$, $\zeta/s = 0.01$, the particle spectra and pion HBT radii were in reasonable agreement with available experimental data. We also made predictions for pion mean transverse momentum and HBT radii for C + C and Al + Al collisions at $\sqrt{s} = 200$ GeV. The 2 + 1 dimensional space-time evolutions of the temperature obtained with SONIC are publicly available [31] in order to be of use in future studies of jet energy loss or photon emission.

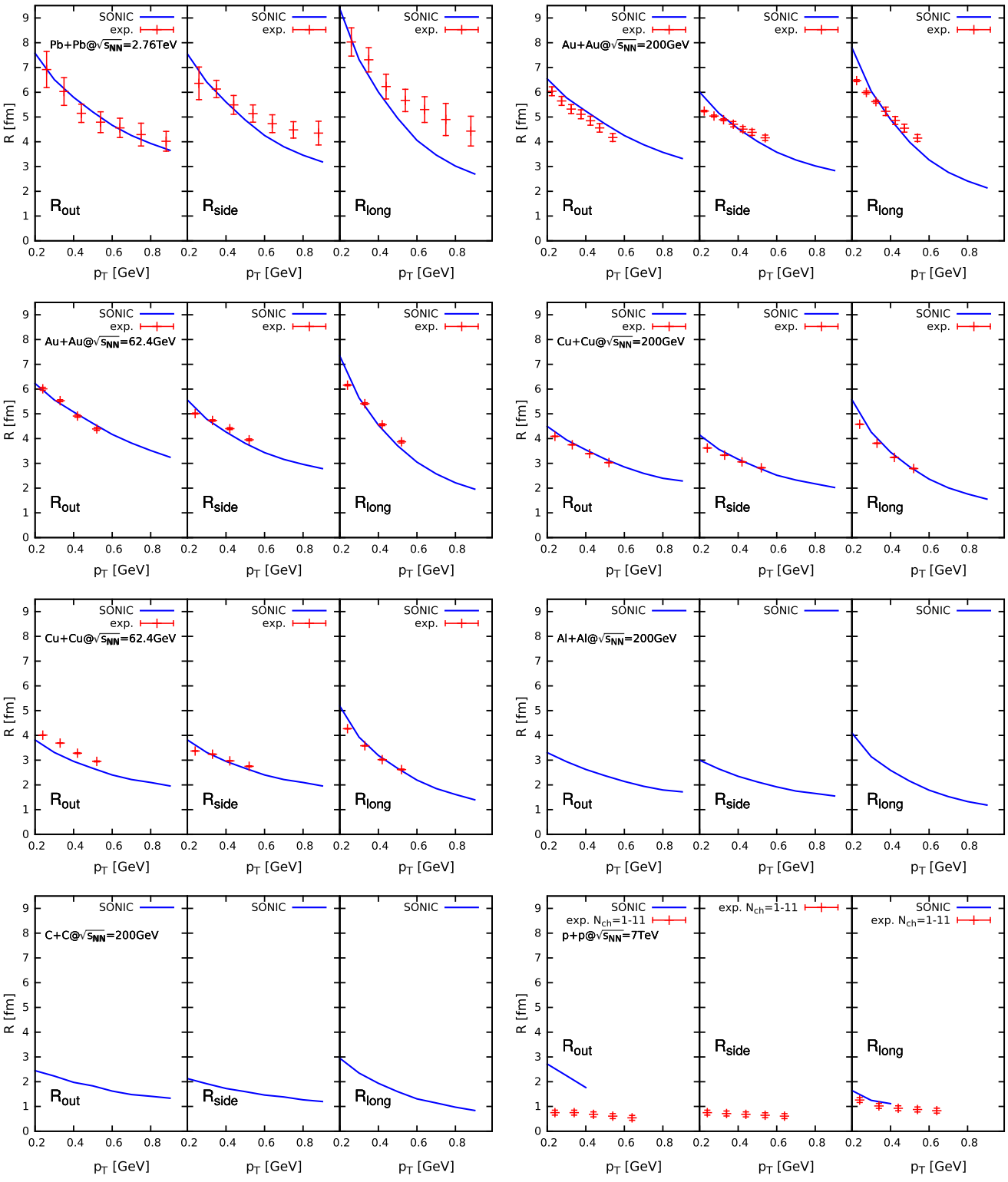

Fig. 4 Pion HBT radii for the different collision systems. Shown are model results (SONIC) and experimental results where available [24,34–36]. For p + p collisions, our numerical method to calculate HBT radii is breaking down, so we only report partial results. Experimental data is for 0–5 % most central events for Pb + Pb and Au + Au collisions, 0–10 % most central events for Cu + Cu collisions and minimum-bias events for p + p collisions

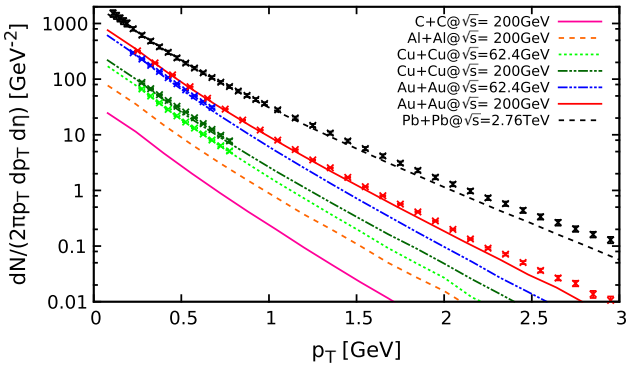

Fig. 5 Pion spectra from SONIC compared to experimental data where available [25–27,33]. Experimental data is for 0–5 % most central events for Pb + Pb and Au + Au collisions and 0–10 % most central events for Cu + Cu collisions

Acknowledgments This work was supported by the Department of Energy, Awards No. DE-SC0008027, DE-SC0008132 and DE-FG02-00ER41244. We would like to thank the JET Collaboration, Chun Shen, and Ulrike Romatschke for discussions.

References

1. W. van der Schee, P. Romatschke, S. Pratt, Phys. Rev. Lett. **111**, 222302 (2013). arXiv:1307.2539
2. M. Luzum, P. Romatschke, Phys. Rev. C **78**, 034915 (2008). arXiv:0804.4015 [nucl-th]
3. J. Novak, K. Novak, S. Pratt, J. Vredevoogd, C. Coleman-Smith et al., Phys. Rev. C **89**, 034917 (2014). arXiv:1303.5769 [nucl-th]
4. D. Li, J. Liao, M. Huang, Phys. Rev. D **89**, 126006 (2014). arXiv:1401.2035 [hep-ph]
5. T. Renk, Phys. Rev. C **89**, 067901 (2014). arXiv:1402.5798 [hep-ph]
6. H. van Hees, M. He, R. Rapp, Nucl. Phys. A **933**, 256 (2014). arXiv:1404.2846 [nucl-th]
7. A.M. Adare, M.P. McCumber, J.L. Nagle, P. Romatschke, Phys. Rev. C **90**, 024911 (2014). arXiv:1307.2188 [nucl-th]
8. C. Aidala, N. Ajitanand, Y. Akiba, Y. Akiba, R. Akimoto, et al. (2012). arXiv:1207.6378 [nucl-ex]
9. P. Romatschke, J.D. Hogg, JHEP **1304**, 048 (2013). arXiv:1301.2635 [hep-th]
10. P. Kolb, U.W. Heinz, P. Huovinen, K. Eskola, K. Tuominen, Nucl. Phys. A **696**, 197 (2001). hep-ph/0103234
11. P. Arnold, P. Romatschke, W. van der Schee, JHEP **1410**, 110 (2014). arXiv:1408.2518 [hep-th]
12. H.D. Vries, C.D. Jager, C.D. Vries, Atomic Data Nucl. Data Tables **36**, 495 (1987). ISSN: 0092-640X. http://www.sciencedirect.com/science/article/pii/0092640X87900131
13. C.D. Jager, H.D. Vries, C.D. Vries, Atomic Data Nucl. Data Tables **14**, 479 (1974) (nuclear charge and moment distributions). ISSN: 0092-640X. http://www.sciencedirect.com/science/article/pii/S0092640X74800021
14. M. Laine, Y. Schroder, Phys. Rev. D **73**, 085009 (2006). hep-ph/0603048
15. P. Romatschke, U. Romatschke, Phys. Rev. Lett. **99**, 172301 (2007). arXiv:0706.1522 [nucl-th]
16. S. Borsanyi, Z. Fodor, C. Hoelbling, S.D. Katz, S. Krieg et al., Phys. Lett. B **730**, 99 (2014). arXiv:1309.5258 [hep-lat]
17. A. Bazavov et al., HotQCD Collaboration, Phys. Rev. D **90**, 094503 (2014). arXiv:1407.6387 [hep-lat]
18. S. Pratt, G. Torrieri, Phys. Rev. C **82**, 044901 (2010). arXiv:1003.0413
19. K. Aamodt et al., ALICE Collaboration, Eur. Phys. J. C **68**, 345 (2010). arXiv:1004.3514 [hep-ex]
20. B. Alver et al., PHOBOS Collaboration, Phys. Rev. C **83**, 024913 (2011). arXiv:1011.1940 [nucl-ex]
21. K. Aamodt et al., ALICE Collaboration, Phys. Rev. Lett. **105**, 252301 (2010). arXiv:1011.3916 [nucl-ex]
22. B. Back et al., PHOBOS Collaboration, Phys. Rev. C **65**, 061901 (2002). nucl-ex/0201005
23. B.B. Abelev et al., ALICE Collaboration, Phys. Lett. B **727**, 371 (2013). arXiv:1307.1094 [nucl-ex]
24. B. Abelev et al., STAR Collaboration, Phys. Rev. C **80**, 024905 (2009). arXiv:0903.1296 [nucl-ex]
25. M. Aggarwal et al., STAR Collaboration, Phys. Rev. C **83**, 034910 (2011). arXiv:1008.3133 [nucl-ex]
26. B. Abelev et al., STAR Collaboration, Phys. Rev. C **79**, 034909 (2009). arXiv:0808.2041 [nucl-ex]
27. S. Adler et al., PHENIX Collaboration, Phys. Rev. C **69**, 034909 (2004). nucl-ex/0307022
28. B. Abelev et al., ALICE Collaboration, Phys. Rev. C **88**, 044910 (2013). arXiv:1303.0737 [hep-ex]
29. Y. Pan, S. Pratt (2012). arXiv:1210.1577 [nucl-th]
30. H. Song, S. Bass, U.W. Heinz, Phys. Rev. C **89**, 034919 (2014). arXiv:1311.0157 [nucl-th]
31. https://sites.google.com/site/revihy will contain a list of data tables for public use
32. S. Pratt, Phys. Rev. Lett. **102**, 232301 (2009). arXiv:0811.3363 [nucl-th]
33. B. Abelev et al., ALICE Collaboration, Phys. Rev. Lett. **109**, 252301 (2012). arXiv:1208.1974 [hep-ex]
34. K. Aamodt et al., ALICE Collaboration, Phys. Lett. B **696**, 328 (2011). arXiv:1012.4035 [nucl-ex]
35. J. Adams et al., STAR Collaboration, Phys. Rev. C **71**, 044906 (2005). nucl-ex/0411036
36. K. Aamodt et al., ALICE Collaboration, Phys. Rev. D **84**, 112004 (2011). arXiv:1101.3665 [hep-ex]

A.3. Testing hydrodynamic descriptions of p+p collisions at $\sqrt{s}$=7 TeV

Eur. Phys. J. C (2016) 76:408
DOI 10.1140/epjc/s10052-016-4237-z

THE EUROPEAN PHYSICAL JOURNAL C

Regular Article - Theoretical Physics

Testing hydrodynamic descriptions of p+p collisions at $\sqrt{s} = 7$ TeV

M. Habich[1], **G. A. Miller**[2], **P. Romatschke**[1,3,a], **W. Xiang**[1,4]

[1] Department of Physics, 390 UCB, University of Colorado at Boulder, Boulder, CO, USA
[2] Physics Department, University of Washington, Seattle, WA 98195, USA
[3] Center for Theory of Quantum Matter, University of Colorado, Boulder, CO 80309, USA
[4] Institute for Interdisciplinary Studies, Guizhou University of Finance and Economics, Guiyang 550025, China

Received: 2 May 2016 / Accepted: 28 June 2016 / Published online: 19 July 2016

Abstract In high-energy collisions of heavy ions, experimental findings of collective flow are customarily associated with the presence of a thermalized medium expanding according to the laws of hydrodynamics. Recently, the ATLAS, CMS, and ALICE experiments found signals of the same type and magnitude in ultrarelativistic proton–proton collisions. In this study, the state-of-the-art hydrodynamic model SONIC is used to simulate the systems created in p+p collisions. By varying the size of the second-order transport coefficients, the range of applicability of hydrodynamics itself to the systems created in p+p collisions is quantified. It is found that hydrodynamics can give quantitatively reliable results for the particle spectra and the elliptic momentum anisotropy coefficient v_2. Using a simple geometric model of the proton based on the elastic form factor leads to results of similar type and magnitude to those found in experiment when allowing for a small bulk viscosity coefficient.

1 Introduction

The experimental heavy-ion program at the Relativistic Heavy Ion Collider (RHIC) and the Large Hadron Collider (LHC) has provided strong evidence for the creation of an equilibrated state of matter in ultrarelativistic collisions of heavy ions such as gold or lead [1–7]. Comparing the wealth of experimental data available over a large range of collision energies to theoretical model calculations, the current consensus in the field is that the matter created in ultrarelativistic heavy-ion collisions behaves like an almost ideal fluid with very low shear viscosity over entropy ratio [8–13]. This form of matter has been dubbed the 'quark–gluon plasma'.

Only a few years ago, there was a similar consensus in the field that the systems created in proton–nucleus collisions (or d+Au collisions in the case of RHIC) did not equilibrate to form a quark gluon plasma because these systems were too small, too short-lived, and contained too few particles to behave collectively. In fact, experimental data from these light-on-heavy-ion collisions was regarded as a reference system in which the quark–gluon plasma component was 'known' to be absent. Similarly, the notion that quark–gluon plasmas could be formed in high-energy proton–proton collisions was mostly regarded as preposterous: how could a system consisting of a handful of particles behave as a fluid?

The consensus in the field was severely challenged, if not shattered, when experimental data for anisotropic collective flow in p+Pb, p+Au, d+Au, ^{3}He+Au, and most recently in proton–proton collisions became available [14–18]. In all of these small systems, the experimental signals turned out to be similar in type and magnitude to those found in heavy-ion collisions. Furthermore, the measurements could again be well described (and in some cases predicted) by theoretical hydrodynamic model calculations [19–23], such as the SONIC model [24].

The experimental finding of a large elliptic flow coefficient v_2 in high-energy proton–proton collisions is particularly intriguing, because a large v_2 coefficient is typically indicative of a hydrodynamic phase in the system evolution [25]. Is it at all possible for hydrodynamics to quantitatively describe the real-time evolution of system with a linear dimension of less than 1 fm and an average of five to six particles per unit rapidity? What constraints would result on QCD transport coefficients such as shear and bulk viscosity? These questions provide the motivation for performing a hydrodynamic study of high-energy proton–proton collisions.

One of the key differences of the present study with respect to most previous hydrodynamic studies of proton–proton collisions such as those in Refs. [26–29] is the inclusion of both shear and bulk viscous effects in the hydrodynamic evolution. (Note that shear-viscous effects were already included in Ref. [30], which will be discussed below

[a] e-mail: paul.romatschke@colorado.edu

in more detail.) Another perhaps novel aspect of the present study is that 'typical' proton–proton collisions (as opposed to high-multiplicity events such as those studied in Ref. [31]) will be discussed. Finally, the main emphasis of the present study will be a quantitative test of applicability of hydrodynamics to small systems, which has never been attempted before.

2 Methodology

In the present study, we use the hydrodynamic model SONIC [24] to simulate the matter created in proton–proton collisions. SONIC simulates the dynamics in the plane transverse to the beam axis using causal relativistic hydrodynamics in the presence of shear and bulk viscosity, followed by the hadron cascade afterburner B3D [32] in the hadronic phase for temperatures $T < 0.17$ GeV, while assuming boost-invariance in the longitudinal direction (see Ref. [24] for a detailed discussion of SONIC's components). It should be noted that while SONIC implements shear-viscous effects when switching from hydrodynamics to the hadron cascade simulation [33], the consistent implementation of bulk viscous effects on particle spectra is currently poorly understood [34]. For this reason, bulk viscous contributions to the initial particle spectra in the hadron cascade are not included in the present description. This is different from other work in the literature (e.g. [35,36]), which uses a form of the bulk viscous corrections based on a quasi-particle model [37].

SONIC is known to successfully describe experimental data for p+Pb and d+Au collisions at $\sqrt{s} = 5.02$ TeV and $\sqrt{s} = 0.2$ TeV collision energies, respectively, and has been used to make accurate predictions for v_2, v_3 for ^{3}He+Au collisions and p+Au collisions at $\sqrt{s} = 200$ GeV [20,23]. In order to simulate proton–proton collisions, a model for the hydrodynamic initial conditions, such as the energy density distribution in the transverse plane, is needed. These initial conditions are poorly constrained from first-principles calculations, so a basic model built on the proton form factor was used, which are described below. Besides the initial conditions, the hydrodynamic evolution in SONIC requires specification of the simulated ratios of shear viscosity and bulk viscosity to entropy density, $\frac{\eta}{s}$, $\frac{\zeta}{s}$, respectively. In the following, both of these ratios were taken to be constant in temperature for simplicity. Finally, SONIC requires specification of second-order transport coefficients, such as the shear and bulk relaxation times τ_π, τ_Π, respectively (cf. Ref. [38]). For simplicity, we have set $\tau_\pi = \tau_\Pi$ (cf. Ref. [39]).

The value of these relaxation times controls the size of second-order gradient terms in the hydrodynamic expansion. Varying the relaxation times thus allows one to quantify the importance of second-order gradient terms in final results, and thus provides a measure of the quantitative reliability of the hydrodynamic gradient expansion. The "conventional" criterion for the applicability of hydrodynamics states that the mean free path λ needs to be much smaller than the system size L. The ratio $\frac{\lambda}{L}$ is referred to as Knudsen number, and the conventional criterion quantifies the size of first-order gradient corrections (viscous effects) to ideal hydrodynamics. In recent years there has been mounting evidence from exact solutions of far-from-equilibrium quantum field theories that (second-order) hydrodynamics quantitatively applies in the cases where first-order (viscous) corrections to ideal hydrodynamics are large (order unity, cf. Refs. [40–43]). Thus it may be that the "conventional" Knudsen number criterion considerably underestimates the applicability of hydrodynamics. Instead, it has been suggested that the true criterion for the applicability of hydrodynamics is set by the location of the first non-hydrodynamic singularity in the complex frequency plane [44]. In second-order hydrodynamics, the location of this pole is controlled by the value(s) of the relaxation time. Hence it is plausible that varying the relaxation time τ_π allows a modern, realistic, quantitative, and easily implementable test for the applicability of hydrodynamics. This is consistent with the notion of large first, but small second-order hydrodynamic corrections.

It is well known that for fixed shear-viscosity over entropy ratio, the value of τ_π varies very little (only by about a factor of two) when the interaction strength in a quantum field theory is changed from zero to infinity [45,46]. With this result in mind, we choose to quantify the applicability of hydrodynamics by varying the relaxation times by 50 % around a fiducial value of $\tau_\pi = 6\frac{\eta}{sT}$. If the resulting variations in the final results are large, then hydrodynamics does not apply. Conversely, if the variations turn out to be small, then this provides evidence that hydrodynamics can give a quantitatively reliable description of the system.

Basic model for the proton We consider the initial transverse energy density distribution ε to be given by

$$\varepsilon(x, y, \tau_0) = \kappa(\tau_0) T_1\left(x + \frac{b}{2}, y\right) T_2\left(x - \frac{b}{2}, y\right), \qquad (1)$$

where $\mathbf{x}_\perp = (x, y)$ are the coordinates in the transverse plane, τ_0 is the initialization time of hydrodynamics, b is the impact parameter of the collision, $\kappa(\tau_0)$ is an overall normalization that is fixed by the experimental multiplicity in minimum-bias collisions, and $T_{1,2}$ is the transverse charge density distribution of proton 1 and 2, respectively. The expert reader will recognize Eq. (1) as an optical-Glauber model for protons, where it should be pointed out that for protons the binary collision scaling coincides with the number of participants scaling because $A = 1$. Indeed, in the basic initial condition model (referred to as 'RND' for 'round' in the fol-

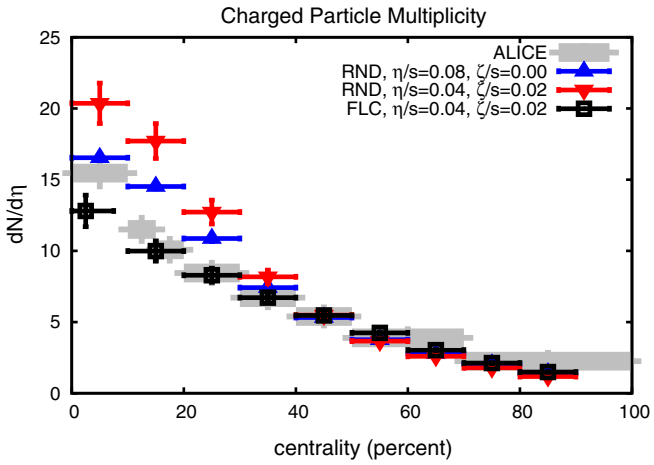

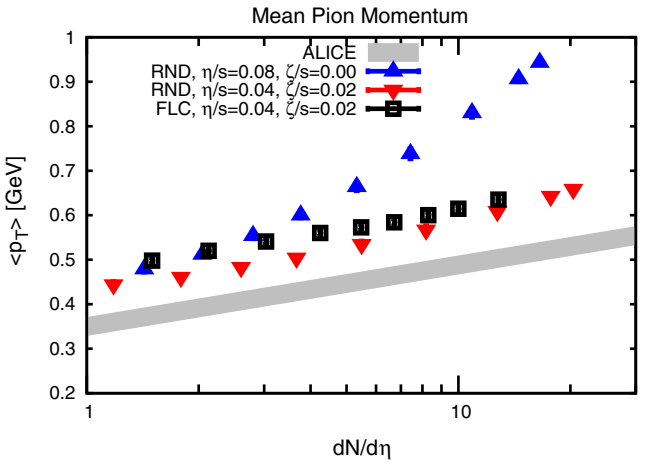

Fig. 1 Unidentified charged hadron multiplicity (*left*) and pion mean transverse momentum (*right*) for p+p collisions at $\sqrt{s} = 7$ TeV. Shown are experimental results from ALICE (cf. [49]) and SONIC simulations for proton models based on the proton form factor. The *error bars* for the SONIC simulations include systematic uncertainties for the applicability of hydrodynamics obtained from varying second-order transport coefficients; as can be seen, those *error bars* are significant for neither the multiplicity nor the pion $\langle p_T \rangle$, thus indicating robust applicability of hydrodynamics for these quantities. Note that the 'RND' model has been run with different shear and bulk viscosities. While the effect of changing the shear viscosity on the multiplicity and transverse momentum is minor (not shown), even a very small bulk viscosity has a large effect on the final pion transverse momentum

lowing), we take $T(x, y)$ to be given by the Fourier-transform of the proton form factor $F(Q^2)$,

$$T_{\mathrm{RND}}(\mathbf{x}_\perp) = \int \frac{\mathrm{d}^2 q}{(2\pi)^2} e^{-i\mathbf{q}\cdot\mathbf{x}_\perp} F(Q^2 = \mathbf{q}^2), \tag{2}$$

where we take the parametrization of the form factor from Ref. [47]. In the RND model, the proton is always round, and initial conditions for ε are generated by Monte-Carlo sampling of impact parameters $b \in [0, b_{\mathrm{max}}]$, where the upper limit $b_{\mathrm{max}} = 1.6$ fm corresponds to approximately twice the proton radius.

In a variation of the 'RND' model for initial conditions, referred to as 'FLC' for 'fluctuating' in the following, spin fluctuations of the proton are considered. Using the model from Ref. [48], the overlap function is defined as

$$T_{\mathrm{FLC}}(\mathbf{x}_\perp) = \int_{-\infty}^{\infty} \mathrm{d}z \left[\frac{\rho_U(r)\left(1 + \hat{n}\cdot\hat{s}\right)}{2N} + \frac{\rho_L(r)\left(1 + 2\hat{r}\cdot\hat{s}\hat{r}\cdot\hat{n} - \hat{n}\cdot\hat{s}\right)}{2N} \right], \tag{3}$$

where $\mathbf{r} = (x, y, z)$, $r = |\mathbf{r}|$ and $N = 4\pi \int_0^\infty \mathrm{d}r r^2 \left[\rho_U(r)\frac{1+\hat{n}\cdot\hat{s}}{2} + \rho_L(r)\frac{3-\hat{n}\cdot\hat{s}}{6}\right]$ is a normalization to ensure that protons have electric charge of unity for arbitrary unit vectors $\hat{s}$, $\hat{n}$. In the FLC model, the proton's shape may fluctuate event-by-event, and initial conditions for ε are generated by Monte-Carlo sampling of the two unit vectors $\hat{s}$, $\hat{n}$ as well as the impact parameter of the collision $b \in [0, b_{\mathrm{max}}]$.

3 Results

Using the basic model of the proton described in the previous section, the hydrodynamic plus cascade model SONIC was initialized at $\tau_0 = 0.25$ fm/c and results for particle spectra and momentum anisotropies were obtained that can be directly compared to experimental measurements (cf. [24]). In Fig. 1, results for the multiplicity of unidentified charged hadrons[1] and mean pion transverse momentum are shown for proton–proton collisions at $\sqrt{s} = 7$ TeV. The multiplicity in the 40–50 % centrality class obtained by ALICE [49] was used to set the overall constant κ in the SONIC simulations. The error bars shown for the SONIC results include the systematic uncertainties for the applicability of hydrodynamics obtained from varying second-order transport coefficients, as described above. From Fig. 1 it becomes apparent that systematic uncertainties of hydrodynamics for the particle multiplicity and mean transverse momentum are small, providing evidence that a hydrodynamic description of these quantities is feasible for proton–proton collisions. The centrality dependence of multiplicity in SONIC is broadly consistent with the experimental measurements from ALICE, with a level of disagreement that can be expected given the simplicity of the initial conditions used. Considering the mean transverse pion momentum, Fig. 1 indicates that SONIC results are extremely sensitive to the presence of bulk viscosity, as is apparent from comparing the 'RND' model results for $\frac{\zeta}{s} = 0$ and $\frac{\zeta}{s} = 0.02$.

[1] In the simulation, $\frac{\mathrm{d}N}{\mathrm{d}Y}$ is reduced by 10 % to obtain the experimentally determined pseudo-rapidity distribution $\frac{\mathrm{d}N}{\mathrm{d}\eta}$.

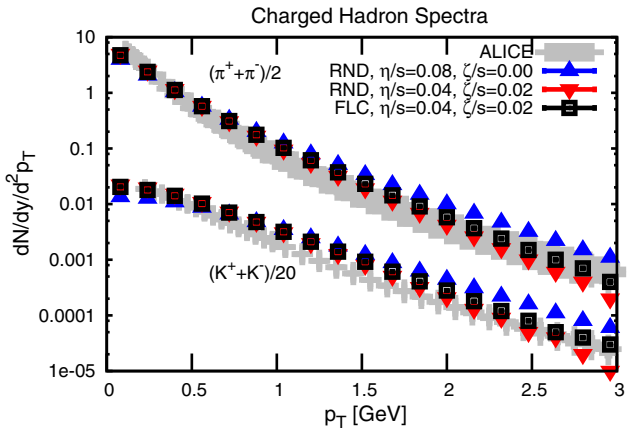

Fig. 2 Pion and kaon spectra for the 40–50 % centrality class compared to measured minimum-bias spectra for $\sqrt{s} = 7$ TeV from the ALICE experiment [50]. The *error bars* for the SONIC simulations include systematic uncertainties for the applicability of hydrodynamics obtained from varying second-order transport coefficients; these *error bars* are smaller than the symbol size for particle spectra, thus indicating robust applicability of hydrodynamics for this quantities. Note that the 'RND' model has been run with different shear and bulk viscosities, indicating the sensitivity of particle spectra to a small bulk viscosity coefficient

This effect originates from the modification of the fluid flow from bulk viscosity, and thus is expected to be a robust feature irrespective of the hadronization prescription used (see also the discussion in the appendix). For the proton models used, a minimum non-zero value of $\frac{\zeta}{s}$ was needed to bring any of the theory calculation close to the experimental data from the ALICE experiment [49] for pion mean transverse momentum. Because of the crudeness of the proton model, no effort has been made to the tune transport coefficient in order to match the experimental data.

Comparisons of identified particle spectra for mid-central collisions to minimum-bias experimental data are shown in Fig. 2. Again, one observes reasonable overall agreement between simulations and experiment except for the case when bulk viscosity was set to zero.

The qualitative effect of bulk viscosity reducing the mean particle momenta was observed before in heavy-ion collisions, e.g. in [34,36]. However, the effect of including the bulk viscosity in proton–proton collisions is much more pronounced than in heavy-ion collisions. Specifically, we find a factor two decrease in pion momentum originating from a bulk viscosity coefficient of $\frac{\zeta}{s} = 0.02$, while Ref. [36] found approximately 25 % reduction for a bulk viscosity coefficient peaking at $\frac{\zeta}{s} = 0.3$ (note that such high values would likely cause cavitation in the fluid [51–53]).

In Fig. 3, the momentum anisotropy coefficient v_2 for unidentified charged particles with $p_T > 0.5$ GeV from SONIC, including the estimated systematic uncertainty from the hydrodynamic gradient expansion is shown. (Note that v_2 is considerably smaller when a smaller p_T cut is used, cf. Ref. [54]). As outlined in the methodology section above, a large systematic uncertainty compared to the mean value indicates that hydrodynamic is very sensitive to the detailed treatment of higher-order gradient terms and/or non-hydrodynamic degrees of freedom. Thus a large uncertainty signals the breakdown of hydrodynamics. There are no established criteria in the literature for what constitutes an unacceptably large uncertainty, so in the following we declare a breakdown of hydrodynamics to occur if the ratio of uncertainty to mean value exceeds 50 %. In the case of the v_2 values shown in the left-hand panel of Fig. 3, this threshold is reached for $\frac{\mathrm{d}N}{\mathrm{d}\eta} \lesssim 2$ and $\frac{\eta}{s} = 0.08$, indicating that the hydrodynamic description of v_2 has broken down in this case.

On the other hand, while the systematic uncertainty originating from higher-order gradient terms is sizable, it seems that hydrodynamics nevertheless is still applicable to describing v_2 in proton–proton collisions for $\frac{\mathrm{d}N}{\mathrm{d}\eta} \gtrsim 2$ when $\frac{\eta}{s} \leq 0.08$. Since this finding disagrees with an earlier prediction by one of us in Ref. [30], this point deserves further clarification. Unlike the earlier study in Ref. [30], the present study does not use hydrodynamics for temperatures below the QCD phase transition, but instead employs a hadronic cascade simulation, thus increasing overall reliability of the model.

As can be seen by e.g. comparing the results for $\frac{\eta}{s} = 0.08$ and $\frac{\eta}{s} = 0.04$ in Fig. 3, the hydrodynamic systematic uncertainties decrease when lowering $\frac{\eta}{s}$. This is a trivial consequence of the fact that uncertainties are calculated by varying τ_π and $\tau_\pi \propto \frac{\eta}{s}$, so decreasing $\frac{\eta}{s}$ also decreases the extent of the variation. In the ideal hydrodynamic limit when $\frac{\eta}{s} \to 0$, second-order hydrodynamics no longer depends on the relaxation time nor does it possess a non-hydrodynamic pole, so an effective ideal hydrodynamic description never breaks down. This somewhat counter-intuitive finding can be justified physically by noting that in the ideal hydrodynamic limit, the mean free path λ tends to zero, so that even for very small system sizes L (or strong gradients) one always has $\frac{\lambda}{L} \to 0$. There are strong indications to support the notion that a lower bound on $\frac{\eta}{s}$ exist, effectively prohibiting to ever reach the ideal hydrodynamic limit in practice. However, this information is not part of a hydrodynamic description or the calculation of systematic uncertainties in this framework.

Also shown in Fig. 3 is the range of experimental results for v_2 as measured by the ATLAS experiment [18] for p+p collisions at $\sqrt{s} = 2.76$ TeV and $\sqrt{s} = 13$ TeV for $N_{\mathrm{ch}} = 50-60$, which roughly corresponds to the 0.5–4 % centrality class (cf. [55]). The SONIC model simulation results include no (RND) or only limited (FLC) event-by-event fluctuations, thereby invalidating the model results for the most central collisions ($\frac{\mathrm{d}N}{\mathrm{d}\eta} \gtrsim 10$) and the most periph-

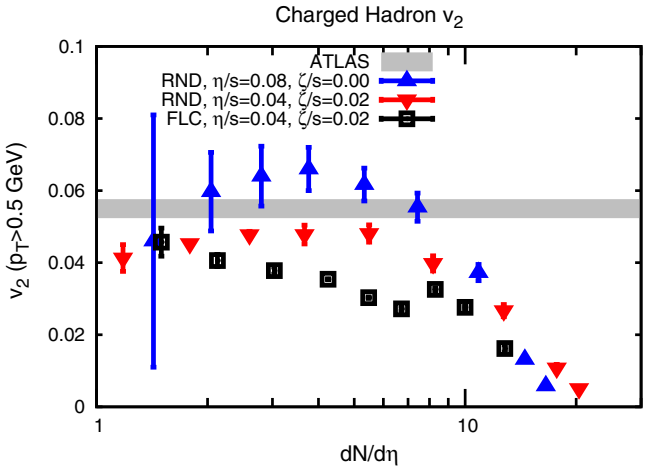

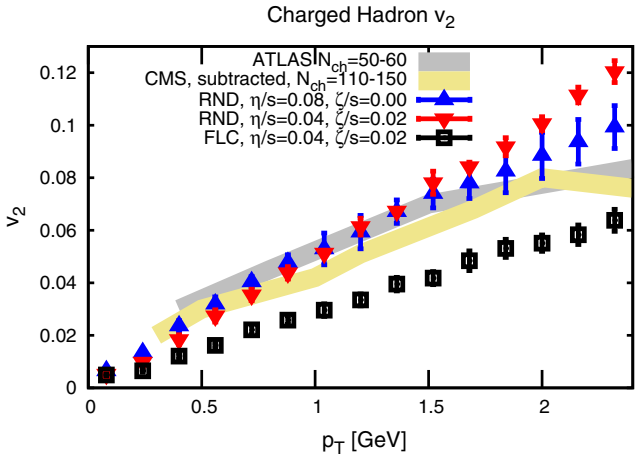

Fig. 3 *Left* Integrated momentum anisotropy v_2 for unidentified charged hadrons with $p_T > 0.5$ GeV in proton–proton collisions. Shown are the range of experimental results from ATLAS (cf. [18]) for $\sqrt{s} = 2.76$, 13 TeV and SONIC simulations for $\sqrt{s} = 7$ TeV. The *error bars* for the SONIC simulations include systematic uncertainties for the applicability of hydrodynamics obtained from varying second-order transport coefficients. *Right* Unintegrated momentum anisotropy for unidentified charged hadrons for the 40–50 % centrality class compared to experimental results from ATLAS [18] with $N_{\rm ch} = 50-60$ and for the 0.5–4 % centrality class ($N_{\rm ch} = 110-150$) from CMS [55]. We expect the $v_2(p_T)$ result from the 40–50 % centrality class in our simple proton models to be most representative of the experimental results for all centralities, including central collisions

eral collisions ($\frac{dN}{d\eta} \lesssim 1$). For mid-central collisions, however, the 'RND' and 'FLC' model are broadly consistent with the magnitude of the measured v_2 coefficient by the ATLAS experiment. This finding is corroborated by the second panel in Fig. 3, where the momentum dependence of the v_2 coefficient for mid-central collisions (40–50 % centrality class) is compared to experimental data for more central collisions from the ATLAS and CMS experiments.

SONIC simulation results for v_2 are sensitive to both shear and bulk viscosity coefficients, and no attempt has been made to tune the value of those coefficients in order to match the experimental data in view of the crudeness of the initial condition model. Rather, one observes that with 'typical' values for $\frac{\eta}{s}$, $\frac{\zeta}{s}$ the SONIC model predicts a v_2 response that is of comparable to that measured by experiment.

4 Conclusions

The hydrodynamic model SONIC was used to study proton–proton collisions at $\sqrt{s} = 7$ TeV by employing a simple parametrization of proton based on the elastic form factor. By varying the size of the second-order transport coefficients, the applicability of hydrodynamics itself to the systems created in p+p collisions could be quantified. It was found that a hydrodynamic description of the momentum anisotropy coefficient v_2 is breaking down for $\frac{dN}{d\eta} \lesssim 2$ when $\frac{\eta}{s} \geq 0.08$. Conversely, it was found that hydrodynamics can give quantitatively reliable results for the particle spectra and the elliptic momentum anisotropy coefficient v_2 when $\frac{dN}{d\eta} \gtrsim 2$. While it is somewhat surprising that hydrodynamics applies even for such low multiplicities, this finding is qualitatively in line with recent results for proton–nucleus collisions in Ref. [23]. In Ref. [23] it was found that a hydrodynamic description of v_2 was found to be reliable whereas hydrodynamics would break down sequentially starting from the higher-order momentum anisotropies (first v_5, then v_4, etc.). The finding that hydrodynamics can be applied to proton–proton collisions is also consistent with recent results from gauge/gravity duality simulations in Ref. [43]. This surprising applicability of hydrodynamics to small systems becomes somewhat less mysterious if one abandons the traditional idea of a handful of quarks and gluons forming a fluid in favor of delocalized and strongly interacting fields forming a plasma. Since hydrodynamics can be derived from a gradient expansion of quantum field theory without ever employing the concept of quasi-particles [45,56], it is perfectly reasonable to expect a tiny droplet of deconfined and strongly interacting QCD matter to behave hydrodynamically, even if this droplet will eventually hadronize into only a handful of hadrons. In principle, this notion could even offer a new interpretation of the apparently thermalized particle spectra seen to e^++e^- collisions.

In the context of a hydrodynamic description, the present study provided evidence that final particle mean transverse momenta in p+p collisions are strongly sensitive to the bulk viscosity coefficient. A non-vanishing minimum value of $\frac{\zeta}{s}$ was required to match experimental measurements of mean transverse momentum. This could indicate a possible experimental path to determining the bulk viscosity coefficient

in QCD. Finally, it was found that typical elliptic momentum anisotropy coefficients v_2 obtained in the hydrodynamic model are of the same magnitude as those measured by experiment.

Clearly, many aspect of the present hydrodynamic study could and should be improved when aiming at a detailed description of experimental data in the future, such as the inclusion of more realistic event-by-event fluctuations for the proton shape, or pre-equilibrium flow. However, we do not expect these future improvements of the treatment of initial conditions to affect the applicability of hydrodynamics.

To conclude, our study provides evidence that the experimental results obtained in high-energy proton–proton collisions can be understood both qualitatively and quantitatively in terms of a hydrodynamic model similar to that used in heavy-ion collisions. While the present hydrodynamic model does not describe details of the experimental measurements, it is likely that more sophisticated parametrizations of the proton could bring the same level of agreement to proton–proton collisions as is now routinely seen in heavy-ion collisions. This implies that an interpretation of the formation of a quark–gluon plasma in proton–proton collisions is consistent with the experimental data, yet does not imply that it is the only such consistent interpretation. Future work is needed to improve our qualitative and quantitative understanding of these fascinating system that link the fields of high-energy and nuclear physics.

Acknowledgments The work of G. A. M. was supported by the U. S. Department of Energy Office of Science, Office of Nuclear Physics under Award Number DE-FG02-97ER-41014. The work of M.H. and P.R. was supported by the U.S. Department of Energy, DOE award No. DE-SC0008132. W.X. was supported by National Natural Science Foundation of China No.11305040 and thanks the Department of Physics The University of Colorado at Boulder for the hospitality when this work was completed. We would like to thank M. Floris for fruitful discussions.

Appendix A: Bulk viscous effects on hydrodynamic flow

In the main text, it was mentioned that bulk viscosity affects the hydrodynamic flow pattern directly. In this appendix, the effect of bulk viscosity on the temperature and fluid velocity evolution are demonstrated through snapshots during the system evolution for an 'RND' proton collision at small impact parameter (0–10 % centrality class), shown in Fig. 4. The panels in the figure show that adding bulk viscosity changes the hydrodynamic evolution through reducing the local fluid velocity and slowing down the temperature decrease. Since particles are sampled from the local fluid cells, smaller velocities imply smaller particle momenta, which is consistent with the finding in the main text.

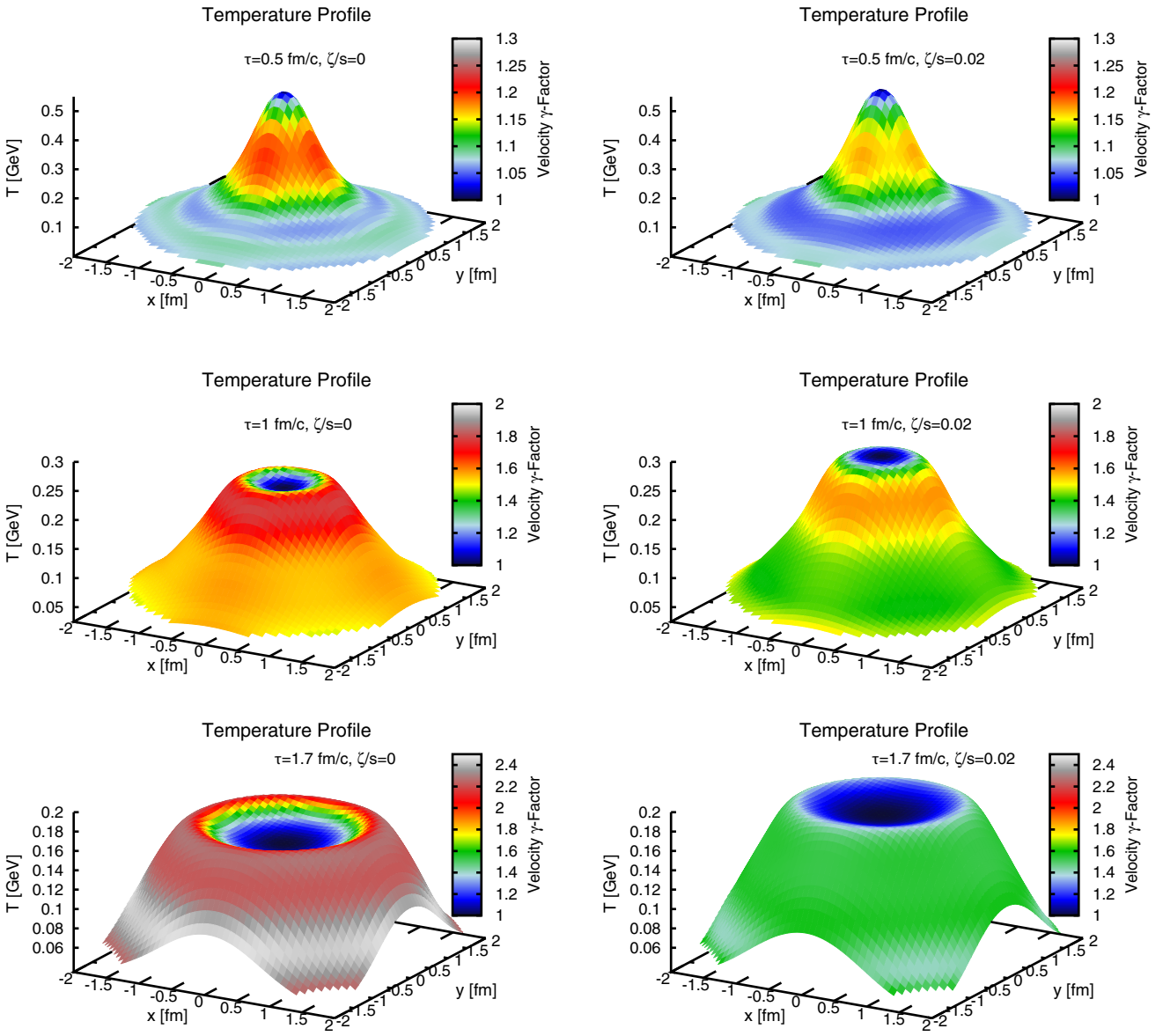

Fig. 4 Time snapshot of the temperature distribution in the transverse plane, with color coding corresponding to the local fluid velocity $|\mathbf{v}|$ (in terms of $\gamma = \frac{1}{\sqrt{1-\mathbf{v}^2}}$). *Left panels* show results without bulk viscosity, while *right panels* are for $\frac{\zeta}{s} = 0.02$

References

1. J. Adams et al. (STAR), Nucl. Phys. A **757**, 102 (2005). arXiv:nucl-ex/0501009
2. K. Adcox et al. (PHENIX), Nucl. Phys. A **757**, 184 (2005). arXiv:nucl-ex/0410003
3. B.B. Back et al., Nucl. Phys. A **757**, 28 (2005). arXiv:nucl-ex/0410022
4. I. Arsene et al. (BRAHMS), Nucl. Phys. A **757**, 1 (2005). arXiv:nucl-ex/0410020
5. K. Aamodt et al. (ALICE), Phys. Rev. Lett. **105**, 252302 (2010). arXiv:1011.3914
6. G. Aad et al. (ATLAS), Eur. Phys. J. C **74**, 3157 (2014). arXiv:1408.4342
7. S. Chatrchyan et al. (CMS), Phys. Rev. C **84**, 024906 (2011). arXiv:1102.1957
8. P. Huovinen, P.F. Kolb, U.W. Heinz, P.V. Ruuskanen, S.A. Voloshin, Phys. Lett. B **503**, 58 (2001). arXiv:hep-ph/0101136
9. D. Teaney, Phys. Rev. C **68**, 034913 (2003). arXiv:nucl-th/0301099
10. T. Hirano, U.W. Heinz, D. Kharzeev, R. Lacey, Y. Nara, Phys. Lett. B **636**, 299 (2006). arXiv:nucl-th/0511046
11. M. Luzum, P. Romatschke, Phys. Rev. C **78**, 034915 (2008). arXiv:0804.4015. **(Erratum: Phys. Rev. C 79, 039903 (2009))**
12. B. Schenke, S. Jeon, C. Gale, Phys. Rev. Lett. **106**, 042301 (2011). arXiv:1009.3244
13. U. Heinz, R. Snellings, Ann. Rev. Nucl. Part. Sci. **63**, 123 (2013). arXiv:1301.2826
14. B. Abelev et al. (ALICE), Phys. Lett. B **719**, 29 (2013). arXiv:1212.2001
15. G. Aad et al. (ATLAS), Phys. Rev. Lett. **110**, 182302 (2013). arXiv:1212.5198

16. A. Adare et al. (PHENIX), Phys. Rev. Lett. **111**, 212301 (2013). arXiv:1303.1794
17. A. Adare et al. (PHENIX), Phys. Rev. Lett. **115**, 142301 (2015). arXiv:1507.06273
18. G. Aad et al. (ATLAS) (2015). arXiv:1509.04776
19. P. Bozek, Phys. Rev. C **85**, 014911 (2012). arXiv:1112.0915
20. J. Nagle, A. Adare, S. Beckman, T. Koblesky, J.O. Koop, D. McGlinchey, P. Romatschke, J. Carlson, J. Lynn, M. McCumber, Phys. Rev. Lett. **113**, 112301 (2014). arXiv:1312.4565
21. B. Schenke, R. Venugopalan, Phys. Rev. Lett. **113**, 102301 (2014). arXiv:1405.3605
22. I. Kozlov, M. Luzum, G. Denicol, S. Jeon, C. Gale (2014). arXiv:1405.3976
23. P. Romatschke, Eur. Phys. J. C **75**, 305 (2015a). arXiv:1502.04745
24. M. Habich, J.L. Nagle, P. Romatschke, Eur. Phys. J. C **75**, 15 (2015). arXiv:1409.0040
25. P. Romatschke, Eur. Phys. J. C **75**, 429 (2015b). arXiv:1504.02529
26. S.K. Prasad, V. Roy, S. Chattopadhyay, A.K. Chaudhuri, Phys. Rev. C **82**, 024909 (2010). arXiv:0910.4844
27. P. Bozek, Acta Phys. Polon. B **41**, 837 (2010a). arXiv:0911.2392
28. G. Ortona, G.S. Denicol, P. Mota, T. Kodama (2009). arXiv:0911.5158
29. K. Werner, I. Karpenko, T. Pierog, Phys. Rev. Lett. **106**, 122004 (2011). arXiv:1011.0375
30. M. Luzum, P. Romatschke, Phys. Rev. Lett. **103**, 262302 (2009). arXiv:0901.4588
31. J. Casalderrey-Solana, U.A. Wiedemann, Phys. Rev. Lett. **104**, 102301 (2010). arXiv:0911.4400
32. J. Novak, K. Novak, S. Pratt, J. Vredevoogd, C. Coleman-Smith, R. Wolpert, Phys. Rev. C **89**, 034917 (2014). arXiv:1303.5769
33. S. Pratt, G. Torrieri, Phys. Rev. C **82**, 044901 (2010). arXiv:1003.0413
34. A. Monnai, T. Hirano, Phys. Rev. C **80**, 054906 (2009). arXiv:0903.4436
35. P. Bozek, Phys. Rev. C **81**, 034909 (2010b). arXiv:0911.2397
36. S. Ryu, J.F. Paquet, C. Shen, G.S. Denicol, B. Schenke, S. Jeon, C. Gale, Phys. Rev. Lett. **115**, 132301 (2015). arXiv:1502.01675
37. C. Sasaki, K. Redlich, Phys. Rev. C **79**, 055207 (2009). arXiv:0806.4745
38. P. Romatschke, Class. Quant. Grav. **27**, 025006 (2010). arXiv:0906.4787
39. I. Kanitscheider, K. Skenderis, JHEP **04**, 062 (2009). arXiv:0901.1487
40. M.P. Heller, R.A. Janik, P. Witaszczyk, Phys. Rev. Lett. **108**, 201602 (2012). arXiv:1103.3452
41. B. Wu, P. Romatschke, Int. J. Mod. Phys. C **22**, 1317 (2011). arXiv:1108.3715
42. W. van der Schee, Phys. Rev. D **87**, 061901 (2013). arXiv:1211.2218
43. P.M. Chesler, Phys. Rev. Lett. **115**, 241602 (2015). arXiv:1506.02209
44. M.P. Heller, R.A. Janik, P. Witaszczyk, Phys. Rev. Lett. **110**, 211602 (2013). arXiv:1302.0697
45. R. Baier, P. Romatschke, D.T. Son, A.O. Starinets, M.A. Stephanov, JHEP **04**, 100 (2008). arXiv:0712.2451
46. M.A. York, G.D. Moore, Phys. Rev. D **79**, 054011 (2009). arXiv:0811.0729
47. S. Venkat, J. Arrington, G.A. Miller, X. Zhan, Phys. Rev. C **83**, 015203 (2011). arXiv:1010.3629
48. G.A. Miller, Phys. Rev. C **68**, 022201 (2003). arXiv:nucl-th/0304076
49. J. Adam et al. (ALICE), CERN-EP-2016-153 (2016). arXiv:1606.07424
50. J. Adam et al. (ALICE), Eur. Phys. J. C **75**, 226 (2015). arXiv:1504.00024
51. K. Rajagopal, N. Tripuraneni, JHEP **03**, 018 (2010). arXiv:0908.1785
52. M. Habich, P. Romatschke, JHEP **12**, 054 (2014). arXiv:1405.1978
53. S.M. Sanches, D.A. Fogaa, F.S. Navarra, H. Marrochio, Phys. Rev. C **92**, 025204 (2015). arXiv:1505.06335
54. M. Luzum, Phys. Rev. C **83**, 044911 (2011). arXiv:1011.5173
55. V. Khachatryan et al. (CMS), CMS-PAS-HIN-15-009 (2015)
56. S. Bhattacharyya, V.E. Hubeny, S. Minwalla, M. Rangamani, JHEP **02**, 045 (2008). arXiv:0712.2456

— End of included papers —